Nanoscale
Horizons

REVIEW

View Article Online
View Journal | View Issue

Cite this: *Nanoscale Horiz.*, 2018, **3**, 464

# Review on nanoscale Bi-based photocatalysts

Rongan He,[ab] Difa Xu,[ab] Bei Cheng,[a] Jiaguo Yu*[a] and Wingkei Ho*[c]

Received 15th March 2018,
Accepted 9th May 2018

DOI: 10.1039/c8nh00062j

rsc.li/nanoscale-horizons

Nanoscale Bi-based photocatalysts are promising candidates for visible-light-driven photocatalytic environmental remediation and energy conversion. However, the performance of bulk bismuthal semiconductors is unsatisfactory. Increasing efforts have been focused on enhancing the performance of this photocatalyst family. Many studies have reported on component adjustment, morphology control, heterojunction construction, and surface modification. Herein, recent topics in these fields, including doping, changing stoichiometry, solid solutions, ultrathin nanosheets, hierarchical and hollow architectures, conventional heterojunctions, direct Z-scheme junctions, and surface modification of conductive materials and semiconductors, are reviewed. The progress in the enhancement mechanism involving light absorption, band structure tailoring, and separation and utilization of excited carriers, is also introduced. The challenges and tendencies in the studies of nanoscale Bi-based photocatalysts are discussed and summarized.

**Conceptual insights**

Photocatalytic technology is effective for environmental remediation and energy conversion. Nano Bi-based photocatalysts are an important family of visible-light-excitable photocatalysts. Therefore, enhancing the activity of these photocatalysts by adjusting their nanostructure is one of the hot topics in photocatalysis. In this paper, we have reviewed the recent development on the improvement of the performance of nanoscale Bi-based photocatalysts to provide general and new insights into this family.

## Introduction

Escalating serious environment and energy crises have resulted in a growing demand for effective environmental remediation and energy conversion techniques. These needs can be addressed using photocatalysis, which is an increasingly developed photochemical strategy. In a photocatalytic procedure, electrons and holes are generated from semiconductors under light irradiation and participate in reduction and oxidization reactions, respectively. Thus, photocatalysis promotes redox reactions, such as pollutant degradation, water oxidization, $H_2$ evolution, $CO_2$ reduction and $N_2$ fixation.[1–19] Consequently, photocatalysis is regarded as a green technique for removing organic pollutants and producing fuel or electricity. Given that visible-light energy constitutes about 43% of solar energy, visible-light-responsive photocatalysts are preferred in photocatalysis and photoelectrocatalysis.

Up to now, many types of semiconductors, including metal oxides ($TiO_2$, ZnO, $Ag_2O$, $Fe_2O_3$, $Cu_2O$, $Ta_2O_5$), metal sulfides (ZnS, CdS, $MoS_2$, $Bi_2S_3$), multi-component oxides ($Bi_2WO_6$, $InTaO_4$, $BiVO_4$, $Ag_3VO_4$, $SrTiO_3$), metal selenides ($MoSe_2$, CdSe), metal phosphides ($Ni_2P$), metal phosphates ($Ag_3PO_4$), metal halides and oxyhalides (AgBr, BiOBr) and metal-free materials (SiC, g-$C_3N_4$, and Si), have been employed as photocatalysts.[3,4,20–24] Among them, those that possess a band gap of $E_g$ > 3 eV are called wide-band-gap photocatalysts, such as $TiO_2$, ZnO, ZnS, $SrTiO_3$, and $KTaO_3$. In contrast, those with a band gap of $E_g \leq 3$ eV are called visible-light-responsive photocatalysts, such as $Ag_2O$, $Bi_2WO_6$, $InTaO_4$, CoO, $BiVO_4$, $Fe_2O_3$, $Cu_2O$, $Ag_3VO_4$, TaON, CdS, $Ta_3N_5$, CdSe, $Bi_2S_3$, SiC, g-$C_3N_4$, and Si. Bi-Based photocatalysts are important visible-light-responsive photocatalysts and have recently attracted rapidly increasing attention, shown not only from the number of publications, but also from the ratio of publications in the field of photocatalysis (see Fig. 1a and b). Considering the stability of $Bi^{3+}$, most studies have focused on $Bi^{3+}$-containing compounds, such as $Bi_2O_3$,[25] $BiVO_4$,[26] $Bi_4Ti_3O_{12}$,[27] $Bi_{12}TiO_{20}$,[28] $Bi_2O_2CO_3$,[29] $Bi_2WO_6$,[30] $BiPO_4$,[31] $BiFeO_3$,[32] BiOX (X = Cl, Br, I),[33] $Bi_3TiNbO_9$,[34] and $Bi_{0.5}K_{0.5}TiO_3$.[35] The majority of these compounds possess a layered structure and plate-like appearance. $Bi^{5+}$-Containing compounds, such as $LiBiO_3$, $NaBiO_3$, and $KBiO_3$,

---

[a] *State Key Laboratory of Advanced Technology for Materials Synthesis and Processing, Wuhan University of Technology, Wuhan 430070, China. E-mail: jiaguoyu@yahoo.com*

[b] *Hunan Province Key Laboratory of Applied Environmental Photocatalysis, Changsha University, Changsha 410022, China*

[c] *Department of Science and Environmental Studies, The Education University of Hong Kong, Tai Po, N. T. Hong Kong, P. R. China. E-mail: keithho@ied.edu.hk*

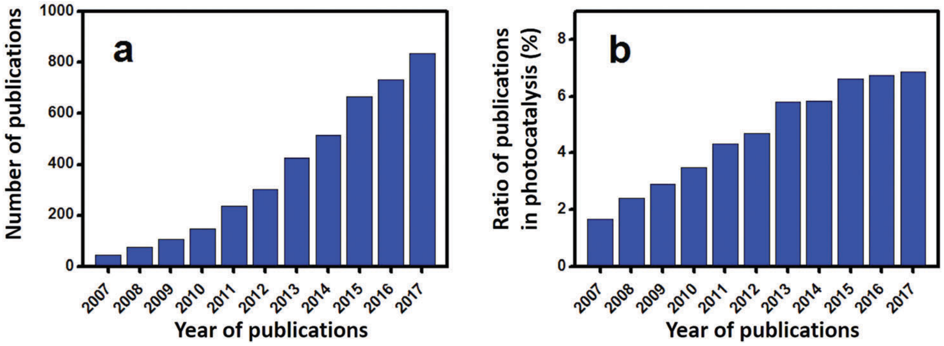

Fig. 1 (a) Number of publications of Bi-based photocatalysts during the last decade (source: web of science; date: 8th April 2018; key word: bismuth and photocatalytic), (b) the ratio of publications of Bi-based photocatalysts in the field of photocatalysis (source: Web of science; date: 8th April 2018; key word: photocatalytic).

can also be excited by visible light. However, such types are less reported than the others because of the instability of $Bi^{5+}$. In Bi(III) compounds, the hybridized O 2p and Bi $6s^2$ orbitals may cause an upshift of the valence bands (VBs).[33] Therefore, the band gaps of Bi compounds are usually smaller than 3.0 eV and can be excited by visible light. Bi-based photocatalysts are regarded as promising candidates for removing toxins from water and air[3,36–38] as well as for the production of fuel.[2,39–41] However, the photocatalytic performance of bulk Bi-based semiconductors is not as high as those of nanoscale Bi-based photocatalysts, because the photogenerated electrons and holes of these materials have not been easily exploited and utilized. Also, bulk photocatalysts have weaker light absorption and smaller surface areas than nanoscale photocatalysts (see Fig. 2). Numerous attempts have been made to enhance bulk Bi-based semiconductors to achieve ideal photocatalytic activity. These studies have focused on nanoscale component adjustment, morphology control, heterojunction construction, and surface modification[2,37,38,42] (Fig. 3).

## Component adjustment

The band structure parameters, such as VB, conduction band (CB), and band gap ($E_g$), are crucial to the photocatalyst activity. Furthermore, component adjustments, such as doping, solid-solution preparation and stoichiometry alteration, are effective methods that can be used to tune the band structures of bismuthal semiconductors. Therefore, suitable component adjustment is favorable for bismuthal photocatalysts.

### Doping

Heteroatom doping is widely adopted to increase the visible-light absorption of photocatalysts, because this process can generate a doping level between the CB and VB (Fig. 4). Consequently, the energy required to excite electrons decreases, and the light response of semiconductors increases.[43–47] Doping can also improve the charge transmission properties of semiconductors and lead to the augmented transfer efficiency of carriers. Doping is commonly employed to enhance the activity of Bi-based semiconductors.

Many bismuthal compounds are visible-light responsive. Thus, doping has been performed more frequently to enhance the visible-light absorption of bismuthal compounds with a wider band-gap, such as in $Bi_2O_2CO_3$,[48] $BiPO_4$,[49] BiOCl,[50] and $Bi_3TiNbO_9$.[34] For example, the band gap of $Bi_3TiNbO_9$ can be reduced from 3.1 eV to 2.6 eV when it is doped with a 10% molar ratio of $Ni^{2+}$.[34] Zheng *et al.*[51] found that the band gap of

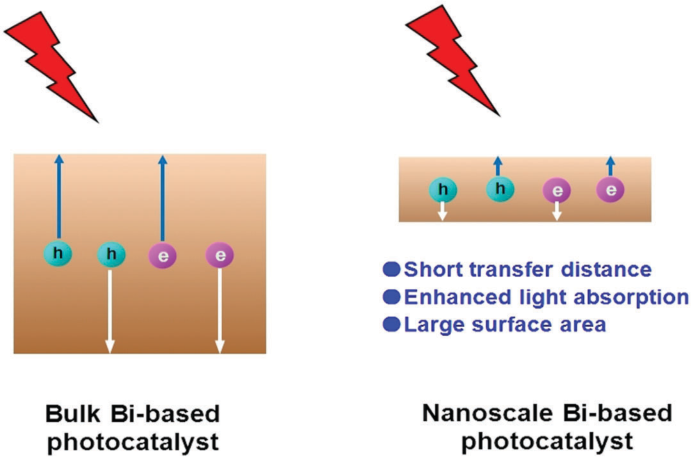

Fig. 2 Schematic illustration showing the superiority of nanoscale photocatalysts.

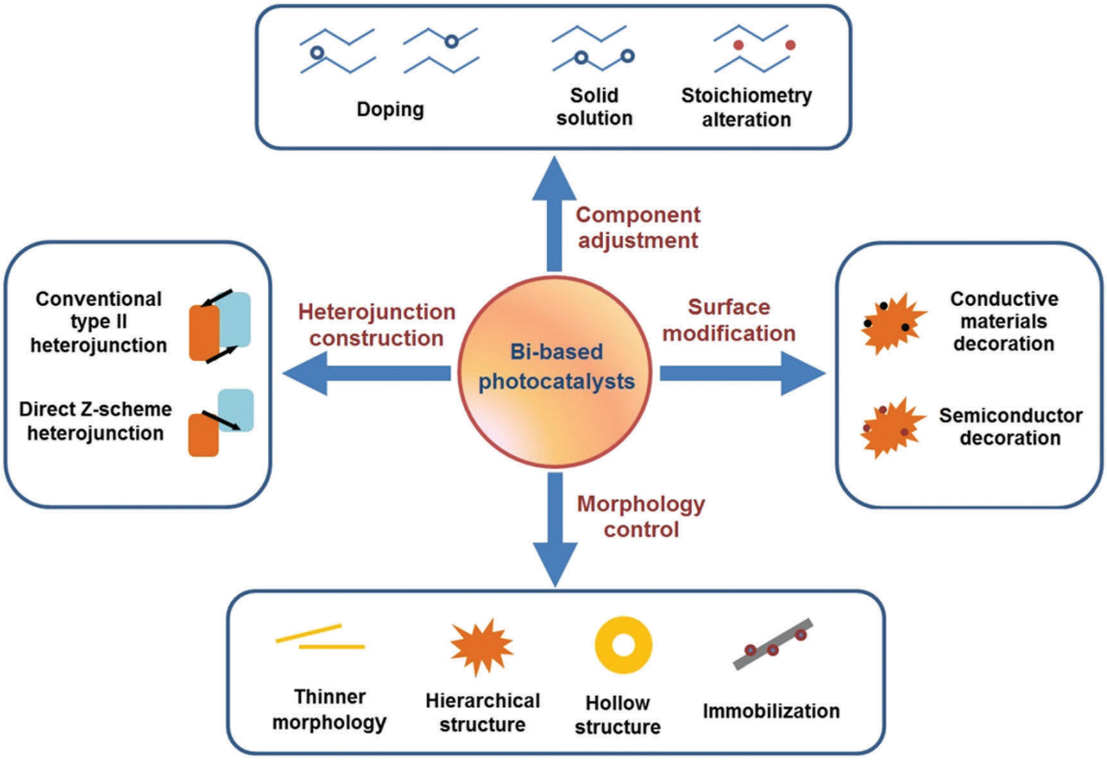

Fig. 3 Enhancement strategies for nanoscale Bi-based photocatalysts.

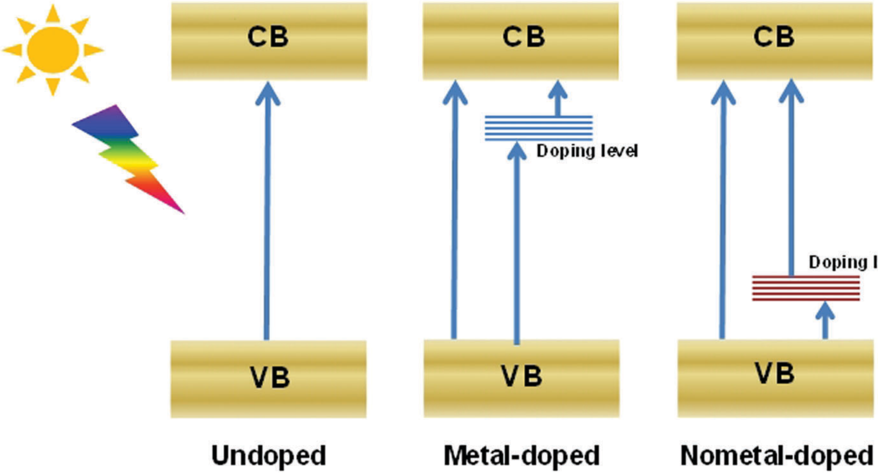

Fig. 4 The energy level mechanisms for metal-doped and nonmetal-doped photocatalysts.

$Bi_2WO_6$ can be narrowed by doping a small amount of Br with the surfactant cetyltrimethylammonium bromide (CTAB) during preparation. Doping by up to approximately 3% can also narrow the band gap of $Bi_2MoO_6$ from 2.96 eV to 2.69 eV and consequently improve the performance of $Bi_2MoO_6$ in the photocatalytic degradation of Rhodamine B (RhB).[52] Zhang *et al.*[53] studied the effects of doping on the electronic structures and optical properties of BiOCl using first-principle calculations. Studies have also proposed that codoping with Sb and I can substantially narrow the band gaps and increase the light absorption of BiOCl because of the difference in the electronegativities between the Sb/I and Bi/Cl atoms.

Doping can further narrow the band gap of visible-light-responsive bismuthal compounds.[54,55] However, the improvement resulting from a narrowed band gap is limited, because visible light response is not the main barrier to the photocatalytic performance of bismuthal compounds. Low utilization efficiency of the generated carriers is the primary issue to be solved for these bismuthal photocatalysts. In this case, doping can also enhance the photocatalyst activity if the dopant can reduce impedance or improve charge separation. For instance, F-doped $\beta$-$Bi_2O_3$ has been shown to exhibit higher photocatalytic activity than that of pure $\beta$-$Bi_2O_3$ in the degradation of methyl orange (MO).[56] This can be attributed to the higher separation efficiency of electron–hole pairs and lower VB position (indicating stronger oxidation capacity). B-Doping can increase the photocatalytic activity of BiOBr on the inactivity of *Escherichia coli*, which is attributed to the role of B as the electron acceptor for the effective separation of electrons and holes.[57] Such a role may have been caused by the empty p-orbital and unpaired electrons in B. Br doping could reduce the effective mass of electrons in $Bi_2WO_6$, by which the transfer and separation of the carrier can be facilitated.[58] Aurivillius-type Ce-doped $SrBi_2Ta_2O_9$ fabricated by Senthil and co-workers[59] exhibited a higher photocatalytic activity than $SrBi_2Ta_2O_9$ for $H_2$ generation. The improvement comes from the enhanced separation of electrons and holes through a dipole moment derived from the bonding of $Ce^{4+}$ with the surrounding oxygen atoms. Zhang and colleagues[60] found that carbon doping increases the internal electric field by 126-fold as a result of the enlarged differences in the electrostatic potentials between the $[Bi_3O_4]$ and [Cl] layers induced by the carbon doping (Fig. 5). Consequently, the separation of holes and electrons was improved. Er-Doped $Bi_{24}O_{31}Br_{10}$,[61] carbon-doped $Bi_2WO_6$,[62] Mo-doped $BiVO_4$,[63] and Er/Yb codoped $BiVO_4$[64] also showed enhanced photocatalytic activities relative to those of the original bismuthal compounds due to increased carrier transfer and separation.

Anion and mixed-valence cation dopants can also improve the photocatalytic performance of bismuthal semiconductors by facilitating the transfer and separation of carriers. For instance, doping with $IO_3^-$ can increase the activity of BiOI in

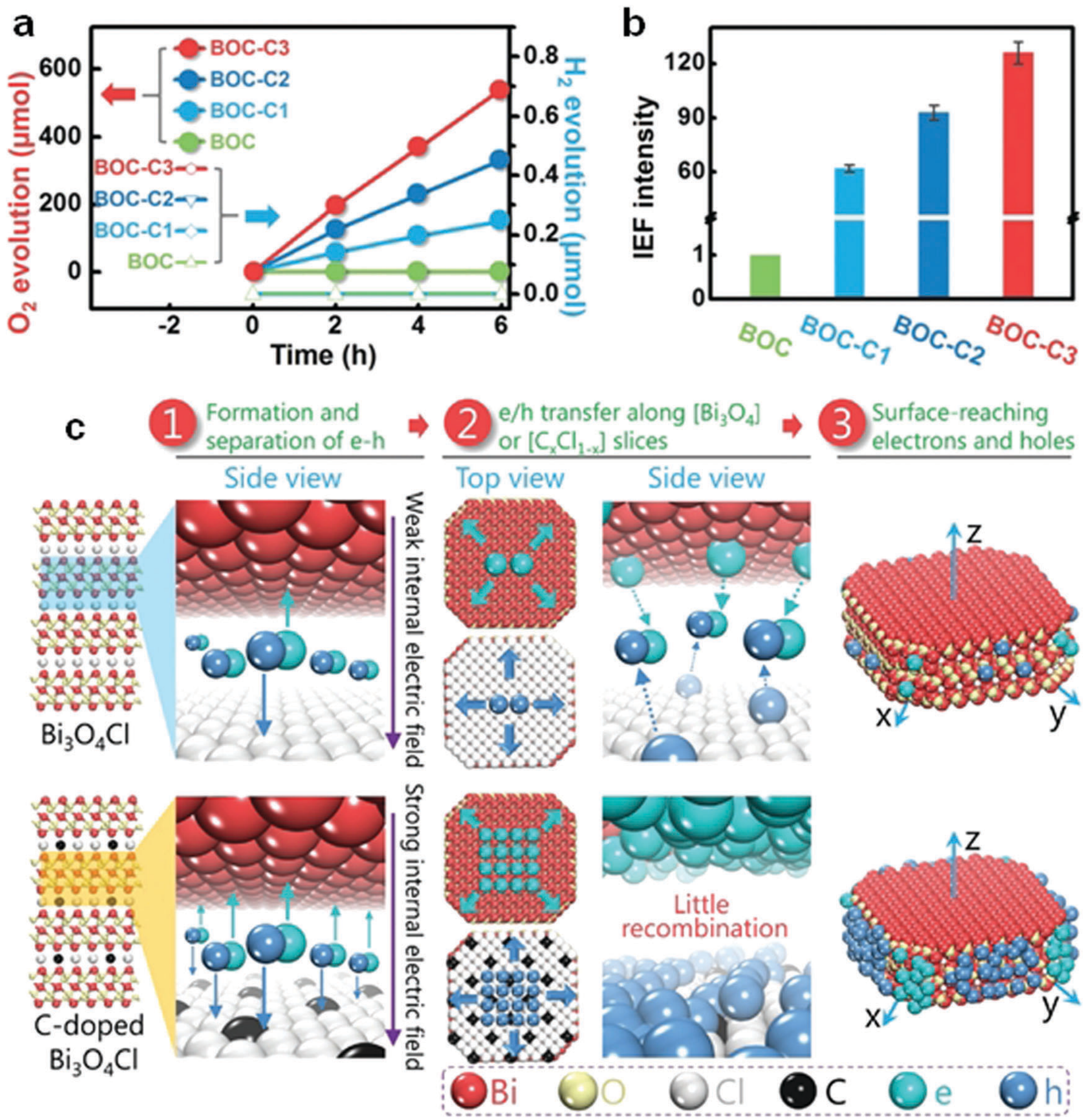

Fig. 5 (a) The performance of visible-light-driven oxygen and hydrogen evolution; (b) internal electric field intensity of C-doped $Bi_3O_4Cl$ (assuming the intensity of BOC to be "1"); and (c) schematic diagram of the carrier migration of pure and C-doped $Bi_3O_4Cl$; BOC-C1, BOC-C2, and BOC-C3 present C-doped $Bi_3O_4Cl$ with carbon concentrations of 0.92%, 1.86%, and 3.16%, respectively. Reproduced with permission from ref. 60. Copyright 2016 John Wiley and Sons.

the photocatalytic degradation of MO because of the key role played by $IO_3^-$ in improving the transfer efficiency of the carriers.[65] In-Doped BiOI exhibited augmented activity in the photocatalytic degradation of *p*-chloroaniline, because the introduced In resulted in the formation of a doping energy level that acted as a scavenger of photo-induced electrons and consequently prevented the recombination of charges.[66] Jiang *et al.*[67] fabricated $Sn^{4+}$-doped $Bi_2S_3$ through a solvothermal method, in which $Sn^{4+}$ acted as an electron scavenger by interconversion between $Sn^{4+}$ and $Sn^{2+}$ and facilitated $O_2$ reduction. Consequently, the photocatalytic performance of $Sn^{4+}$-doped $Bi_2S_3$ was enhanced. Similarly, the dopant Tb acted as an electron-trapping agent through interconversion between $Tb^{4+}$ and $Tb^{3+}$ and improved the photocatalytic activity of $Bi_2MoO_6$ in RhB degradation.[68]

Although the above conventional doping of heteroatoms can enhance the activities of bismuthal compounds, the introduced hetero element may alter the space lattice and cause additional stress. This process suppresses the introduction of the dopant and limits the improvements of visible-light absorption and carrier transfer derived from doping. Hence, doping by substituting the original element, rather than interstitial doping, is desired.

For example, when Bi and Ti in $Bi_4Ti_3O_{12}$ are partially replaced by Cr, the doped $Bi_4Ti_3O_{12}$ exhibits a higher activity in $H_2$ generation because of the considerably narrowed band gap and enlarged light absorption of $Bi_4Ti_3O_{12}$.[69] The cosubstitution of Gd and Mn in $BiFeO_3$ nanoparticles (NPs) reduces the band gap and electrical resistivity of $BiFeO_3$.[70] The band gap of BiOCl was narrowed when $Bi^{3+}$ was partially substituted by $Sn^{2+}$, and this process consequently endowed BiOCl with increased photocatalytic activity for degrading RhB.[71] When O in $BiVO_4$ was partially substituted by F through a solid–vapor reaction, the photoelectrochemical water oxidation on $BiVO_4$ was strongly promoted.[72] This effect may be attributed to the more negative flat band potential (an upshift of approximately 0.1 V) and increased carrier density resulting from the doping of F. The moderate upshift of the flat band potential makes the consumption of electrons easier, which is favorable to the holes in the VB for oxidation reactions. $Bi_3FeMo_2O_{12}$ was found to be superior to $Bi_3GaMo_2O_{12}$ in the photocatalytic degradation of RhB under visible-light irradiation. This result was due to the narrower band gap of $Bi_3FeMo_2O_{12}$ (2.3 eV) than that of $Bi_3GaMo_2O_{12}$ (2.95 eV) as a result of the contribution of Fe 3d orbitals to the CB.[73] Nevertheless, not all elemental substitutions lead to a reduced band gap in bismuthal compounds. If Bi and Fe in $BiFeO_3$ NPs are cosubstituted with Ca and Ti using a sol–gel method, the band gap will increase upon an increase in the amount of Ca and Ti.[74]

Elemental substitution can also improve the separation of carriers and thus boost the performance of photocatalysts. Gu *et al.*[75] obtained Ce-doped $BiVO_4$ by substituting $Bi^{3+}$ with Ce ions in a homogeneous precipitation synthesis. The introduction of Ce enhanced the photocatalytic performance of MB and phenol removal by effectively hindering the recombination of photo-generated carriers. $BiV_{0.8}Mo_{0.2}O_4$ exhibited an improved photoelectrochemical activity in water oxidation because of the more efficient charge transport and electron–hole separation derived from the formation of cation vacancies ($Bi^{5+}$)/oxygen interstitials as a result of high Mo doping.[76]

## Solid solution

Fabricating solid solutions is an effective technique to adjust the band structure of photocatalysts by hybridizing two or more crystalline phases at the atomic scale. A solid solution can be regarded as a special doped semiconductor, in which the anions or cations of the host semiconductor are selectively replaced by introduced ones over the whole range of the composition.[77] By adjusting the concentration of cation and/or anion substitution (by controlling the components and composition), the band structure of a solid solution can be tuned.[78,79] Although the aforementioned doping methods can enhance the performance of bismuthal photocatalysts to some extent, the shortcomings of doping are obvious. The formed doping levels are generally discrete (Fig. 3), and the dopant may also act as the recombination center of carriers and increase the number of recombination sites for electrons and holes.[78,79] Contrary to doping, solid solutions contain no discrete energy levels. The band structures of solid solutions are uniform, and their band gaps usually fall in the region between those of original semiconductors (Fig. 6). Consequently, the electron excitation can be improved with a lower increase in carrier recombination.

Bismuth oxyhalide solid solutions are the most frequently studied among Bi-based solid solutions because of the similar structures of BiOX (X = Cl, Br, I) and easy fabrication of solid solutions comprising these compounds. Hence, several studies have also considered BiOX as a kind of heterooxyhalide-substituted bismuth oxyhalide.[80] Furthermore, along with the ratio of oxyhalides, the absorption edges of bismuth oxyhalide solid solutions usually vary gradually between the absorption edges of the pristine compounds (Fig. 7).[81] This phenomenon renders the tailoring of the band structure as highly convenient. For example, hierarchical Bi-rich $Bi_4O_5Br_xI_{2-x}$ solid-solution nanosheets can be prepared *via* a precursor method and show improved photocatalytic activity for $CO_2$ conversion and Cr(VI) removal.[82] Flower-like $BiOCl_{0.5}Br_{0.5}$ hierarchical solid solutions can be fabricated through reacting $Bi_2O_3$ with a mixed solution of KCl and KBr at room temperature in the presence of glacial acetic acid and exhibit enhanced photocatalytic activity for RhB degradation under visible-light irradiation, compared to pure BiOCl and BiOBr.[83] Similarly, 3D flower-like $BiOCl_xBr_{1-x}$,[84] $BiOCl_xI_y$,[85] and $BiOCl_{1-x}Br_x$ hierarchical microspheres[86] have also been prepared by simple one-pot methods and have exhibited better activities than pure BiOCl, BiOBr, and BiOI. When the three latter halogens were introduced during fabrication, ternary solid solutions $BiOCl_xBr_yI_z$ ($x + y + z = 1$) could be obtained, and the as-prepared solid solutions generally possessed a controllable band gap and highly enhanced visible-light photocatalytic activity.[87] F-Containing bismuth oxyhalide solid solutions are less reported in solid-solution preparations because of the partial miscibility of $BiOF_{1-x}Y_x$, as proposed by Zhao *et al.*[88] They examined the properties of $BiOX_{1-x}Y_x$ (X, Y = F, Cl, Br, I)

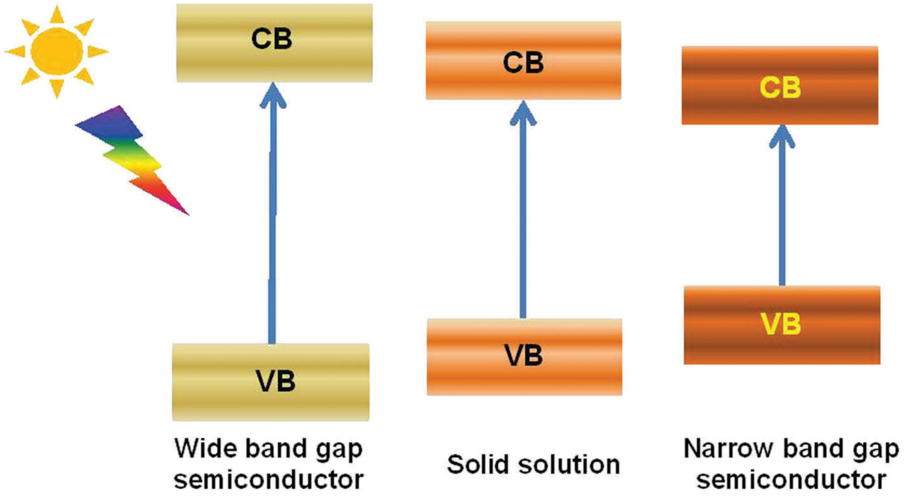

Fig. 6 Schematic diagram of the band structure tuning through solid-solution fabrication.

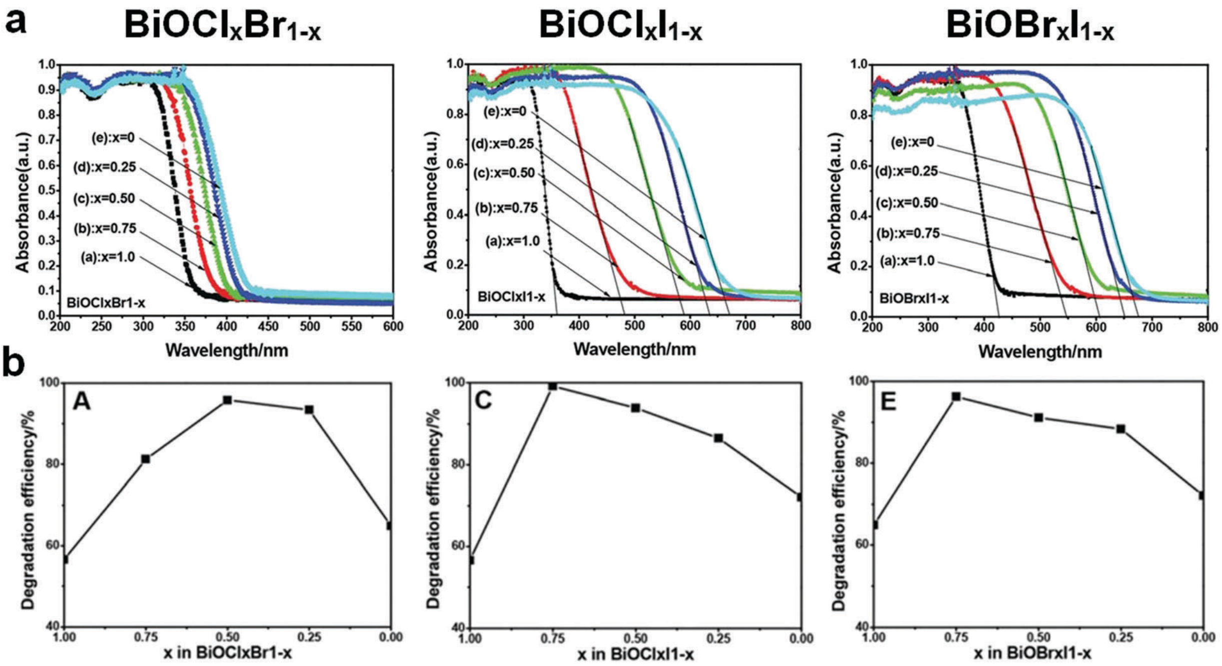

Fig. 7 (a) UV-visible light diffuse reflectance spectra and (b) RhB degradation efficiency of $BiOCl_xBr_{1-x}$, $BiOCl_xI_{1-x}$, and $BiOBr_xI_{1-x}$ solid solutions. Reproduced with permission from ref. 81. Copyright 2013 Royal Society of Chemistry.

solid solutions through density functional theory calculations. The results showed that several properties of $BiOCl_{1-x}Br_x$, $BiOBr_{1-x}I_x$, and $BiOCl_{1-x}I_x$ solid solutions changed almost linearly with $x$, while the properties of $BiOF_{1-x}Y_x$ (Y = Cl, Br, I) solid solutions are partially miscible. In addition, the related calculated data were difficult to fit. Therefore, this behavior has been attributed to the partial miscibility of $BiOF_{1-x}Y_x$.

In addition to bismuth oxyhalides, other Bi-containing solid solutions were found to be more efficient than pure bismuthal compounds for visible-light-driven photocatalysis. For instance, Terebilenko *et al.*[89] fabricated $Bi_{1-x/3}V_{1-x}Mo_xO_4$ solid solutions for photocatalytic water oxidation. The resulting solid solutions possessed the same band gap of 2.25 eV (narrower than that of $BiVO_4$), which endowed such solid solutions with high visible-light absorption. A $Sr_{0.9}Bi_{0.1}Ti_{0.9}Fe_{0.1}O_3$ solid solution synthesized by Lu *et al.*[90] performed more effectively than $SrTiO_3$ in $H_2$ production under full-range irradiation ($\lambda \geq 250$ nm). This finding was attributed to the suitable band gap of the former compound. The resulting band gap can be tuned by adjusting the ratio of Bi to Sr (see Fig. 8).

### Stoichiometry alteration

The layered structures of bismuthal compounds render the component adjustment convenient. Even without introducing a foreign element, the band structures can also be tuned by changing the stoichiometry of the bismuthal semiconductor.

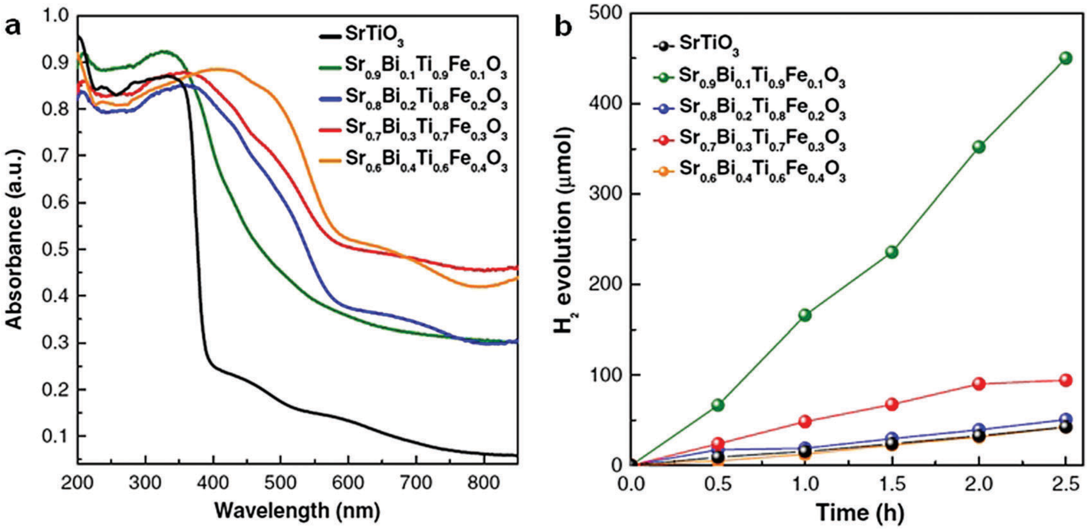

Fig. 8 (a) UV-visible diffuse reflectance spectra and (b) photocatalytic $H_2$ production of $Sr_{0.9}Bi_{0.1}Ti_{0.9}Fe_{0.1}O_3$ solid solutions under full-range irradiation ($\lambda \geq 250$ nm). Reproduced with permission from ref. 90. Copyright 2017 Elsevier.

In this field, similar to solid solutions, bismuth oxyhalides have been extensively studied because the band gap, VB, and CB of oxygen-rich (bismuth-rich) or oxygen-deficient compounds usually changes gradually along with the atomic ratio. Consequently, the compounds can be enhanced by stoichiometric variation. In a bismuth oxyhalide, both the O 2p and X *n*p (*n* = 3, 4, and 5 for X = Cl, Br, and I, respectively) states have a major contribution to the VB, while the Bi 6p states dominate the CB. When the O content increases, the O 2p states of bismuth oxyiodide become more significant than the X *n*p state in the VB, therefore the band gap energies of O-rich bismuth oxyiodides are closer to those of $Bi_2O_3$.[91] That is, the VB can be tuned by changing the O/X ratio.

The band gap of BiOI is very narrow, but its CB is less negative, and its VB is less positive. These characteristics result in the low reduction and oxidation capacities of BiOI. Consequently, the CB upshift and VB downshift become more favorable, but excessive shift in the CB and VB may result in a wide band gap, which is unfavorable for photocatalysis. That is, a moderate upshift of CB and downshift of VB are required. Generally, the VB of bismuth oxyiodides downshifts to a more positive level because of the increased contribution of the O 2p states, while the CB upshifts to a more negative position owing to the additional contribution of I 5p, thus the band gap of the bismuth oxyiodides increases with an increase in the bismuth and oxygen content. Hence, bismuth oxyiodides with moderate overdoses of bismuth and oxygen, such as $Bi_4O_5I_2$ or $Bi_6O_9I_3$, are more advisable. For instance, $Bi_4O_5I_2$ nanosheets (fabricated using a solvothermal method) exhibited a higher activity than BiOI in the photocatalytic degradation of RhB because of the more positive VB of the former.[92] For BiOCl, narrowing the wide band gap is the primary aim of the atomic ratio adjustment. Oxygen-rich bismuth oxychlorides, such as $Bi_{24}O_{31}Cl_{10}$ ($E_g$ = 2.71 eV, ref. 93) and $Bi_{12}O_{17}Cl_2$ ($E_g$ = 2.57 eV, ref. 94), possess narrower band gaps and can be excited by visible light. Therefore, the visible-light photocatalytic performances of these bismuth oxychlorides are better than that of BiOCl. Moreover, Cl-rich bismuth oxychloride was also found to possess a narrower band gap. For instance, the band gap of $Bi_{12}O_{15}Cl_6$ nanosheets fabricated by Wang *et al.*[95] was estimated to be 2.36 eV, and the photocatalytic performance of $Bi_{12}O_{15}Cl_6$ nanosheets for bisphenol A (BPA) removal was superior to that of BiOCl nanosheets. Studies on oxygen-rich bismuth oxybromides have mainly focused on $Bi_4O_5Br_2$ because of its narrow band gap. In reports by Xia and co-workers,[96] $Bi_4O_5Br_2$ nanosheets fabricated using a solvothermal method were shown to possess a narrower band gap (2.37 eV) and lower carrier transfer resistance than those of BiOBr (2.82 eV) and were more effective than BiOBr in the photocatalytic degradation of BPA. For similar reasons, $Bi_4O_5Br_2$ showed much higher activity than BiOBr in the photocatalytic degradation of resorcinol[97] and ciprofloxacin (CIP)[98] under visible light. Furthermore, $Bi_4O_5Br_2$ nanosheets were also discovered to be more suitable than BiOBr nanosheets in the photoreduction of $CO_2$.[99] These results are due to the CB position of $Bi_4O_5Br_2$ being higher than that of BiOBr and thus more favorable for the reduction reaction of $CO_2$.

The band structures of other Bi compounds, such as $BiVO_4$, $Bi_2SiO_5$, and $Bi_2O_3$, can also be altered by varying the stoichiometry for activity enhancement. Batool *et al.*[100] found that $Bi_4(SiO_4)_3$ nanofibers possess lower impedance and exhibit higher photocatalytic performance than $Bi_2SiO_5$ nanofibers in the degradation of MO. Huang and co-workers[101] prepared $Bi_4V_2O_{11}$ through a solvothermal method. The synthesized $Bi_4V_2O_{11}$ had a narrower band gap (2.15 eV) than that of $BiVO_4$ (2.4 eV) and showed high water oxidation activity under 300 W Xe lamp irradiation. In Kalyan's research, a $BiO_{2-x}$ phase with a narrow band gap (1.84 eV) formed on the surface of a $Bi_2O_3$ photoanode during photoelectrochemical testing in the presence of KOH and $H_2O_2$.[102] The formed $BiO_{2-x}$ phase improved the photocurrent because of its narrow band gap.

## Morphology control

The photocatalytic properties of semiconductors are highly dependent on their morphologies and sizes.[103] High specific surface area, low thickness, and hierarchical and hollow structures can increase light absorption and accessibility of photocatalysts. Such properties enable the accelerated migration of carriers to the surface and reduce the dosage of photocatalysts. Accordingly, the performance of Bi-based photocatalysts can be enhanced by building ultrathin and hierarchical and hollow structures or by immobilization on substrates with specific morphologies.

### Thin morphologies

Thickness greatly affects the activities of bismuthal compounds because of the influence of such a variable on the efficiency of light absorption and the distance of the photo-generated carriers from the surfaces. A smaller sized bismuthal compound usually leads to a higher specific surface area and better photocatalytic and photoelectrochemical performance.[104,105] Considering unique layered plate-like structures, the exposed-facet ratio of bismuthal compounds usually changes along with the thickness of the compounds. Therefore, the thickness effect has often been discussed in related reports. Thinner structures can endow bismuthal compounds with a higher specific surface area, increased light absorption efficiency, and enabled utilization of photogenerated electrons and holes. Ultimately, such properties may enhance photocatalytic activity. With a decrease in the thickness, the surface energy of the nanoplates would also largely increase, single plates become thermodynamically unstable and these nanoplates prefer to stack together into one larger particle to reduce surface energy during growth. As a result, many Bi-based photocatalysts usually possess a granular appearance comprising nanoplates. The thin morphology discussed in this section refers to these nanoplates.

Chen and colleagues[106] found that reducing the thickness of BiOBr nanosheets can significantly increase the exposed (001) facets and the photocatalytic activity of the BiOBr nanosheets. The enhanced photocatalytic activity of the BiOBr nanosheets was ascribed mainly to the enhanced absorption of visible light and improved separation efficiency of charge carriers due to the ultrathin structure. Li *et al.*[107] proposed that the photoactivity of the BiOBr nanosheets depends on nanosheet thickness. Similarly, reducing the thickness of $Bi_2O_2CO_3$

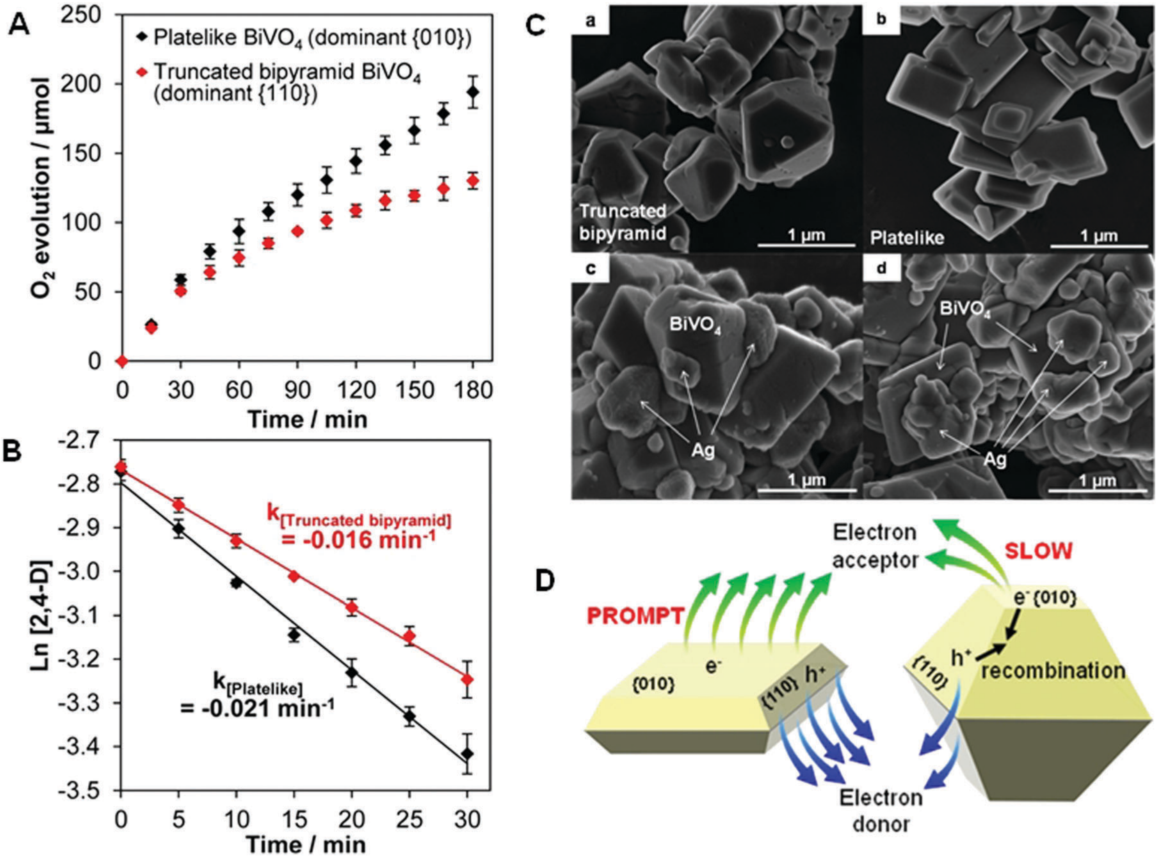

Fig. 9 (A) Photocatalytic $O_2$ evolution from an $AgNO_3$ solution; (B) pseudo-first-order-fitted photocatalytic degradation curves of 2,4-dichlorophenoxyacetic acid (2,4-D) on truncated bipyramid (red) and plate-like (black) $BiVO_4$ under visible light ($\lambda > 420$ nm); SEM images of bare (C-a) truncated bipyramid and (C-b) plate-like $BiVO_4$ and the corresponding Ag-deposited (C-c) truncated bipyramid and (C-d) plate-like $BiVO_4$. (D) Schematic diagram of the promotion induced by increasing the size of the (010) facets in $BiVO_4$. Reproduced with permission from ref. 111. Copyright 2016 American Chemical Society.

[accompanied by an increase in the (001) facets] improved its photocatalytic activity in the degradation of RhB,[108] and the activities of $Bi_2WO_6$ were augmented along with a reduction in thickness.[109]

Thinner structures sometimes result in additional facet and structure differences, which affects the performance of bismuthal photocatalysts. For example, increasing the exposure of (001) facets (accompanied by a reduction in the thickness) can improve the efficiency of RhB degradation on $Bi_2Fe_4O_9$ nanoplates, because a larger exposed (001) surface can provide more $Fe^{3+}$ cations to generate more hydroxyl radicals.[110] A reduction in the thickness can also improve the photocatalytic performance of $BiVO_4$ in $O_2$ evolution, owing to the increased ratio of reduction functional (010) facets *versus* dominating oxidation functional (110) facets (Fig. 9).[111] Hu *et al.*[112] noted that reducing the thickness of $BiTaO_4$ not only increased the specific surface area but also caused upshifts in the VB and CB. Density of states (DOS) calculations showed that the energy levels of the VB and CB of the (010) facets of $BiTaO_4$ are more negative than those of bulk $BiTaO_4$. The (010) facets in $BiTaO_4$ increase along with a reduction in the thickness, therefore, thinner $BiTaO_4$ single-crystal nanoplates possess more {010} facets and higher VB and CB positions.

When the thickness of a bismuthal semiconductor is reduced to below 10 nm, the specific surface area, light absorption, and carrier migration will be further enhanced. Sometimes, new characteristics might also arise. Ultrathin square-like BiOCl nanosheets (3–7 nm in thickness) have been shown to exhibit a higher activity than thicker nanosheets in the photocatalytic degradation of RhB due to a larger specific surface area.[113] Di *et al.*[114] reported the preparation of ultrathin BiOI nanosheets and their composites, which displayed a uniform thickness of approximately 0.9 nm (Fig. 10), approaching the thickness of one [I–Bi–O–Bi–I] unit (0.9149 nm). The CB position of the BiOI nanosheets was determined to be −0.95 eV (NHE), negative to reduce $O_2$ to $^{\bullet}O_2^{-}$. This characteristic is beneficial for $H_2$ generation or $CO_2$ reduction. However, the researchers did not provide results on the reduction application, although their reports on the surface modification of BiOI nanosheets still exhibited improved activity for the photocatalytic degradation of RhB. The ultrathin $H_{1.78}Sr_{0.78}Bi_{0.22}Nb_2O_7$ nanosheets (Fig. 11) prepared by calcination exhibited 5.5 and 26.2 times higher activity than $H_{1.78}Sr_{0.78}Bi_{0.22}Nb_2O_7$ plates and $SrBi_2Nb_2O_9$ platelets for photocatalytic $H_2$ generation, respectively. This result can be ascribed to the higher separation efficiency of the photo-generated carriers and specific surface area.[115]

Preparation of fabric or quantum sized materials is another method for obtaining thin morphologies and high specific surface areas. Bharathkumar *et al.*[116] fabricated $BiFeO_3$ fibers

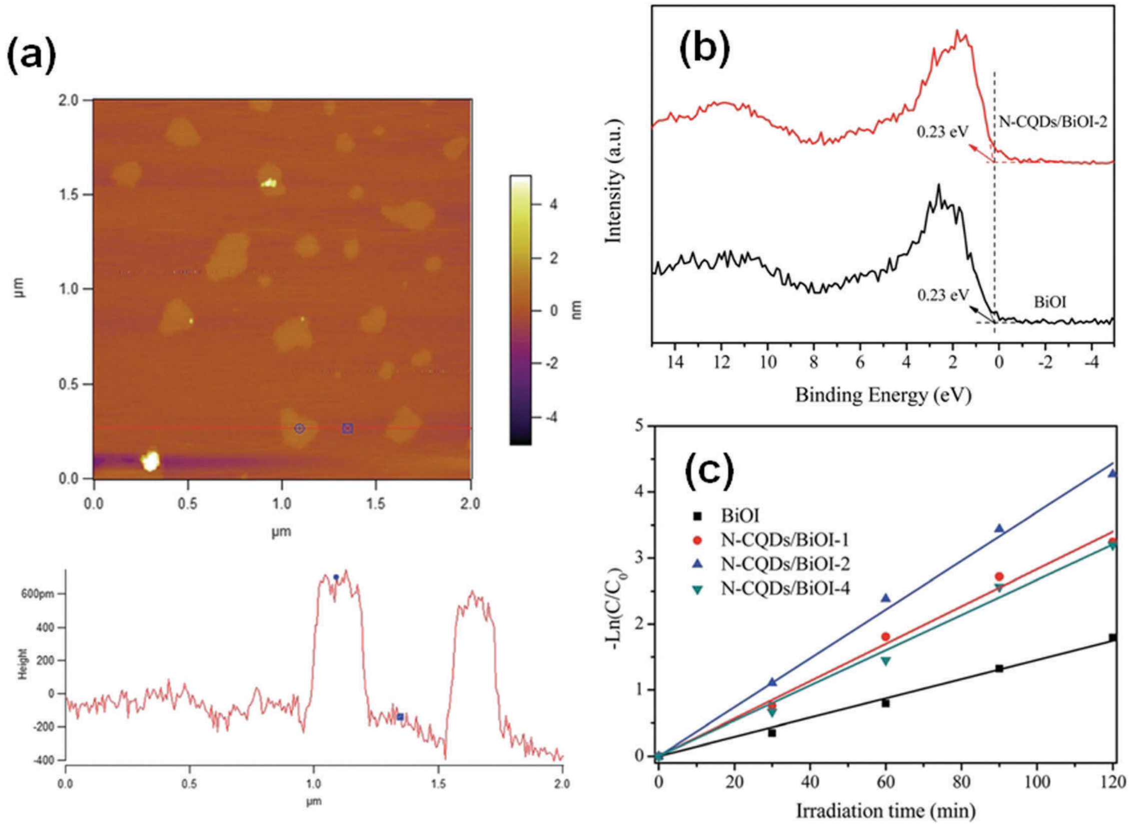

Fig. 10 (a) Atomic force microscopy (AFM) image and corresponding height of the atomically thin BiOI nanosheets; (b) valence-band X-ray photoelectron spectra and (c) pseudo-first-order-fitted kinetic curves (for the RhB degradation) of pure BiOI and N-carbon quantum dot (CQD) decorated BiOI. Reproduced with permission from ref. 114. Copyright 2016 Royal Society of Chemistry.

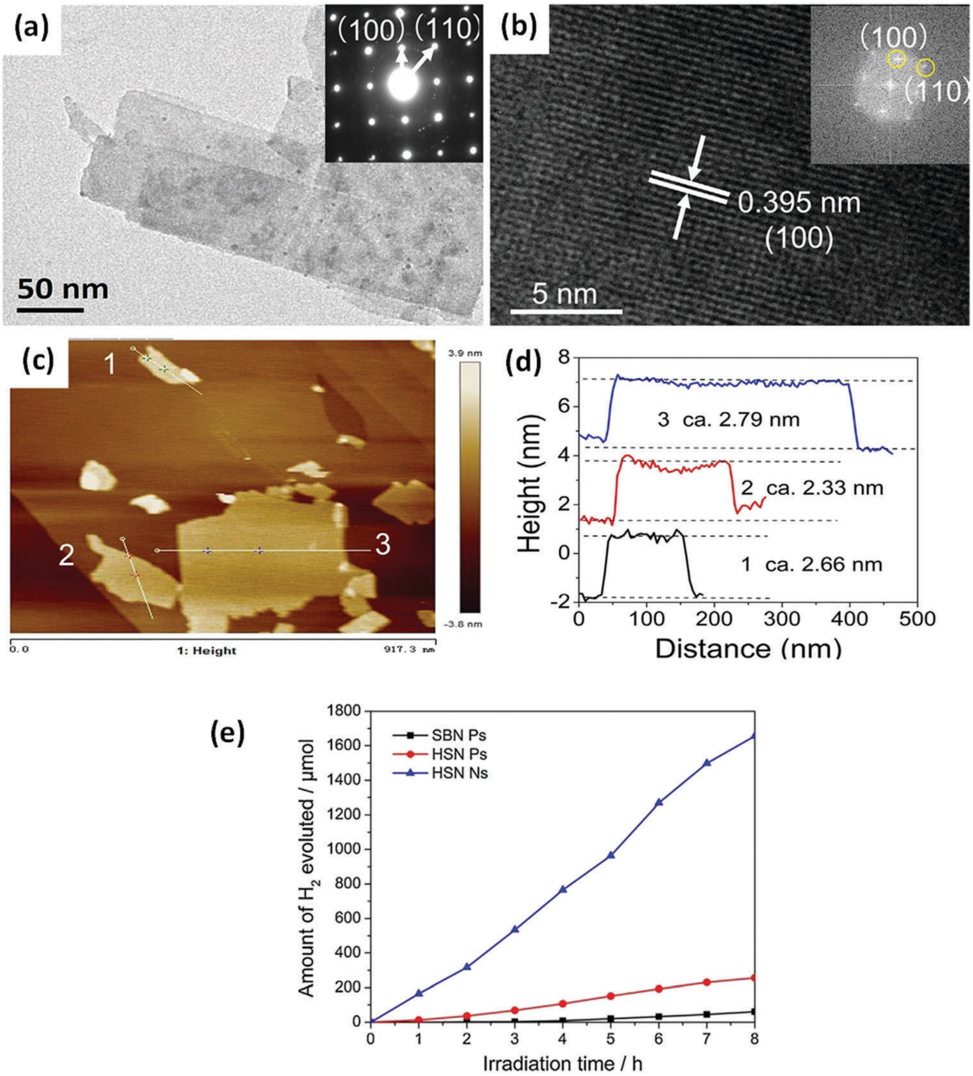

Fig. 11 (a) Transmission electron microscopy (TEM) and (b) high-resolution TEM (HRTEM) images of $H_{1.78}Sr_{0.78}Bi_{0.22}Nb_2O_7$ nanosheets (HSN Ns); (c) AFM image; (d) corresponding height of the HSN Ns; and (e) the $H_2$ evolution curves of the $SrBi_2Nb_2O_9$ platelets (SBN Ps), $H_{1.78}Sr_{0.78}Bi_{0.22}Nb_2O_7$ platelets (HSN Ps), and HSN Ns. Reproduced with permission from ref. 115. Copyright 2017 Elsevier.

using an electrospinning method. The obtained $BiFeO_3$ fibers then exhibited improved relative photocatalytic activity compared with that of $BiFeO_3$ particles for degrading RhB, due to their high specific surface area. Zhao and co-workers[117] prepared metal Bi nanofibers using an aqueous reduction procedure and found that Bi nanofibers exhibited a higher photocatalytic activity than Bi nanoplates and NPs in degrading RhB. Yang *et al.*[118] fabricated bismuth oxide formate (HCOOBiO) nanowires (Fig. 12) with a diameter of 20 nm and a length of up to several hundreds of micrometers in *N*,*N*-dimethylformamide (DMF) solution *via* a solvothermal route. These HCOOBiO nanowires showed a higher activity than HCOOBiO microspheres in the photocatalytic degradation of MO. In the studies of Lu and colleagues,[119] $BiVO_4$ nanofibers were prepared using an electrospinning and calcination method and showed a higher efficiency than $BiVO_4$ rods in the photocatalytic removal of MB under visible-light irradiation. Additionally, $Bi_2S_3$ with a high length-to-width ratio was found to be highly effective in the photocatalytic reduction of $CO_2$ to $CH_3OH$.[120] The high length-to-width ratio not only increases the specific surface area but also enlarges the band gap (by a down-shift of the VB and an upshift of the CB) owing to the increased influence of the surface state resulting from the smaller size. And as it happens, the CB is upshifted to a level sufficient enough for $CO_2$ reduction. Bismuth monoxide quantum dots (QDs) obtained using a hydrothermal method exhibited high efficiency in the photocatalytic reduction of $N_2$.[121] The ammonia production rate reached 1226 μmol $g^{-1}$ $h^{-1}$ in the absence of a sacrificial agent and a cocatalyst. As $Bi_5O_7Br$ was tailored into nanotubes with a diameter of 5 nm, its CB (−1.14 eV) was more negative than that of BiOBr. Though such a CB is still not thermodynamically accessible for direct free $N_2$ fixation, $N_2$ fixation was achieved because the formed oxygen vacancy in samples injects trapped photogenerated electrons directly into the chemically adsorbed $N_2$ and weakens the $N{\equiv}N$ triple bond.[122]

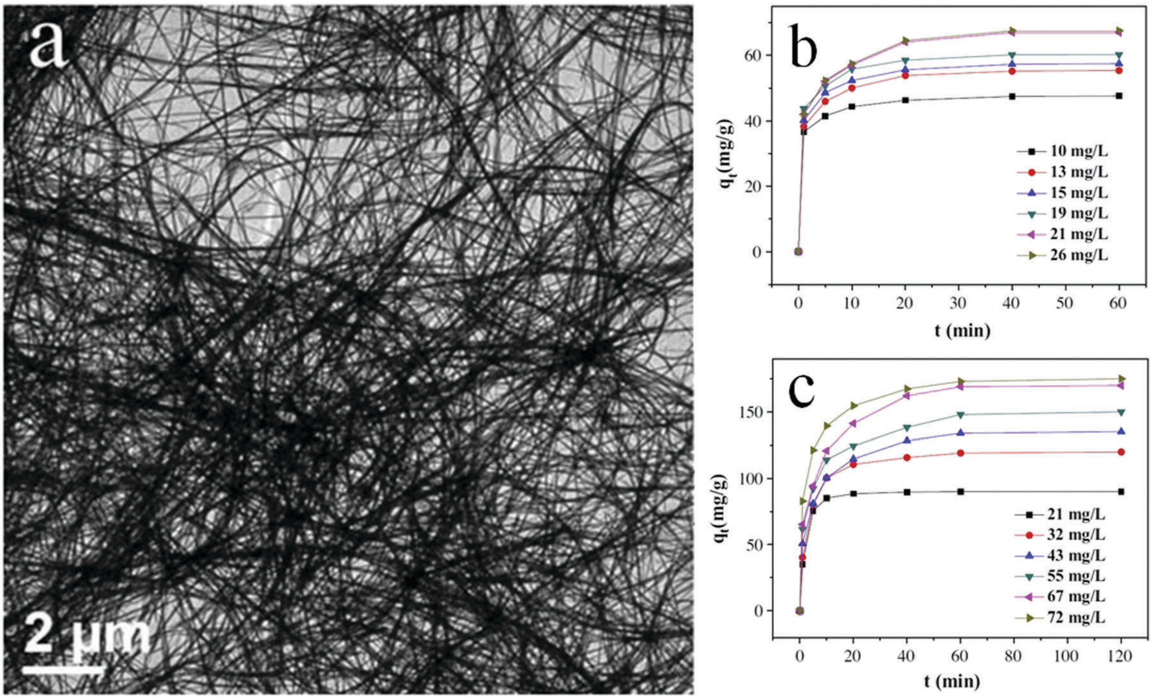

Fig. 12 Scanning electron microscopy (SEM) images (a) of ultra-long HCOOBiO nanowires. Removal of (b) MO and (c) Cr(VI) at various initial concentrations from ultra-long HCOOBiO nanowires. Reproduced with permission from ref. 118. Copyright 2015 Elsevier.

## Hierarchical structures

Photocatalysts with hierarchical structures usually exhibit better performances than bulk photocatalysts. Such superiority is due to the high specific surface area, efficient light harvesting, accessibility, and easy transport of the reactants of the former catalysts. Yang *et al.*[123] accomplished the early work on hierarchical ordered oxides. Since then, the design and synthesis of hierarchical-structured nanomaterials have attracted significant attention.[124–126]

Specific surface area is one of the most important factors that results in the higher activity of bismuthal compounds. Generally, photocatalysts with a hierarchical structure possess relative higher specific surface areas than bulk photocatalysts or individual rods and plates, and work better in photocatalytic reactions. For example, grain-like $Bi_{24}O_{31}Br_{10}$ hierarchical architectures (Fig. 13) fabricated using a solvothermal method in the presence of starch also showed improved photocatalytic activity in the degradation of RhB.[127] Qin and co-workers[128] prepared $BiYO_3$ with a high specific surface area using a hydrothermal method with soft templates. The $BiYO_3$ prepared using disodium ethylenediaminetetraacetate (EDTA) as a template possessed the highest specific surface area and photocatalytic activity for reducing $CO_2$. Jia *et al.*[129] found that hierarchical $Bi_2S_3$ produced using a hydrothermal method [with cetyltrimethylammonium bromide (CTAB) as a surfactant] exhibited higher photocatalytic activity than $Bi_2S_3$ nanorods in the degradation of RhB. This performance was ascribed to the synergetic effect of the shape, surface area, band gap, crystallinity, and size resulting from the 3D hierarchical structure. Han's group[130] fabricated flower-like $\delta$-$Bi_2O_3$ by thermally treating bismuthyl acetate $CH_3COO(BiO)$, which was prepared from $Bi_2O_3$ and glacial acetic acid (HAc) or $Bi(NO_3)_3{\cdot}5H_2O$ and HAc. The obtained $\delta$-$Bi_2O_3$ showed superior activity over that of $\delta$-$Bi_2O_3$ sheets in the photocatalytic degradation of RhB. Zhou *et al.*[131] prepared uniform cylindrical $BiFeO_3$ samples by adjusting the ratio of $HNO_3$ : NaOH to 8 : 12 in the hydrothermal process. The uniform cylindrical $BiFeO_3$ exhibited enhanced photocatalytic activities for removing RhB under visible-light irradiation, because the uniform structures favored charge transport and increased the accessibility to organic matter. Li *et al.*[132] prepared BiOBr strips accumulated from tiny pieces using a solvothermal method with bismuth subsalicylate as a template. They found that the BiOBr strips showed an enhanced performance for the photocatalytic degradation of RhB. Furthermore, the hierarchical structure of bismuthal oxyiodide obviously promoted the performance of the compound in phenol removal.[133]

Even in the construction of a hierarchical structure, the morphologies of bismuthal photocatalysts can be further tuned to different forms by adjusting the solvent, pH, and surfactants, as well as by adding capping agents. For instance, Wang *et al.*[134] synthesized 3D hierarchical flower-like $\alpha$-$Bi_2O_3$ microspheres with various morphologies (Fig. 14) in an ethanol–water mixture. They heated the mixture in an oil bath at 95 °C, and the morphology was controlled by adjusting the amount of added glycerol and oleic acid (capping agents). Sarka *et al.*[135] fabricated $Bi_2S_3$ in different shapes (Fig. 15) using a solvothermal method with various solvents. The performance of $Bi_2S_3$ nanocrystals in removing MB was better than those of the $Bi_2S_3$ nanorods and nanoplates due to the higher specific surface

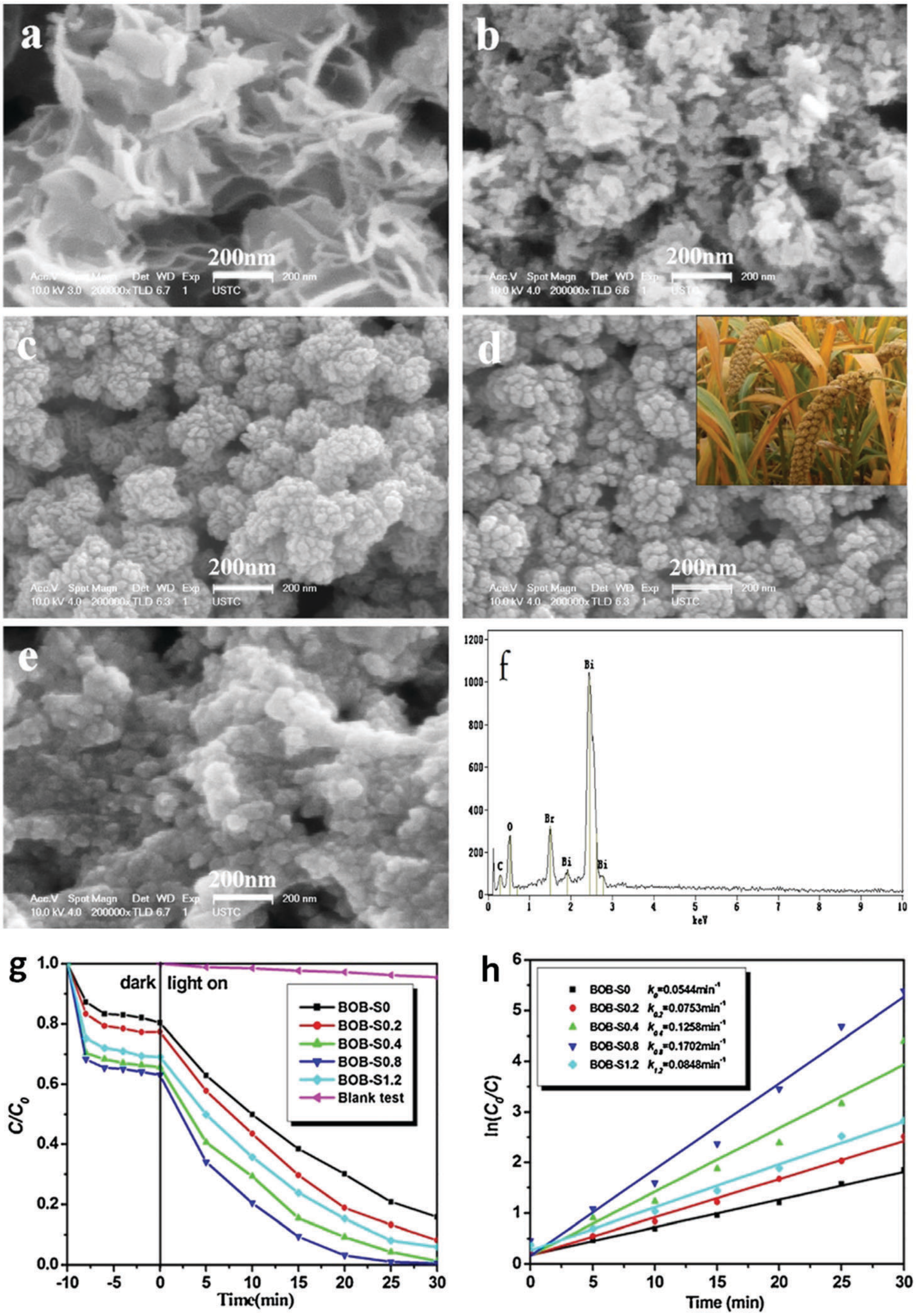

Fig. 13 SEM images of $Bi_{24}O_{31}Br_{10}$ hierarchical architectures (BOB) (a) BOB-S0, (b) BOB-S0.2, (c) BOB-S0.4, (d) BOB-S0.8 (grain-like), and (e) BOB-S1.2 (*e.g.*, -S1.2 indicates that the mass of starch used was 1.2 g); (f) EDS pattern of BOB-S0.8; (g) photocatalytic degradation curves of RhB; and (h) pseudo-first-order-fitted kinetic curves over $Bi_{24}O_{31}Br_{10}$ samples under visible-light irradiation. Reproduced with permission from ref. 127. Copyright 2016 Elsevier.

area and suitable band structure of the $Bi_2S_3$ nanocrystals. Zhao *et al.*[136] altered the morphologies of $BiVO_4$ from olive-shaped to primrose-like, leaf-shaped, or strip-like morphologies (Fig. 16), by adjusting the concentration of glycerol in the aqueous solution during template-free solvothermal synthesis. In addition to solvent control, the morphologies of $BiVO_4$ can also be modified by pH adjustment. Besides this, the hierarchical morphology alteration of $BiVO_4$ can also be achieved through adjusting the pH.[137] The relationship between pH and the morphologies of $BiVO_4$ is illustrated in Fig. 17. If $NaHCO_3$ is added in the solid-state synthesis of $BiVO_4$, the morphology can be turned from polyhedral to a rice-like shape, by increasing the nucleation rate and hindering the continual growth of the original product particles.[138] In the preparation of $Bi_2WO_6$, its morphology can be tuned from accumulated sheets to a complex morphology by adjusting the molecular weight of the

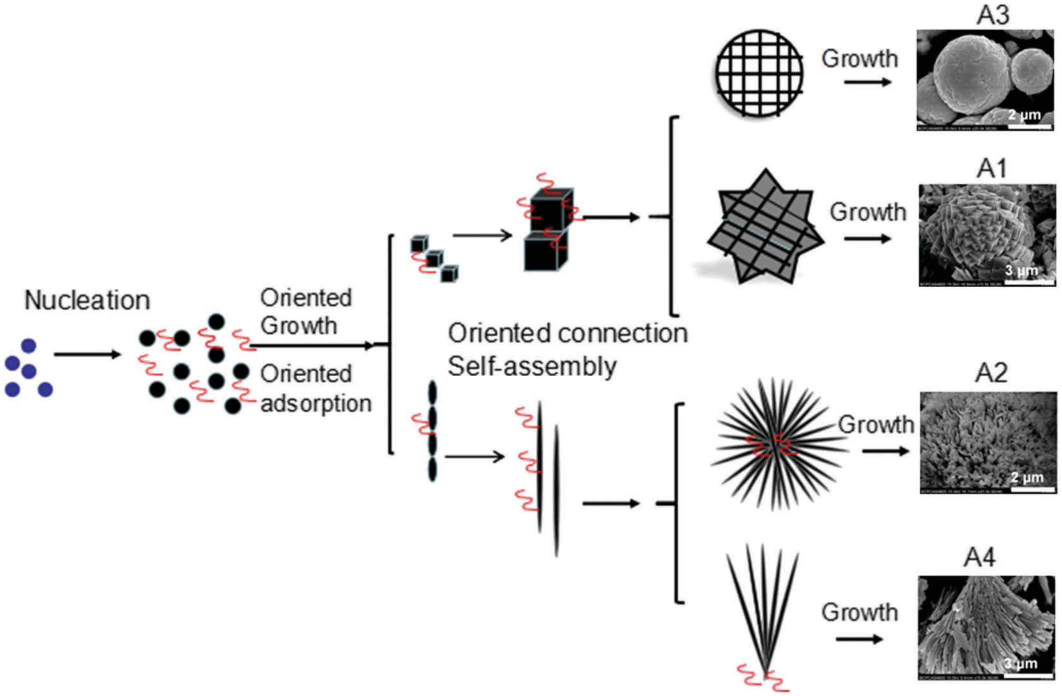

Fig. 14 3D hierarchical flower-like α-$Bi_2O_3$ microspheres fabricated using different solvents: A1 (0.5 mL of glycerol), A2 (1 mL of glycerol), A3 (1 mL of glycerol and 1 mL of oleic acid), and A4 (1 mL of glycerol and 2 mL of oleic acid). Reproduced with permission from ref. 134. Open Access 2016 World Scientific.

added polyvinylpyrrolidone (PVP).[139] Examples of such complex morphology include flower-like, red blood cell-like, and square pillar-like morphologies. $Bi_2WO_6$ with a thin sheet-like appearance showed the best photocatalytic performance in the decomposition of RhB under visible-light irradiation.

### Hollow and porous structures

The hierarchical structure of Bi compounds can be transformed to a hollow structure, which is more preferable for improving the photocatalytic performance, using a suitable method. For instance, Qian *et al.*[140] fabricated mesoporous $Bi_4Ti_3O_{12}$ by calcinating a mixture of $Bi(NO_3)_3$ and tetrabutyl titanate. The product had a markedly higher specific surface area (109.4 $m^2\ g^{-1}$) and exhibited a better performance than that of the bulk compound. Gong and co-workers[141] prepared porous $BiVO_4$ by electrospinning and calcination in the presence of PVP. The obtained porous $BiVO_4$ had a larger specific surface area and enhanced photocatalytic activity for the degradation of MB. Kashfi-Sadabad *et al.*[142] synthesized Sm-doped $Bi_2MoO_6$ hollow spheres by developing a solvothermal pathway in the presence of pluronic P123 copolymer. During the synthesis, no spherical structures formed in the absence of P123 (Fig. 18b). At a low dosage of P123, the products became solid spheres without hollow structures (Fig. 18c). Hollow spheres formed gradually and became enlarged upon further P123 addition. Finally, $Bi_2MoO_6$ hollow spheres with diameters of 1–1.5 μm and a thickness of approximately 100 nm (Fig. 18d) were obtained when the P123 amount reached 3 g. The formation of these spheres is illustrated in Fig. 18a. Hollow spherical bismuthal photocatalysts can also be fabricated using a solvothermal method in the absence of a template. Zhou and colleagues[143] fabricated hollow $Bi_2WO_6$ microspheres (Fig. 19) using a template-free solvothermal route with a mixed solvent composed of ethylene glycol (EG) and ethanol. The well-defined hollow $Bi_2WO_6$ microspheres exhibited considerably better photocatalytic activity in the degradation of RhB than $Bi_2WO_6$ with other morphologies under visible-light irradiation. Li *et al.*[144] synthesized hollow $Bi_2MoO_6$ spheres using a solvothermal route in a $Bi_2MoO_6$ precursor solution. The obtained yolk shell-like $Bi_2MoO_6$ displayed markedly higher efficiency in removing RhB. Such improvement was attributed to the hollow structure accompanied by enhanced light absorption, increased specific surface area, and augmented charge transfer. If a mixed solution containing glycerol, ethanol, and deionized water was adopted, hollow $Bi_2MoO_6$ was still obtained during the solvothermal synthesis.[145] Multishell hollow structures are more attractive than other structural types because of their higher surface area and unique nested structure, which ensure highly efficient light utilization. Zong *et al.*[146] achieved Bi–V–O heterostructured multishell hollow spheres (composed of interconnected $BiVO_4$ and $Bi_4V_2O_{11}$) (Fig. 20) using NaOH-treated carbonaceous microsphere templates and a suitable heating rate. The double-shell Bi–V–O hollow spheres were more effective than their single-shell counterparts in removing MB under visible-light irradiation because of the multiple light reflections and effective light utilization achieved through the multishell hollow structure.

Hollow structures are not restricted to hollow spheres. Hollow tubes and cross-linked net-like structures are also favorable

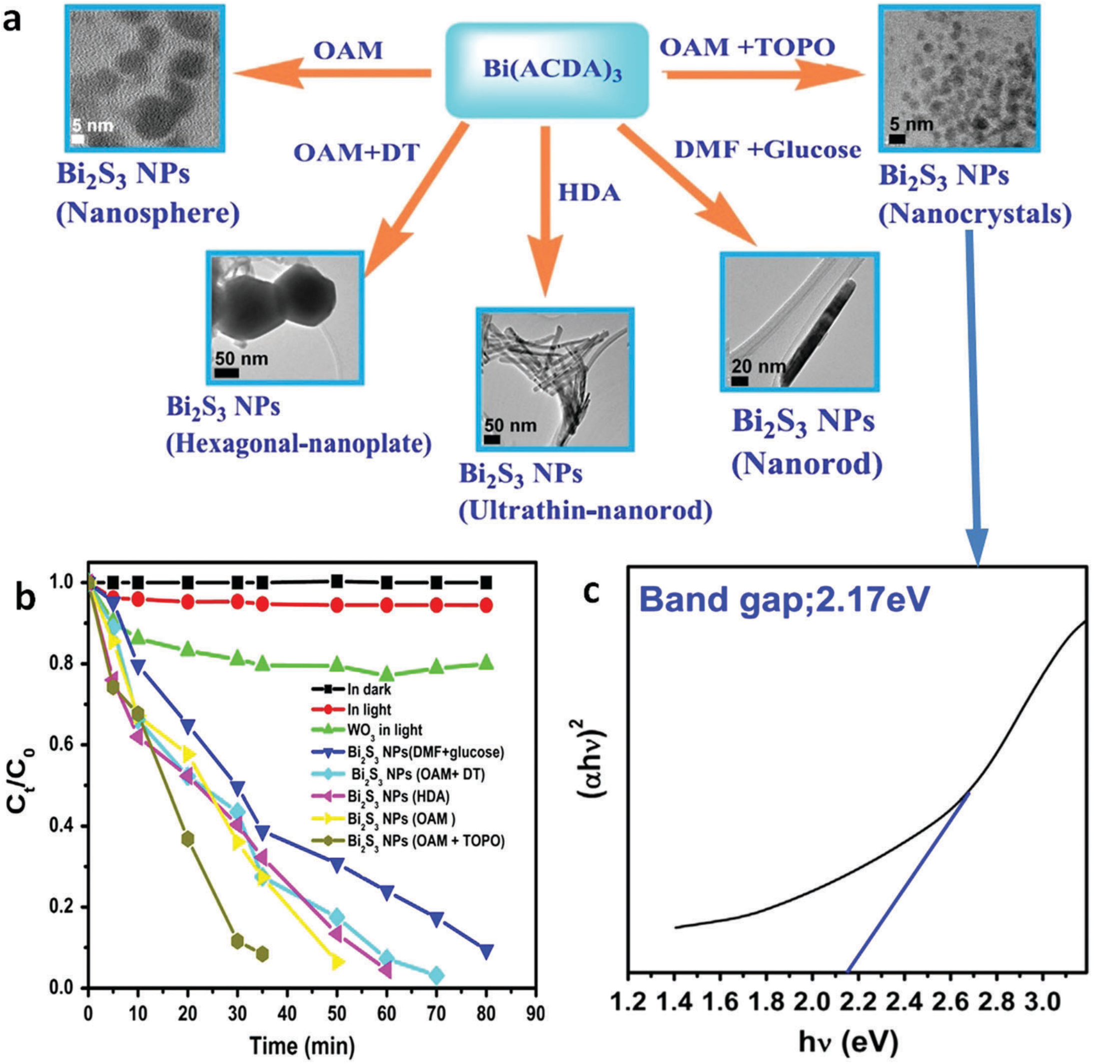

Fig. 15 (a) Synthesis pathways of $Bi_2S_3$ NPs with tuned morphologies from $Bi(ACDA)_3$ (ACDA = 2-aminocyclopentene-1-dithiocarboxylic acid radical) using solvent comprising glucose, oleylamine (OAM), hexadecylamine (HDA), dodecanethiol (DT), trioctylphosphine oxide (TOPO), and dimethylformamide (DMF); (b) photocatalytic degradation curves of MB under visible-light irradiation and (c) the Tauc plot of the $Bi_2S_3$ NPs using a mixed solvent composed of OAM and TOPO. Reproduced with permission from ref. 135. Copyright 2016 Elsevier.

morphologies for bismuthal photocatalysts. These alternative structures can be constructed with assistance from directed surfactant agents or substrates. For example, $Bi_2O_2CO_3$ nanotubes (Fig. 21) can grow on a graphene substrate through hydrolysis by adjusting the pH to 10.5 using urea.[147] In the presence of CTAB (as a morphology director), $BiVO_4$ can grow into nanotubes during hydrothermal synthesis.[148] The formed $BiVO_4$ nanotubes exhibit improved activity relative to that of $BiVO_4$ nanorods in the photocatalytic degradation of MO. When dual templates of polystyrene latex spheres (PS) and P123 are adopted in the preparation of $Bi_2O_3/TiO_2$ composites (sol–gel method), a series of 3D-ordered macroporous profiles are produced (Fig. 22).[149] The composites present a significantly higher activity than P25 and $Bi_2O_3$ in the photocatalytic removal of crystal violet. Such an advantage can be ascribed to the formed porous structure and heterojunction. Lee *et al.*[150] fabricated a type of porous $\beta$-$Bi_2O_3$ from $Bi(NO_3)_3$ using a rapid phase and surface transformation with structure-guided combustion waves. The compound showed a higher photocatalytic performance in the degradation of RhB than those of $\alpha$-$Bi_2O_3$ rods and $Bi(NO_3)_3{\cdot}H_2O$ rods.

### Immobilization

During an application, the undesired aggregation of NPs would seriously affect the performance of Bi-based photocatalysts, so an effective separation method should be employed to reduce the aggregation. The cyclic utilization of Bi-based photocatalysts should also be considered. Immobilization has been considered as an effective means to solve these two issues. Furthermore, with the aid of substrate materials, the profile of bismuthal photocatalysts can be tuned to achieve photocatalytic reactions. Hence, suitable immobilizations have been explored for improving the performance of Bi-based photocatalysts.

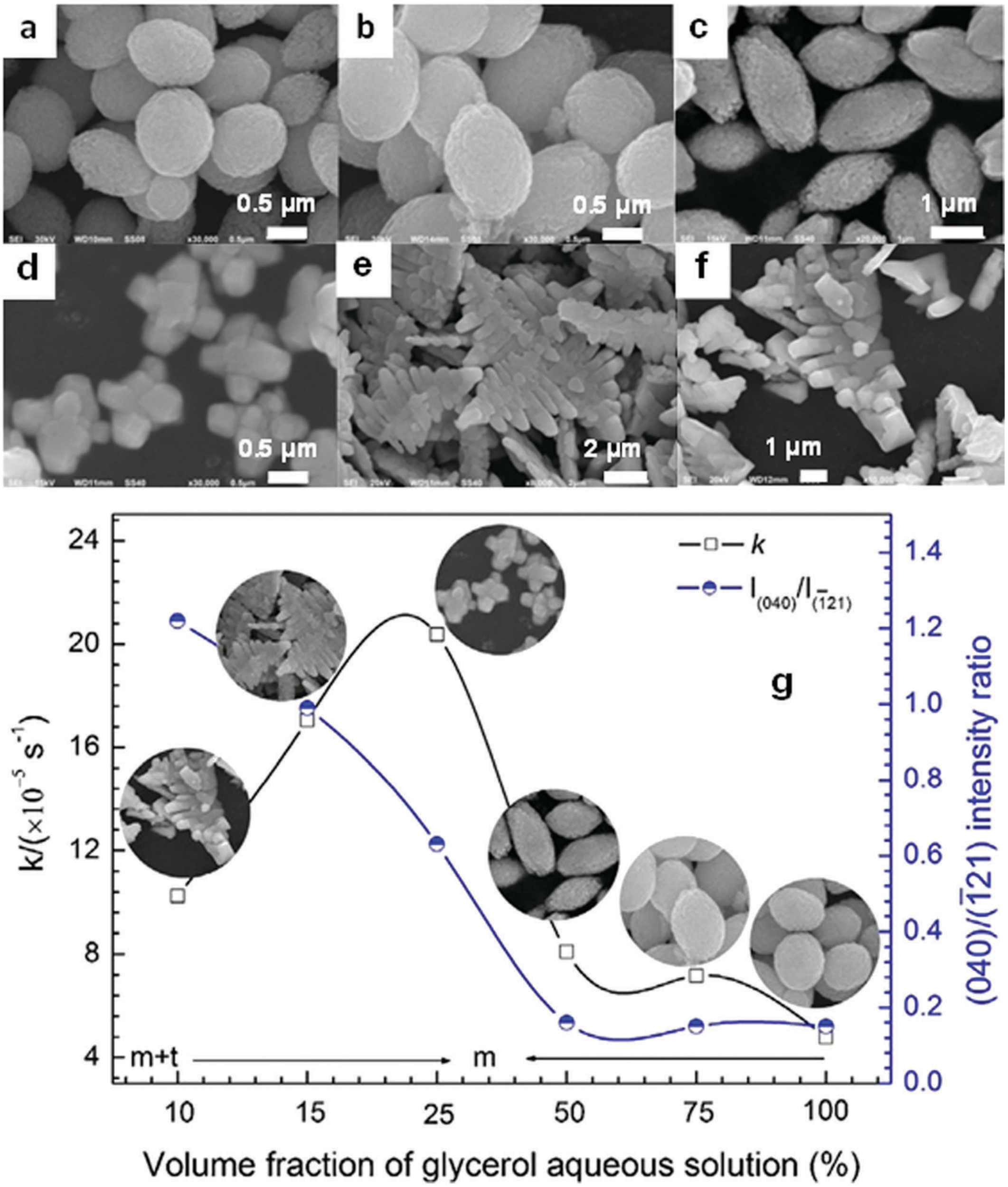

Fig. 16 SEM images of the $BiVO_4$ samples prepared with the following volume fractions of glycerol aqueous solution: (a) 100%, (b) 75%, (c) 50%, (d) 25%, (e) 15%, and (f) 10%; (g) relationship between the glycerol fraction, the (040)/($\bar{1}$21) intensity ratio, the morphology, and the photocatalytic performance of the $BiVO_4$ samples. Reproduced with permission from ref. 136. Copyright 2016 Elsevier.

Immobilization requires the increased dispersion of bismuthal photocatalysts, which increases the availability of photocatalysts and improves the attachment between the photocatalysts and reactants. Wang and co-workers[151] prepared a BiOCl film on a Bi plate using a room-temperature reaction, and the product exhibited a high photocatalytic activity in the degradation of RhB because of the good dispersion of the formed BiOCl nanonuclei. Sonawane and colleagues[152] immobilized $Bi_2O_3$ on bentonite using an intercalation method. The obtained $Bi_2O_3$/bentonite composite exhibited improved performance relative to the separate use of $Bi_2O_3$ and bentonite in the photocatalytic degradation of RhB because of the increased adsorption capacity brought about by the use of bentonite. Similarly, Wang *et al.*[153] immobilized phosphotungstic acid-modified BiOBr on the surface of a zeolite. This process endowed the composites with enhanced photocatalytic activity for the degradation of MO. Li *et al.*[154] immobilized BiOI on diatomite and obtained composites with improved photocatalytic performance in the degradation of RhB. Tong and co-workers[155] used nickel foam as a substrate to immobilize a $Bi_2WO_6/TiO_2$ composite and increase the efficiency of $Bi_2WO_6/TiO_2$ in the photocatalytic degradation of RhB. Shi *et al.*[156] found that the performance of $BiVO_4$ in the photocatalytic removal of tetracycline hydrochloride could be enhanced when supported

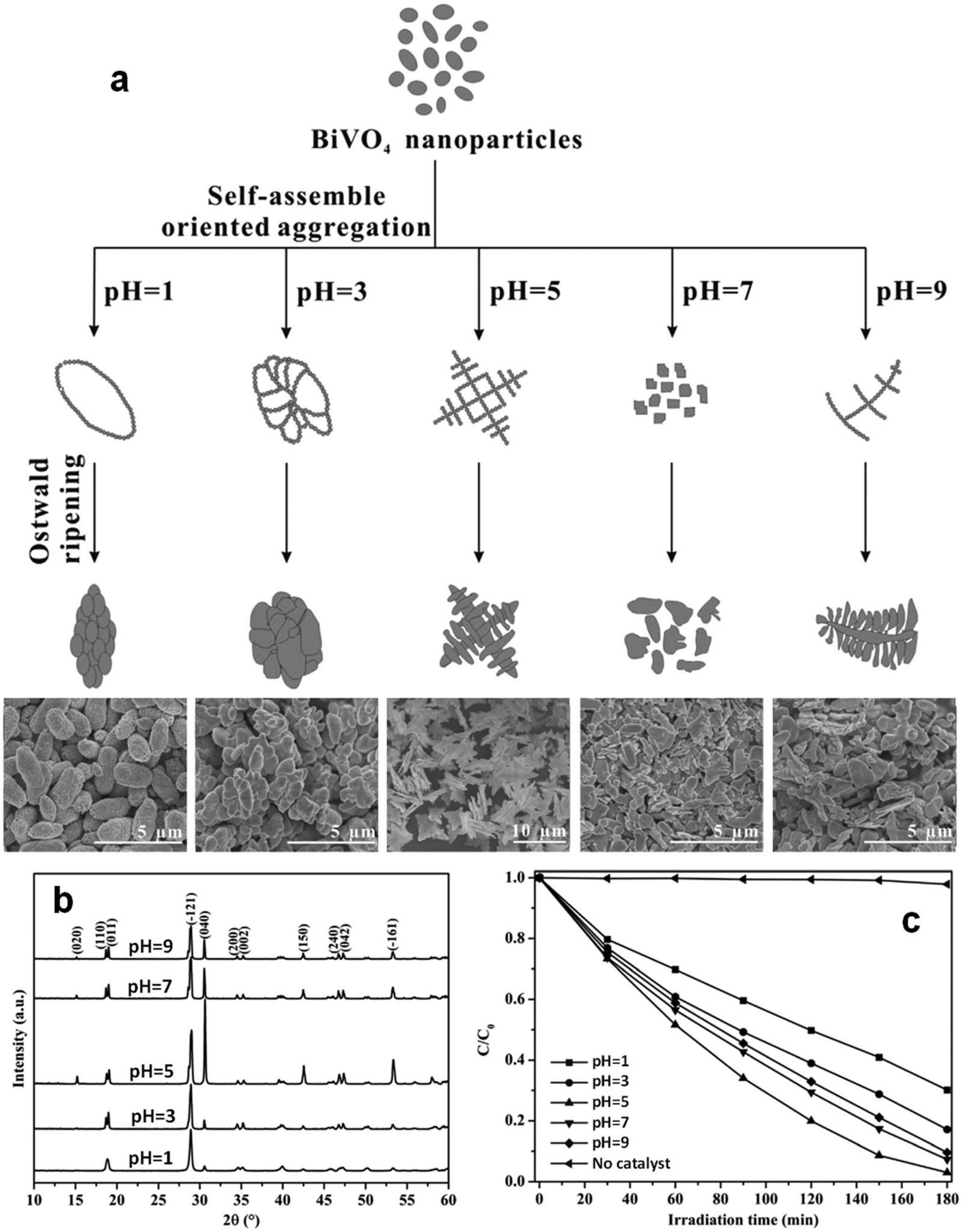

Fig. 17 (a) Schematic diagram of the possible formation mechanism and (b) powder X-ray diffraction patterns (PXRD) patterns of BiVO$_4$ samples with various morphologies prepared at different pH values; (c) photocatalytic activities of the BiVO$_4$ samples in the degradation of MB under visible light. Reproduced with permission from ref. 137. Copyright 2016 Elsevier.

on palygorskite. Zhang and colleagues[157] demonstrated that $Bi_4Ti_3O_{12}$ immobilized on $SiO_2$ spheres could more effectively decolorize Brilliant Red-X3B because of the good dispersion and smaller size of $Bi_4Ti_3O_{12}$.

If the substrates are semiconductor materials, a heterojunction will form and facilitate the separation of electrons and holes. Mu and co-workers[158] deposited spindle-like $BiVO_4$ on $TiO_2$ nanofibers (Fig. 23) using a solvothermal method, and the composite exhibited enhanced visible-light activity than that of a mechanical mixture of $BiVO_4$ and $TiO_2$ in the photocatalytic degradation of RhB. This result could be ascribed not only to the thorough dispersal of the $BiVO_4$ NPs by immobilization, but also to the improved separation of electrons and holes by the formed heterojunction between $BiVO_4$ and $TiO_2$. Zhang and co-workers[159] reported the enhanced performance of BiOCl nanosheets in the photocatalytic degradation of RhB by immobilizing the BiOCl sheets on $TiO_2$ arrays over FTO (Fig. 24). This effect was achieved, because the reflection within the ordered array structure endowed the composites with enhanced light absorption. Moreover, the heterojunction between BiOCl and

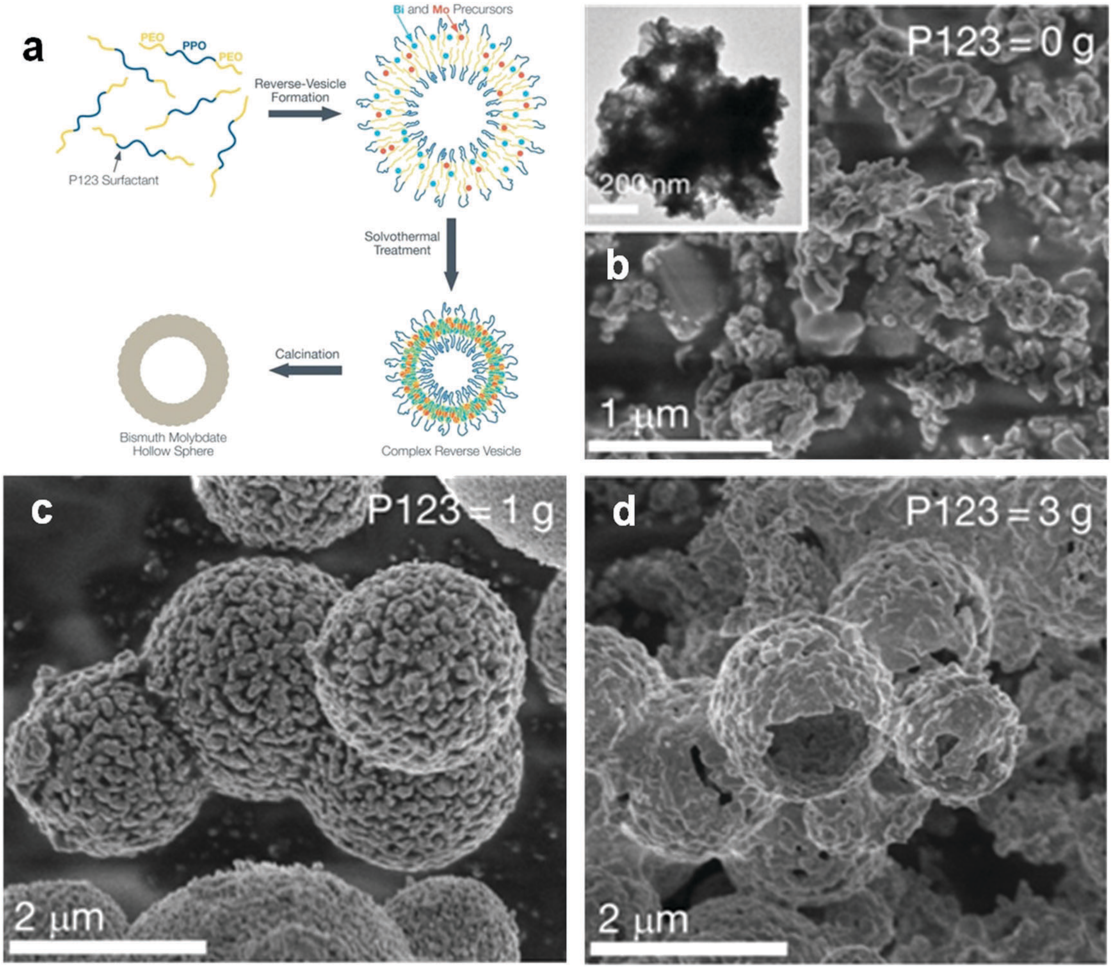

Fig. 18 (a) Schematic diagram of the formation of hollow-structured $Bi_2MoO_6$ and SEM images of $Bi_2MoO_6$ fabricated (b) without P123, (c) with 1 g of P123, and (d) with 3 g of P123. Reproduced with permission from ref. 142. Copyright 2016 American Chemical Society.

$TiO_2$ significantly decreased the charge transfer resistance and facilitated the separation of photo-generated holes and electrons. Kumar *et al.*[160] prepared $Bi_2S_3/TiO_2$ composites from $Bi_2S_3$ nanotubes and $TiO_2$ NPs. The acquired composites showed improved photocatalytic performance in the degradation of amaranth.

Conductive substrates not only affect the morphologies of the composites, but also act as electron acceptors. For example, when a BiOCl sheet was immobilized on carbon fibers, the performance of the sheet in the photocatalytic degradation of 4-nitrophenol was enhanced due to the good dispersion of BiOCl nanoplates and the electron trapping role of the carbon fibers.[161] Likewise, Weng and co-workers[162] loaded $Bi_4Ti_3O_{12}$ on carbon fibers using a hydrothermal method with carbon-fiber-supported $TiO_2$ nanosheets as a precursor. The prepared composite exhibited better performance than that of $Bi_4Ti_3O_{12}$ nanosheets in the photocatalytic degradation of MO. Di *et al.*[163] deposited small $Bi_4O_5Br_2$ nanosheets on multi-walled carbon nanotubes (MWCNTs) *via* an ionic liquid-assisted solvothermal method and found that the activity of the composites in the photocatalytic degradation of tetracycline hydrochloride was obviously improved.

Immobilization plays a more important role in gaseous reactions than in other reactions, because well-dispersed photocatalysts are crucial to the external and internal diffusions of gaseous molecules. Dong's group[164] immobilized Bi NPs on g-$C_3N_4$ and observed that an NO removal efficiency of 60.8% was achieved when Bi NPs of 12 nm were decorated on g-$C_3N_4$. This efficiency was higher than that of g-$C_3N_4$ (38.6%). Meanwhile, Dong's group[165] deposited metal Bi NPs on $TiO_2$ for NO removal and noted that Bi can act as a cocatalyst, similar to a noble metal, due to surface plasmon resonance and can effectively photoactivate $TiO_2$ during NO oxidation under visible-light irradiation. Xia *et al.*[166] loaded BiOI on porous $Al_2O_3$ using a hydrothermal method and observed that the obtained $BiOI/Al_2O_3$ composite exhibited photocatalytic performance by simultaneously eliminating gaseous NO and $SO_2$.

## Heterojunction construction

Heterojunction construction is an effective pathway for enhancing the performance of photocatalysts, because photo-generated electrons and holes can be effectively separated by a heterojunction.[29,42,167–175] For most Bi-based photocatalysts, a narrow band gap ensures that electrons can be excited by visible light.

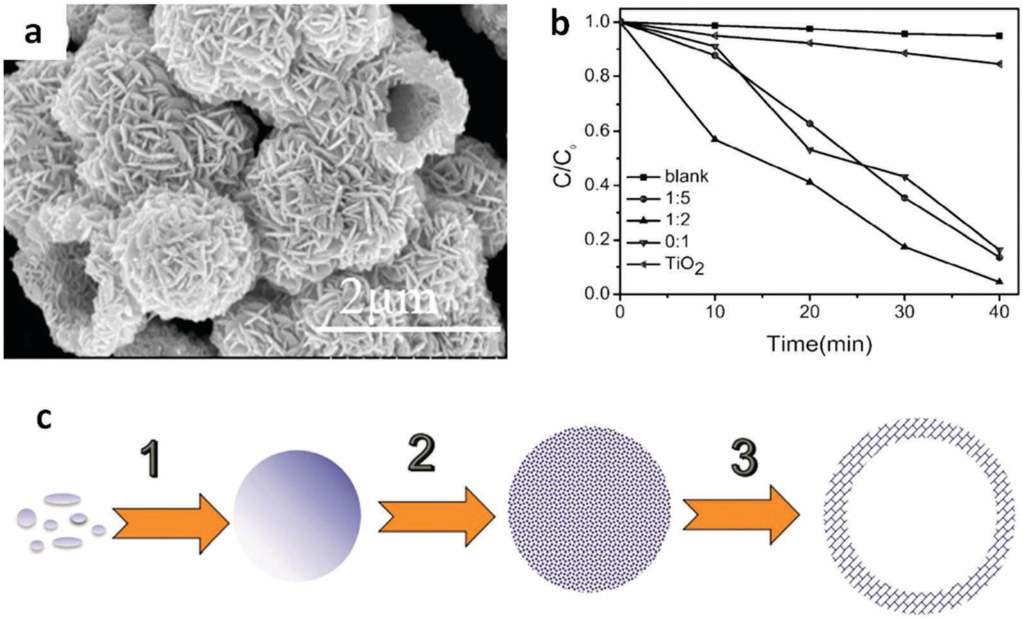

Fig. 19 (a) SEM images of $Bi_2WO_6$ hollow spheres prepared using a mixed solvent of EG and ethanol (EA) ($V_{EG}:V_{EA}$ = 1 : 2) at 160 °C for 2 h; (b) photocatalytic degradation curves of RhB on $Bi_2WO_6$ samples prepared using solvents with different $V_{EG}:V_{EA}$ ratios, and (c) schematic diagram of the formation of hollow structures, involving the formation (1), surface roughening (2) and hollowing (3) of amorphous solid microspheres. Reproduced with permission from ref. 143. Open Access 2016 MDPI.

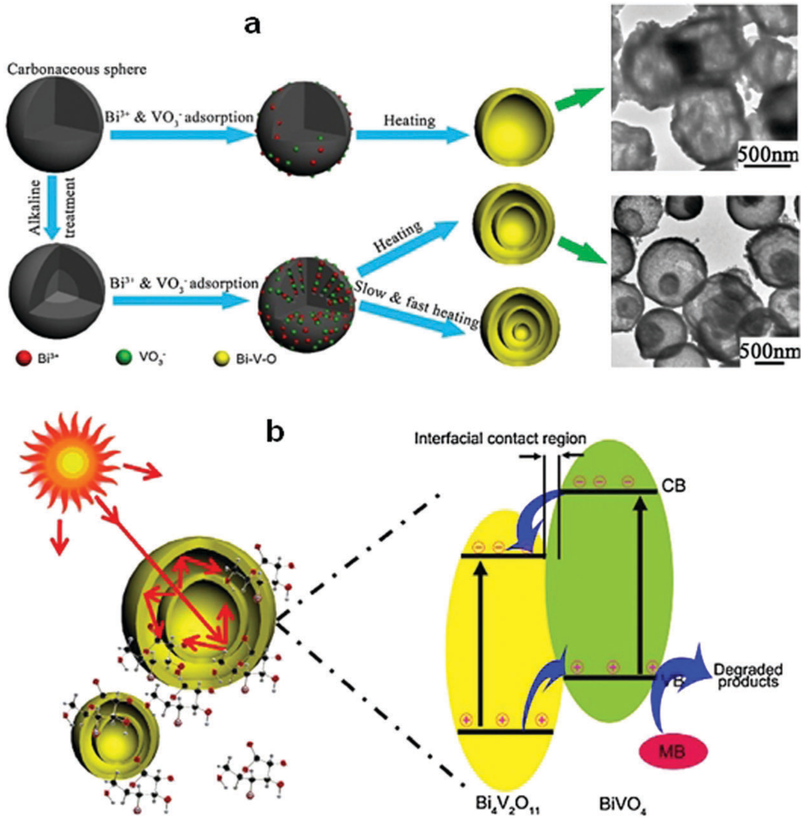

Fig. 20 (a) Schematic diagram of the formation of Bi–V–O multishell hollow spheres and (b) photoabsorption and photocatalytic mechanism of the Bi–V–O multishell hollow spheres. Reproduced with permission from ref. 146. Copyright 2017 Elsevier.

However, the excited electrons recombine with holes soon after. Therefore, heterojunction construction plays a key role in improving the performance of Bi-based photocatalysts. Bi-Based heterojunctions include conventional and Z-scheme heterojunctions.

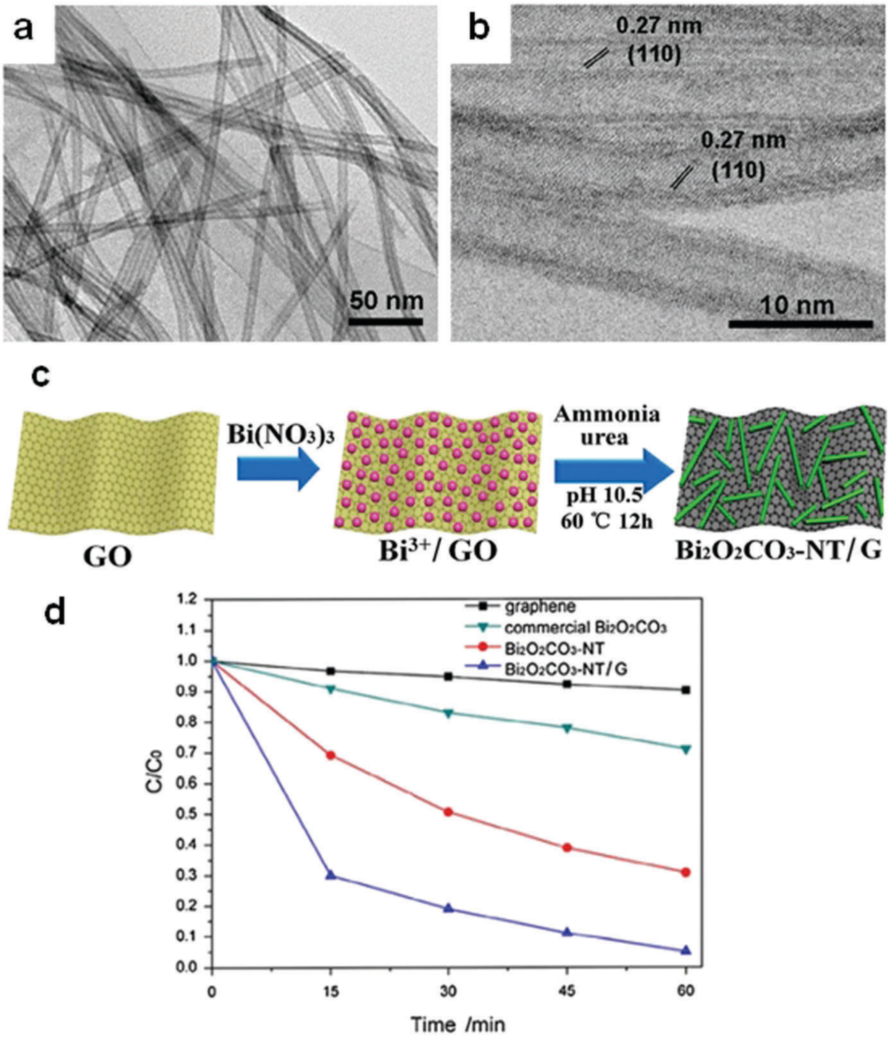

Fig. 21 (a) TEM and (b) HRTEM images and (c) formation mechanism of $Bi_2O_2CO_3$ nanotubes on a graphene substrate; (d) photocatalytic degradation behavior of samples toward reactive red (X-3B). Reproduced with permission from ref. 147. Copyright 2017 Elsevier.

Among the conventional heterojunctions, the type II junction is the most common one, while in Z-scheme systems, the newly-emerged direct Z-scheme heterojunction appears to be the most effective junction structure used for exploring the capacity of photo-generated carriers.

### Conventional type II heterojunctions

Conventional heterojunctions are the most commonly reported in Bi-based photocatalysts, and the two main carrier migrations are illustrated in Fig. 25. In the type I mode, photo-induced holes migrate from the lower VB of semiconductor B (SC-B) to the higher VB of semiconductor A (SC-A), whereas electrons migrate from the higher CB of SC-B to the lower CB of SC-A. During the process, electrons and holes migrate in the same direction, but electrons and holes migrate at different speeds due to their different effective mass or other factors. Consequently, holes and electrons are separated. In the type II mode, holes migrate from the lower VB of SC-B to the higher VB of SC-A, while electrons migrate from the higher CB of SC-A to the lower CB of SC-B. During the process, electrons and holes migrate in opposite directions, resulting in their separation. In any of these two heterojunctions, the electrons and holes can be separated, and the photocatalytic activity of the photocatalysts can be enhanced.

Among the different types of heterojunctions, the type II junction is the most reported one. This kind of heterojunction usually forms between bismuthal compounds and semiconductors with a narrow band gap, when the CB and VB of one semiconductor are lower than that of the coupled one. For example, Zhu and co-workers[176] reported the fabrication of a binary Bi and non-Bi $Bi_4Ti_3O_{12}/CeO_2$ composite by coupling $Bi_4Ti_3O_{12}$ with $CeO_2$ using a molten salt and ion-impregnation method. The obtained $Bi_4Ti_3O_{12}/CeO_2$ composite exhibited enhanced activity in the photocatalytic degradation of BPA. This phenomenon can be attributed to the important role of the heterojunction between $Bi_4Ti_3O_{12}$ and $CeO_2$, which facilitates carrier separation (Fig. 26). In addition, Fan *et al.*[177] constructed a binary Bi-based $Bi_2MoO_6$/BiOI composite heterojunction (Fig. 27a and b) using an anion exchange method with BiOI as a precursor. The as-prepared $Bi_2MoO_6$/BiOI exhibited

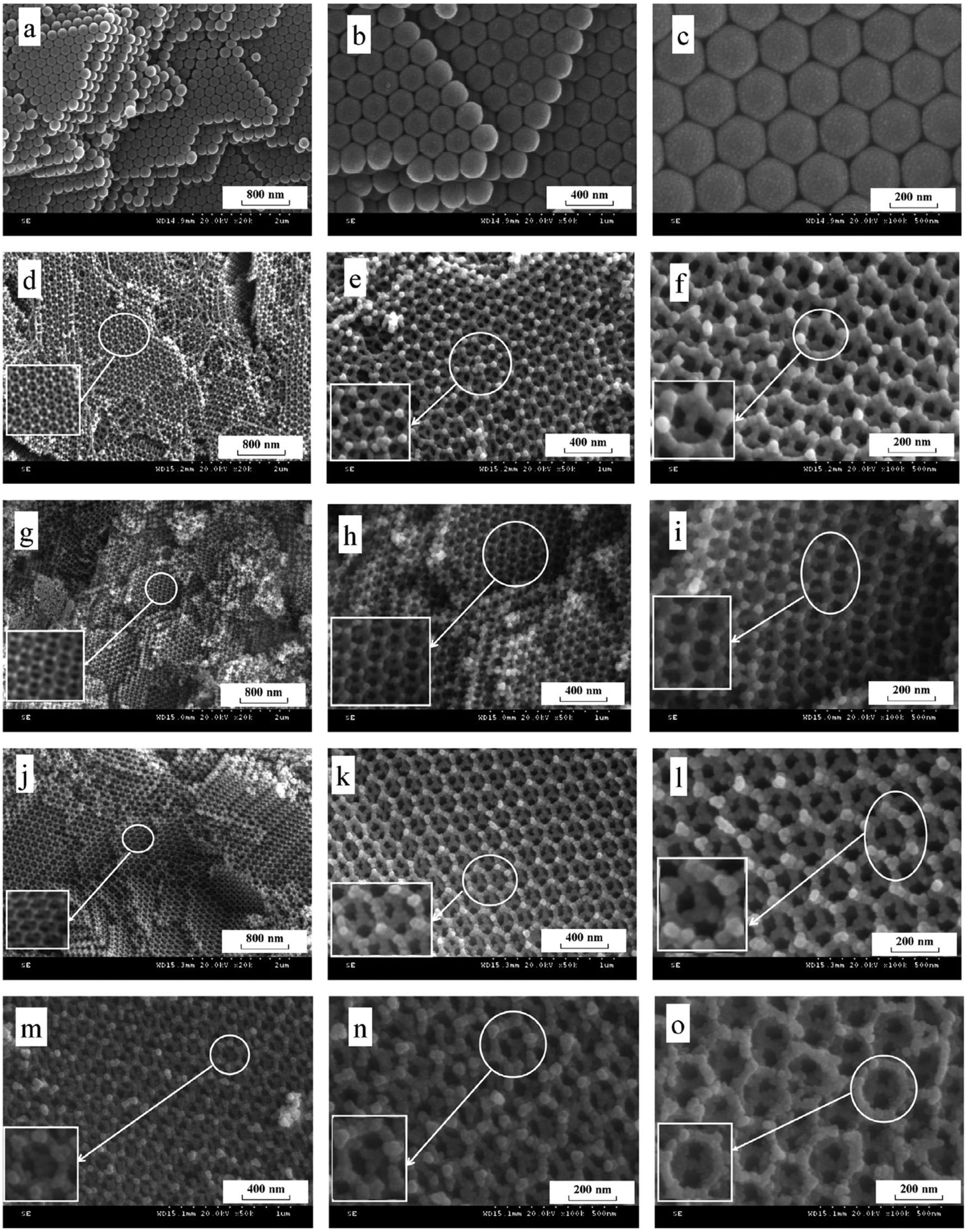

Fig. 22 SEM images of (a–c) polystyrene latex spheres, (d–f) 3DOM $Bi_2O_3/TiO_2$-1 ($n_B : n_{Ti}$ = 0.015 : 1), (g–i) 3DOM $Bi_2O_3/TiO_2$-2 ($n_{Bi} : n_{Ti}$ = 0.03 : 1), (j–l) 3DOM $Bi_2O_3/TiO_2$-3 ($n_{Bi} : n_{Ti}$ = 0.06 : 1) and (m–o) 3DOM $Bi_2O_3/TiO_2$-4 ($n_{Bi} : n_{Ti}$ = 0.09 : 1). Reproduced with permission from ref. 149. Copyright 2015 Elsevier.

improved photocatalytic activities in the degradation of RhB (Fig. 27c). The sample with a Mo/I molar ratio of 50% exhibited the best activity under visible light excitation due to the formation of a type II heterojunction between $Bi_2MoO_6$ and BiOI (Fig. 27d). This type of charge migration and separation were also observed for heterojunctions formed between ZnO/BiOI and BiOCl/$Bi_3PO_4$ couples.[178,179] If three matched bismuthal semiconductors are coupled together, a ternary heterojunction such as $Bi_2S_3/Bi_2O_3/Bi_2O_2CO_3$ can be constructed that exhibits a better performance.[180] The enhancement in the activity of $Bi_2S_3/Bi_2O_3/Bi_2O_2CO_3$ is ascribed to the increased light absorption and efficient charge separation by the double type II

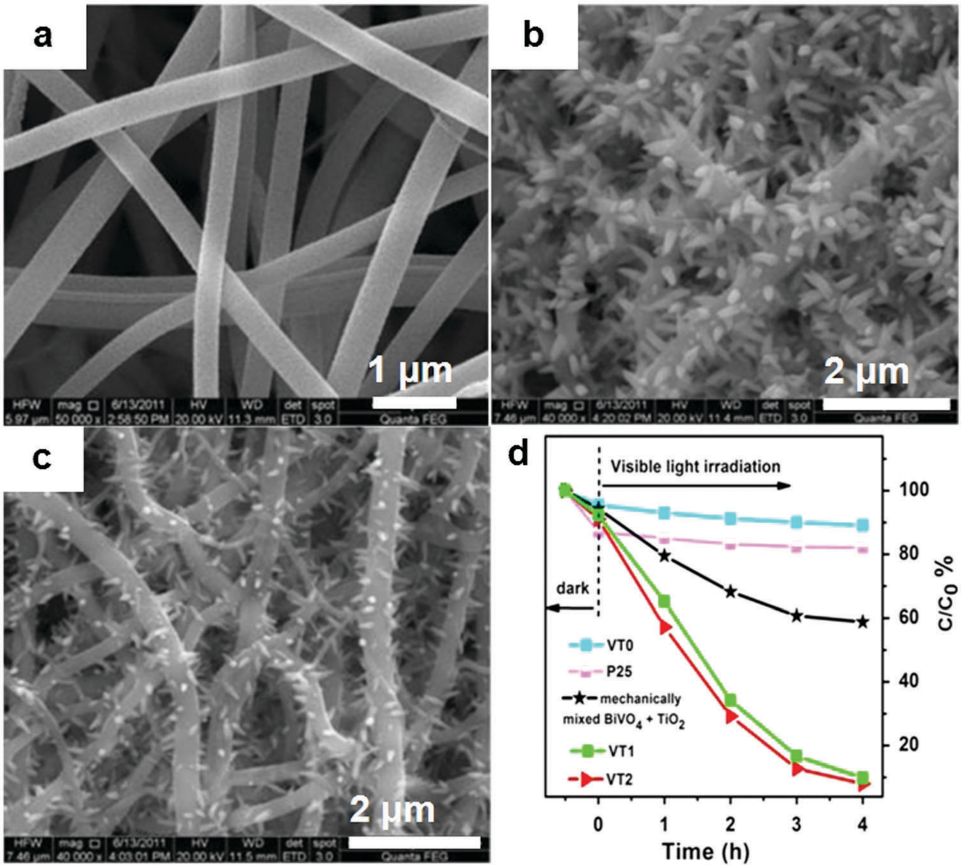

Fig. 23 SEM images of (a) $TiO_2$ nanofibers (VT0), (b and c) $BiVO_4$ immobilized on $TiO_2$ nanofibers using a low (VT1) and high (VT2) concentration of raw material solution, and (d) the degradation curves of RhB over different photocatalysts under visible light. Reproduced with permission from ref. 158. Copyright 2016 Elsevier.

heterojunction (Fig. 28). Type II carrier migrations can also occur in homojunctions. In a homojunction, the interface between two homogenous semiconductors forms due to different phase structures.[181,182]

Numerous preparation strategies for conventional heterojunctions (mainly Type II) have been reported, and most of these techniques have revealed enhanced photocatalytic activities (Table 1). Nevertheless, conventional heterojunctions have evident limitations. Photo-generated electrons migrate from a more negative CB to a less negative CB and the holes from a more positive VB to a less positive VB. This type of migration for electrons and holes reduces the redox capacity of the photocatalyst. Consequently, any improvement in the performance of the photocatalysts will be significantly limited.

Given the limited improvement of a simple conventional heterojunction, several strategies combining heterojunction and morphology control, such as the preparation of a $MoS_2/Bi_{12}O_{17}Cl_2$ 2D bilayer heterostructure[183] and a $Bi_2S_3$ nanorods/$Bi_2O_3$ microtubes composite,[184] have been developed to further enhance the performance of bismuthal photocatalysts. In our previous work, we found that heterojunctions can form between two adjacent (001) and (110) facets of BiOI, whereas their CBs and VBs are located in different positions. Consequently, BiOI with a hierarchical morphology and an optimal ratio of (001) and (110) facets was found to possess the highest photocatalytic activity.[185] However, the combination of heterojunction and morphology control is still unable to overcome the inherent limitations of a conventional heterojunction, although this characteristic results in the better performance of as-prepared photocatalysts.

## Direct Z-scheme heterojunctions

In 2013, Yu *et al.* proposed a direct Z-scheme heterojunction concept to explain the enhancement in the photocatalytic activity of a $TiO_2/g\text{-}C_3N_4$ composite photocatalyst.[285] This direct Z-scheme heterojunction is different from conventional liquid-phase Z-scheme heterojunctions and all-solid-state Z-scheme heterojunctions. The direct Z-scheme heterojunction does not require an electron medium.[286–290] The transfer of charge carriers in this heterojunction is through the built-in electric field between the interface of SC-A and SC-B (Fig. 29a). However, the transfer of charge carriers in the liquid-phase (Fig. 29b) and all-solid-state (Fig. 29c) Z-scheme heterojunction is through the use of ions in the solution and noble metal NPs as electron conductors, respectively.[291–295]

The structure of a direct Z-scheme heterojunction is similar to that of a type-II heterojunction (Fig. 25b) but with different charge carrier transport mechanisms. In a typical type-II

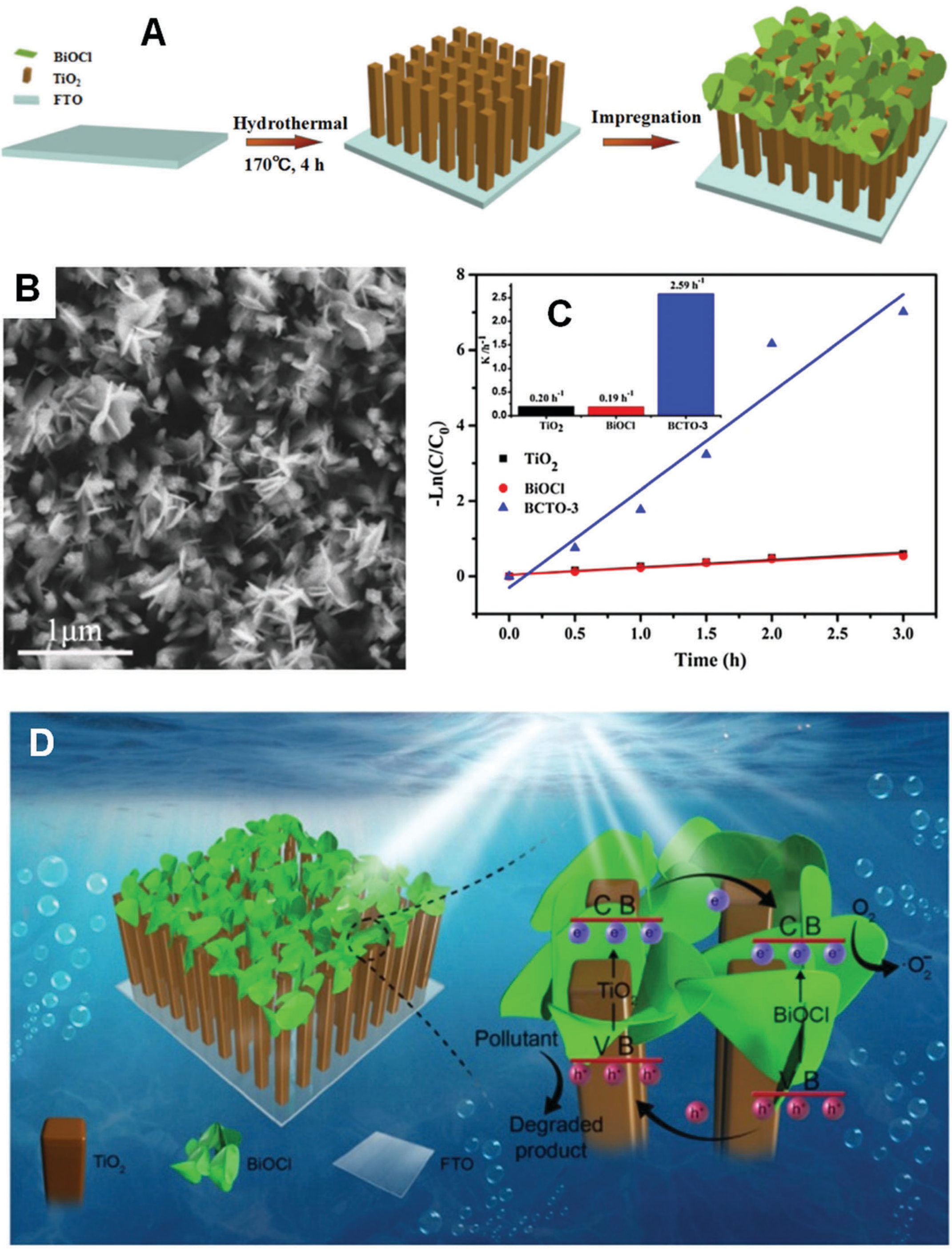

Fig. 24 (A) Schematic diagram of BiOCl/$TiO_2$ composite formation; (B) FESEM images of a BiOCl/$TiO_2$ composite (BCTO-3); (C) kinetic curves of RhB photocatalytic degradation on $TiO_2$, BiOCl, and BCTO-3; (D) schematic diagram of the reaction mechanism over the immobilized BiOCl/$TiO_2$ composite under visible light. Reproduced with permission from ref. 159. Copyright 2017 Elsevier.

heterojunction photocatalyst, SC-A has higher CB and VB positions than SC-B. Under light irradiation, the electrons in SC-A and holes in SC-B will transfer to the CB of SC-B and VB of SC-A, respectively. This process results in the spatial separation of the electron–hole pairs. However, the reduction ability of photo-generated electrons in the CB of SC-B and the oxidation ability of holes in the VB of SC-A are greatly reduced.

In contrast, the direct Z-scheme heterojunction exhibits a completely different mechanism of charge carrier migration. A photo-generated electron with a low reduction potential in SC-B will recombine with a photo-generated hole with a low oxidation potential in SC-A (Fig. 29a). Finally, the photo-generated electron and hole will remain in the CB of SC-A and VB of SC-B, respectively. The direct Z-scheme heterojunction will result in

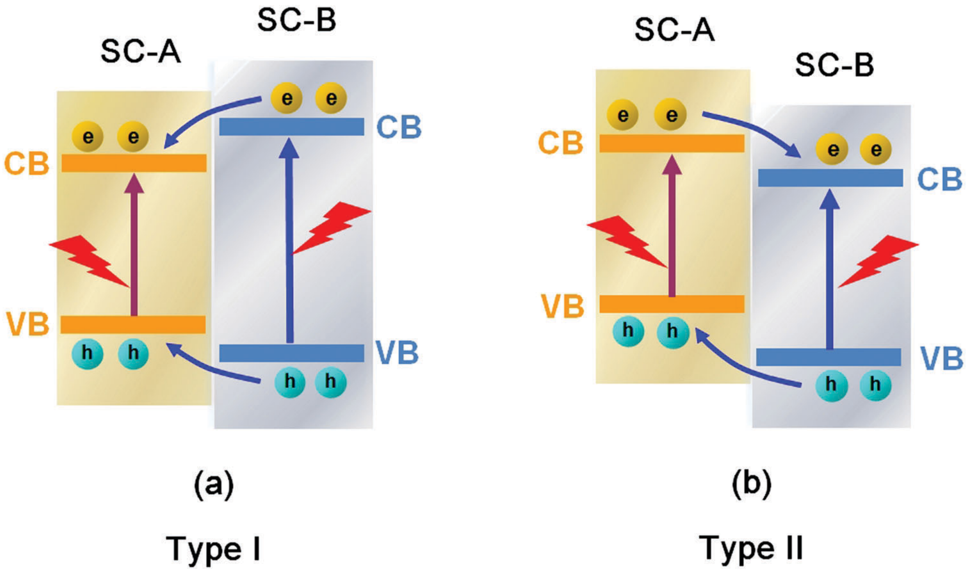

Fig. 25 Schematic diagram of the carrier migrations in conventional (a) type I and (b) type II heterojunctions between semiconductor A (SC-A) and semiconductor B (SC-B).

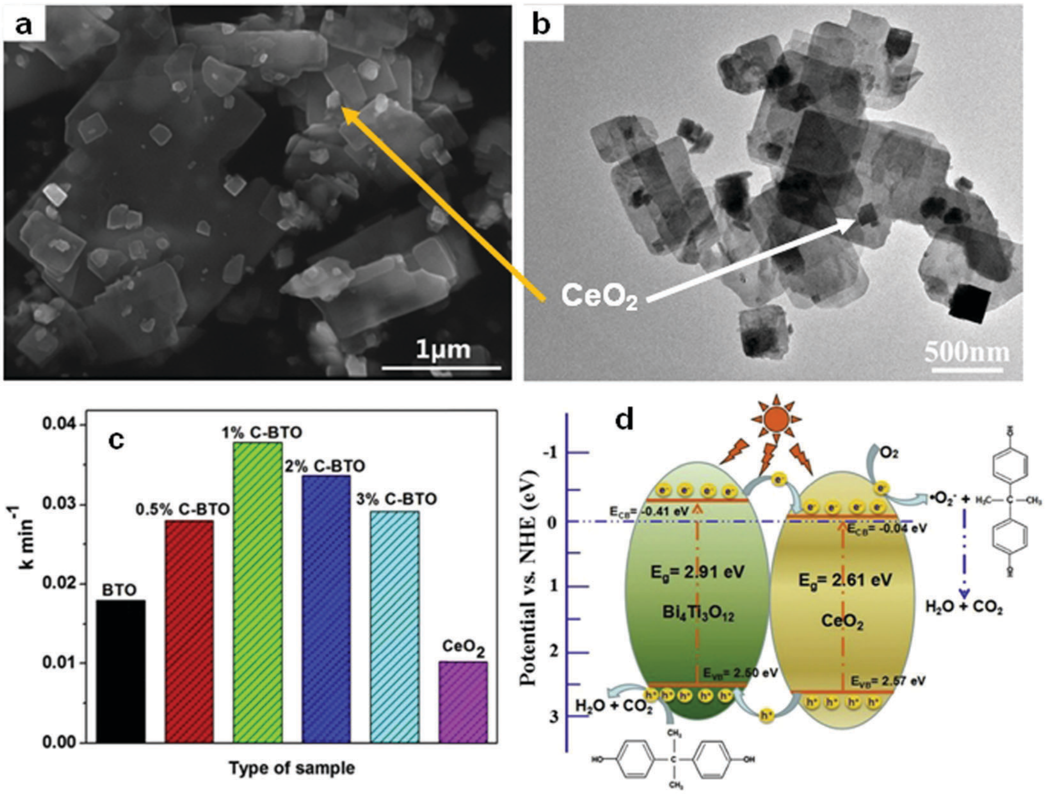

Fig. 26 (a) SEM and (b) TEM images of $CeO_2/Bi_4Ti_3O_{12}$ composites (1%C–BTO); (c) comparison of pseudo-first-order kinetic constants of different photocatalysts for BPA; and (d) a schematic illustration of the charge migration in the 1%C–BTO composites under light irradiation. Reproduced with permission from ref. 176. Copyright 2016 Elsevier.

the spatial separation of useful charge carriers, remove useless charge carriers, and optimize the redox ability of the SC-A and SC-B composition system. Therefore, an enhanced photocatalytic performance can be observed in a direct Z-scheme heterojunction photocatalyst. In addition, the transfer mechanism of the charge carriers in a direct Z-scheme heterojunction is also different from that of conventional liquid-phase and all solid-state Z-scheme heterojunctions. No electron conductor is

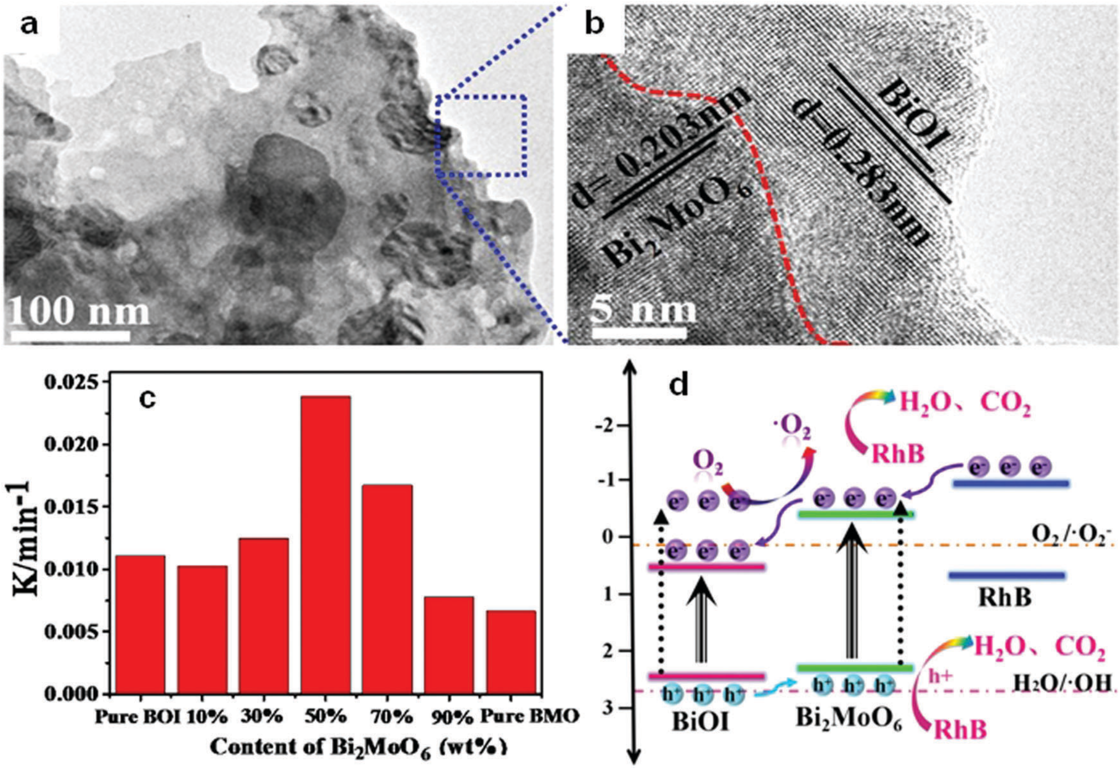

Fig. 27 (a) TEM images and (b) the corresponding HRTEM images of $Bi_2MoO_6$/BiOI composites (BMO/BOI = 50%); (c) reaction rate constants for RhB degradation on BiOI (BOI), $Bi_2MoO_6$ (BMO) and BMO/BOI; and (d) a schematic diagram showing the charge transfer of a BMO/BOI heterostructure. Reproduced with permission from ref. 177. Open Access 2016 World Scientific.

needed in a direct Z-scheme heterojunction, and the charge carrier can directly migrate using the built-in field at the SC-A and AC-B interfaces. Moreover, the fabrication cost of the direct Z-scheme photocatalyst is greatly reduced. Significantly, the direct Z-scheme heterojunction offers at least two obvious merits, namely, a low fabrication cost and high redox ability.

Many Bi-based direct Z-scheme heterojunction photocatalysts have been prepared and reported. For example, Liu *et al.*[296] prepared a CdTe/$Bi_2S_3$ direct Z-scheme heterojunction photocatalyst using an electrostatic adsorption and self-assembly method. The obtained CdTe/$Bi_2S_3$ exhibited higher photocurrent responses and microcystin-LR sensitivity than the individual CdTe and $Bi_2S_3$ nanorod components. Meanwhile, Dai and colleagues[297] formed a g-$C_3N_4$/$Bi_2MoO_6$ direct Z-scheme heterojunction between g-$C_3N_4$ and $Bi_2MoO_6$ using a hydrothermal method. This g-$C_3N_4$/$Bi_2MoO_6$ photocatalyst exhibited a higher activity than the individual g-$C_3N_4$ and $Bi_2MoO_6$ components in the photocatalytic degradation of MB (Fig. 30). Ullah and coworkers[298] reported the synthesis of a Se/$BiVO_4$ direct Z-scheme heterojunction photocatalyst and its higher photocurrent density than that of its individual Se and $BiVO_4$ components. Huang and colleagues[299] demonstrated a direct Z-scheme electron migration mechanism between g-$C_3N_4$ and $BiOIO_3$ in their prepared g-$C_3N_4$/$BiOIO_3$ composite under UV-visible light irradiation. The photocatalytic activity of the g-$C_3N_4$/$BiOIO_3$ composite was shown to be markedly higher than those of g-$C_3N_4$ and mechanically mixed g-$C_3N_4$/$BiOIO_3$ for the removal of RhB. We recently fabricated a $Bi_2O_3$/g-$C_3N_4$ direct Z-scheme heterojunction photocatalyst using an *in situ* room-temperature approach, including photoreduction deposition of $Bi^{3+}$ and subsequent air-oxidation of the resultant metallic Bi.[300] In the prepared composite, $Bi_2O_3$ quantum dots were uniformly distributed on the surface of g-$C_3N_4$ sheets (Fig. 31a), and the photocatalytic activity of $Bi_2O_3$/g-$C_3N_4$ was found to be higher than those of pure $Bi_2O_3$ and g-$C_3N_4$ in the photocatalytic degradation of phenol under visible light (Fig. 31b). This phenomenon can be attributed to the formed direct Z-scheme heterojunction (Fig. 31c). More reports on direct Z-scheme heterojunctions are listed in Table 2 for reference.

# Surface modification

Surface modification is an effective and widely used method for enhancing the activity of a photocatalyst.[314] It also plays an important role in improving the performance of Bi-based photocatalysts. An extensive range of materials can be adopted to modify surfaces. Carbon-based materials, metals, ions, polymers, and semiconductors can be used to modify bismuthal photocatalysts. If a semiconductor is used as a modifier, a nanosized heterojunction will be formed, and the carriers will transfer faster in the tiny heterojunction than in bulk junctions because of the larger interface ratio. For example, the dandelion-like $MoS_2$-decorated $Bi_2S_3$ prepared by Li *et al.*[315] exhibited improved

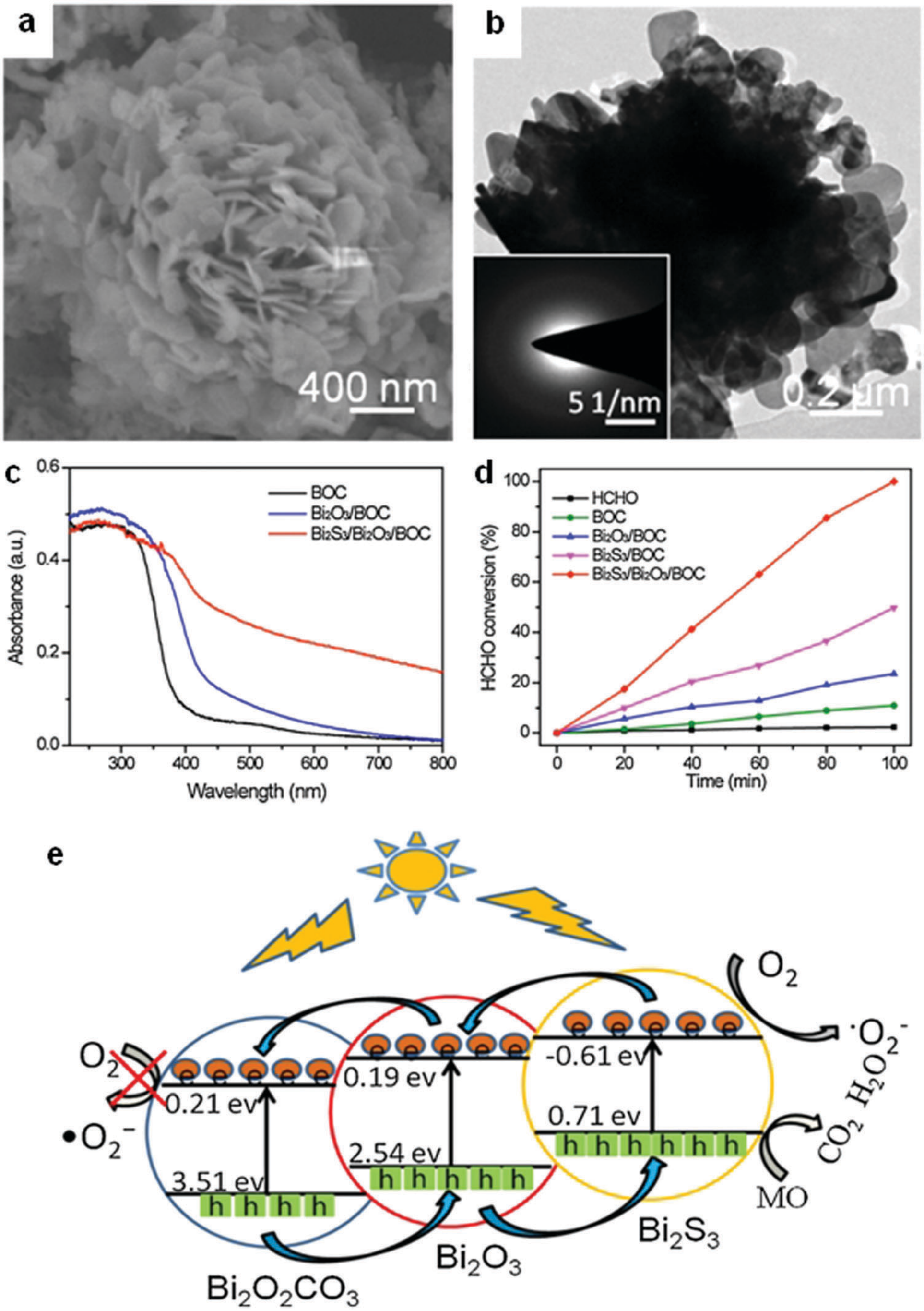

Fig. 28 (a) SEM and (b) TEM images of a ternary $Bi_2S_3/Bi_2O_3/Bi_2O_2CO_3$ composite photocatalyst; (c) UV-visible absorption spectra of $Bi_2O_2CO_3$(BOC), $Bi_2O_3$/BOC, and $Bi_2S_3/Bi_2O_3$/BOC; (d) comparison of the photocatalytic HCHO removal of $Bi_2O_2CO_3$(BOC), $Bi_2O_3$/BOC, $Bi_2S_3$/BOC, and $Bi_2S_3/Bi_2O_3$/BOC; and (e) a schematic diagram showing the charge-transfer process in ternary $Bi_2S_3/Bi_2O_3/Bi_2O_2CO_3$ double heterojunctions. Reproduced with permission from ref. 180. Copyright 2016 Elsevier.

photocatalytic performance in the degradation of RhB due to the tiny heterojunctions formed between $MoS_2$ and $Bi_2S_3$ (Fig. 32). Further to this, $SnO_2$ modified $BiVO_4$ was found to be able to reduce $CO_2$ to $CH_4$, with the introduced $SnO_2$ acting as a redox reaction platform capable of accepting the photogenerated electrons from $BiVO_4$ nanoplates during the conversion of $CO_2$.[316] AgBr, graphene-like BN (g-BN), and some bismuthal compounds with a narrow band gap have also been reported as semiconductor modifiers for Bi-based photocatalysts (Table 3).

Coupling bismuthal photocatalysts with conductive materials is another effective surface modification strategy. The conductive materials usually act as electron acceptors to promote the migration of photo-generated electrons and consequently facilitate the separation of carriers. Metals, carbon-based materials,

Table 1 Conventional heterojunction strategies of nanoscale Bi-based photocatalysts

| Bismuthal compound | Coupled material | Method | Application | Ref. |
|---|---|---|---|---|
| Binary Bi and non-Bi heterojunction | | | | |
| $Bi_2O_3$ | $FeVO_4$ | Grounding and calcination | Malachite green | 186 |
| $Bi_2O_3$ | $TiO_2$ | Hydrothermal synthesis and calcination | MB | 187 |
| $Bi_2O_3$ | g-$C_3N_4$ | Self-assembly | RhB | 188 |
| $Bi_2O_3$ | g-$C_3N_4$ | Mixing-calcination | RhB | 189 |
| $Bi_2S_3$ | ZnS | Cation exchange | MB | 190 |
| $Bi_2S_3$ | ZnS | Solvothermal method | $H_2$ generation | 191 |
| $Bi_2S_3$ | Pd4S | Thermal reduction and cation exchange | Atrazine | 192 |
| $Bi_2O_2CO_3$ | CdS | Reflux | MB | 193 |
| $Bi_2Ti_2O_7$ nanosheets | $TiO_2$ fibers | Hydrothermal method | RhB | 194 |
| $Bi_{12}TiO_{20}$ | g-$C_3N_4$ | Hydrothermal method | Gaseous HCHO | 195 |
| $Bi_4Ti_3O_{12}$ | g-$C_3N_4$ | Ball milling | Acid orange II (AO-7) | 196 |
| $Bi_4Ti_3O_{12}$ | $CeO_2$ | Molten salt and ion impregnation | BPA | 176 |
| $Bi_2O_2CO_3$ | g-$C_3N_4$ | Calcination | Dibutyl phthalate and MO | 197 |
| $Bi_2O_2CO_3$ | $Ag_3PO_4$ | Hydrothermal method and precipitation | RhB | 198 |
| $BiFeO_3$ | g-$C_3N_4$ | Hydrothermal method | Guaiacol | 199 |
| $BiFeO_3$ | CuO | Hydrothermal synthesis and impregnation | MO | 200 |
| $Bi_2Sn_2O_7$ | $In_2O_3$ | Impregnation | RhB | 201 |
| BiOCOOH | $Ag_2O$ | Solvothermal deposition | RhB and *p*-chlorophenol | 202 |
| $BiVO_4$ | $TiO_2$ fibers | Hydrothermal method | Brilliant red X-3B | 203 |
| $BiVO_4$ | 3DOM $TiO_2$ | Hydrothermal method | RhB | 204 |
| $BiVO_4$ | g-$C_3N_4$ | Ultrasonic assembly | $CO_2$ reduction | 205 |
| $BiVO_4$ | $CeO_2$ | Coprecipitation and subsequent annealing | RhB | 206 |
| $BiVO_4$ | $Ag_2O$ | Impregnation and evaporation | MO | 207 |
| $BiVO_4$ | ZnO | Annealing of mixture | RhB | 208 |
| $BiVO_4$ | $SnO_2$ | Hydrothermal method | MB | 209 |
| $BiVO_4$ | $Co_3O_4$ | Drop-casting method | Water oxidation | 210 |
| $BiVO_4$/FTO | PEDOT:PSS | Electrodeposition | Photo-photocurrent | 211 |
| $Bi_2WO_6$ | $TiO_2$ | Hydrothermal method | RhB and MO | 212 |
| $Bi_2WO_6$ | $TiO_2$ fibers | Hydrothermal method | RhB and phenol | 213 |
| $Bi_2WO_6$(001) | $TiO_2$(001) | Hydrothermal method | MB | 214 |
| $Bi_2WO_6$ | $WO_3$ | Hydrothermal method | RhB | 215 |
| $Bi_2WO_6$ | $\alpha$-$Fe_2O_3$ | Electrospinning with sintering | RhB | 216 |
| $Bi_2WO_6$ | $CeO_2$ | Hydrothermal method | RhB | 217 |
| $Bi_2WO_6$ | AgCl | Hydrothermal method | RhB | 218 |
| $Bi_2WO_6$ | $Ag_2O$ | Chemical precipitation | RhB | 219 |
| $Bi_2WO_6$ | CdS and ZnS | Surface functionalization | RhB | 220 |
| $Bi_2MoO_6$ | $TiO_2$ | Solvothermal method | Phenol and nitrobenzene | 221 |
| $Bi_2MoO_6$ | g-$C_3N_4$ | Liquid chemisorption and thermal treatment | RhB | 222 |
| $Bi_2MoO_6$ | $Ag_3VO_4$ | Hydrothermal method and precipitation | RhB | 223 |
| $Bi_2MoO_6$ | AgBr | Precipitation–deposition | RhB | 224 |
| $Bi_2MoO_6$ | AgI | Precipitation–deposition | RhB and BPA | 225 |
| $Bi_2MoO_6$ | $MoO_3$ | Chemical vapor deposition | $O_2$ evolution and glycerol oxidation | 226 |
| $Bi_2MoO_6$ | $MoO_3$ | Hydrothermal method | Photoanode | 227 |
| $Bi_2SiO_5$ | AgI | Precipitation | Acid red G and gaseous HCHO | 228 |
| BiOCl | g-$C_3N_4$ | Solvothermal method | RhB | 229 |
| BiOCl | CuS | Hydrothermal method | RhB | 230 |
| BiOCl | $TiO_2$ | Solvothermal method | Benzene | 231 |
| BiOBr | N doped graphene | Wet chemical method | Chlorpyrifos detection | 232 |
| BiOBr | $CoFe_2O_4$ | Solvothermal method | Congo red | 233 |
| BiOBr | $NiFe_2O_4$ | Hydrothermal method | MB | 234 |
| p-Type BiOBr | n-Type $La_2Ti_2O_7$ | Refluxed in oil bath | RhB | 235 |
| BiOBr | $CdWO_4$ | Hydrothermal synthesis and precipitation | RhB | 159 |
| BiOBr | $CeO_2$ | Precipitation–deposition | RhB | 236 |
| BiOBr | $Ag_3PO_4$ | Precipitation–deposition | RhB | 237 |
| BiOI | $TiO_2$ nanotube | Impregnating-hydroxylation | MO | 238 |
| BiOI | $TiO_2$ fibers | Successive ionic layer adsorption and reaction | MO | 239 |
| BiOI | $Fe_2O_3$ | *In situ* hydrolysis | RhB | 240 |
| BiOI | $La(OH)_3$ | Chemical impregnation | NO | 241 |
| BiOX (X = Cl, Br, I) | AgX (X = Cl, Br and I) | Precipitation | RhB | 242 |
| $Bi_4O_5I_2$ | g-$C_3N_4$ | Solvothermal method using an ionic liquid | RhB and endocrine | 243 |
| Binary Bi-based heterojunctions | | | | |
| $\alpha$-$Bi_2O_3$/$\beta$-$Bi_2O_3$ | | Solid-state reaction | Indigo carmine and RhB | 244 |
| $\alpha$-$Bi_2O_3$/$\beta$-$Bi_2O_3$ | | *In situ* phase transformation by calcination | RhB | 245 |
| $Bi_2O_3$-$Bi_2S_3$ | | Hydrothermal method | RhB | 184 |

Table 1 (*continued*)

| Bismuthal compound | Coupled material | Method | Application | Ref. |
|---|---|---|---|---|
| $Bi_2O_3/BiVO_4$ | | Solvothermal synthesis followed by annealing | Phenol | 246 |
| $Bi_2O_3/BiVO_4$ | | Hydrothermal method | RhB | 247 |
| $Bi_2O_3$ QDs/$BiVO_4$ fibers | | Direct heat treatment | RhB | 248 |
| $Bi_2WO_6/Bi_2O_3$ | | Solid-state reaction | RhB | 249 |
| $Bi_2O_3/BiOCl$ | | Alkaline treatment | MO | 250 |
| $\beta$-$Bi_2O_3/BiOI$ | | *In situ* reaction | MO | 251 |
| $Bi_5O_7I/Bi_2O_3$ | | Chemical etching | Malachite green | 252 |
| $Bi_2S_3/BiOCl$ | | Solvothermal synthesis | Salicylic acid, RhB | 253 |
| $Bi_2S_3/Bi_2WO_6$ | | Anion exchange approach | RhB | 254 |
| $Bi_2S_3/Bi_2WO_6$ | | Hydrothermal method | Reduction of Cr(VI) | 255 |
| $Bi_2S_3/Bi_4Ti_3O_{12}$ nanofibers | | *In situ* ion exchange | RhB | 256 |
| $Bi_2S_3/Bi_2O_2CO_3$ | | Anion exchange | Gaseous NO | 257 |
| $Bi_2S_3/Bi_2O_2CO_3$ hollow microspheres | | One-pot room temperature route | RhB | 258 |
| $Bi_2Ti_2O_7/Bi_4Ti_3O_{12}$ | | One-step molten salt method | MO, RhB | 259 |
| $Bi_{12}TiO_{20}/Bi_2WO_6$ | | Hydrothermal method | RhB | 260 |
| $BiVO_4/Bi_2O_2CO_3$ | | Hydrothermal method | RhB | 261 |
| $BiPO_4/BiOBr$ | | Mixing in solvent | Gaseous *o*-dichlorobenzene | 262 |
| $Bi_2MoO_6/BiVO_4$ | | Spin-coating | Photoelectrode | 263 |
| $Bi_2MoO_6/BiPO_4$ | | Hydrothermal method | RhB | 264 |
| $Bi_2W_xMo_{1-x}O_6/BiOCl$ | | Solvothermal method | RhB | 265 |
| $Bi_{3.64}Mo_{0.36}O_{6.55}/Bi_2MoO_6$ | | Hydrothermal method | RhB | 266 |
| $BiOI/BiVO_4$ | | Coprecipitation | *Pseudomonas aeruginosa* | 267 |
| $BiOI/BiVO_4$ | | Precipitation–deposition | MO | 268 |
| $BiOCl/BiVO_4$ | | Coprecipitation method | RhB | 269 |
| $BiOCl/Bi_{12}O_{17}C_{l2}$ | | Hydrothermal method | MO | 270 |
| $BiOI/Bi_2MoO_6$ | | Precipitation–deposition | BPA | 271 |
| $Bi_2MoO_6/BiOI$ | | hydrothermal method | RhB | 177 |
| $Bi_{24}O_{31}Cl_{10}/BiOCl$ | | Phase transformation by annealing | Conversion of benzyl alcohol | 272 |
| $Bi_4O_5I_2/Bi_5O_7I$ | | *In situ* phase transformation | BPA and RhB | 273 |
| $Bi_4O_5I_2/Bi_5O_7I$ | | Hydrothermal method | Propylparaben | 274 |
| $Bi_2O_2CO_3/BiOI$ | | Pore impregnation | RhB | 275 |
| $Bi_2O_4$-Decorated BiOBr | | Alkali posttreatment assisted light irradiation | MO | 276 |
| Monoclinic $BiVO_4$/tetragonal $BiVO_4$ | | Hydrothermal method | RhB | 277 |
| $BiVO_4/Bi_4V_2O_{11}$ | | Precursor conversion | Photoelectrodes | 278 |
| Ternary heterojunctions | | | | |
| $Bi_2O_3/Bi_2S_3/MoS_2$ | | Hydrothermal method | $O_2$ evolution and MB degradation | 279 |
| $AgI/BiOI–Bi_2O_3$ | | Etching-deposition | Cr(VI) reduction | 280 |
| $BiOCl_x/BiOBr_y/BiOI_z$ | | Electrospinning and the sol–gel methods | Trichloroethylene | 281 |
| $Bi_2S_3/Bi_2O_3/Bi_2O_2CO_3$ | | Heat treatment and ion exchange | HCHO, MO, and phenol | 180 |
| $Bi_7O_9I_3/AgI/AgIO_3$ | | Chemical deposition | MO and gaseous NO | 282 |
| $Bi_7O_9I_3/Bi_5O_7I$/g-$C_3N_4$ | | Hydrothermal method | Crystal violet | 283 |
| $BiOBr/Co(OH)_2/PVP$ | | Solvothermal synthesis | MO | 284 |

Rhodamine B, RhB; methylene blue, MB; methyl orange, MO; bisphenol A, BPA; ciprofloxacin, CIP; PEDOT:PSS = Poly(3,4-ethylenedioxythiophene):poly-(styrenesulfonate).

conductive polymers, and metallic Bi have been adopted as electron scavengers to enhance the photocatalytic activities of bismuthal compounds (Table 3). Commonly employed noble metals include Au, Ag, Pt, and Pd. Hirakawa *et al.*[317] obtained a composite by loading Au NPs on $BiVO_4$. The prepared Au/$BiVO_4$ exhibited an enhanced production of $H_2O_2$ from water than that of pure $BiVO_4$ under visible-light irradiation due to the selective two-electron reduction of $O_2$ by Au. In addition to noble metals, other metals can also serve as electron trapping agents. Park and co-workers[318] decorated Ni NPs on W-doped $BiVO_4$ nanofibers and obtained a fibrous composite (Ni@NiO/W:$BiVO_4$ NFs). The process was followed by a calcination method, during which Ni NPs were partly oxidized to NiO. The as-prepared composite exhibited a higher photocurrent and $O_2$ evolution than W-doped $BiVO_4$ nanofibers and Pt-decorated fibers in the photocatalytic oxidation of water. The enhancement was attributed to the unique structure of the Ni@NiO decoration, in which the Ni metal traps the photo-generated electrons and NiO accepted holes. Moreover, the metal Bi-decorated $Bi_2WO_6$ exhibited a photocatalytic efficiency three times higher than that of pure $Bi_2WO_6$ in the degradation of phenol under visible light, because metal Bi not only acts as an electron acceptor, but also promotes the separation of carriers.[319] Finally, the surface plasmon resonance of Bi was also embodied in the Bi/BiOBr composite, which possessed a higher activity for NO oxidation than that of pure BiOBr.[320]

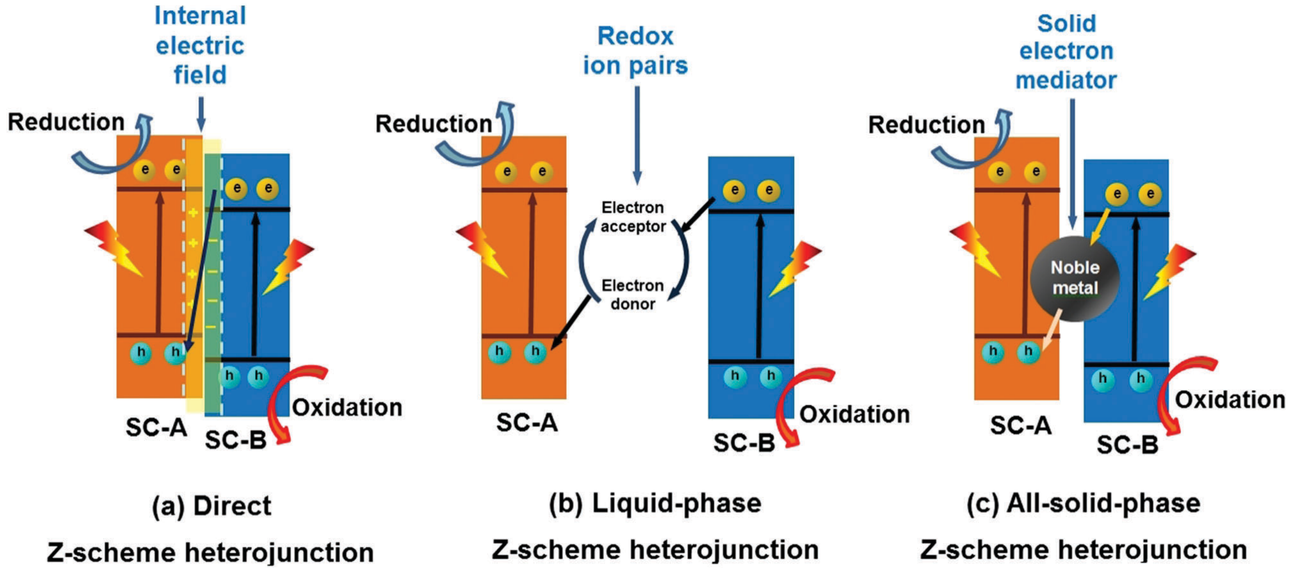

Fig. 29 Schematic illustration of (a) direct Z-scheme, (b) liquid-phase Z-scheme and (c) all-solid-state Z-scheme heterojunctions (SC represents semiconductor).

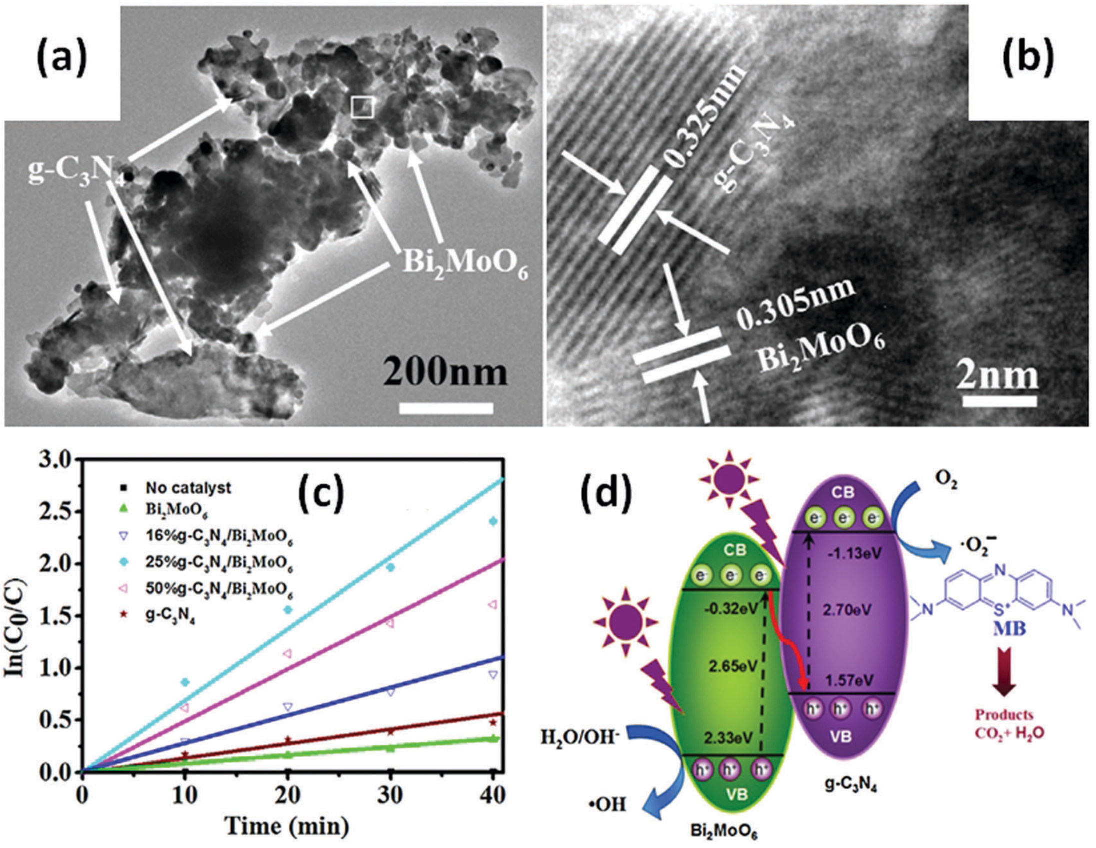

Fig. 30 (a) TEM and (b) HRTEM images of a g-$C_3N_4$/$Bi_2MoO_6$ composite; (c) pseudo first-order fitted kinetic curves of MB degradation on g-$C_3N_4$/$Bi_2MoO_6$ composites (25%g-$C_3N_4$/$Bi_2MoO_6$); and (d) a schematic illustration of electron and hole migration in a g-$C_3N_4$/$Bi_2MoO_6$ direct Z-scheme heterojunction. Reproduced with permission from ref. 297. Copyright 2015 Elsevier.

Carbon materials, such as carbon dots (CDs), CNTs, graphene, graphene oxide (GO), reduced graphene oxide (RGO), carbon quantum dots (CQDs), and graphene quantum dots (GQDs), can be used as modifiers. Among these materials, graphene-based materials are more favorable because of their special graphitic structure and ideal conductivity.[321] Priya *et al.*[322]

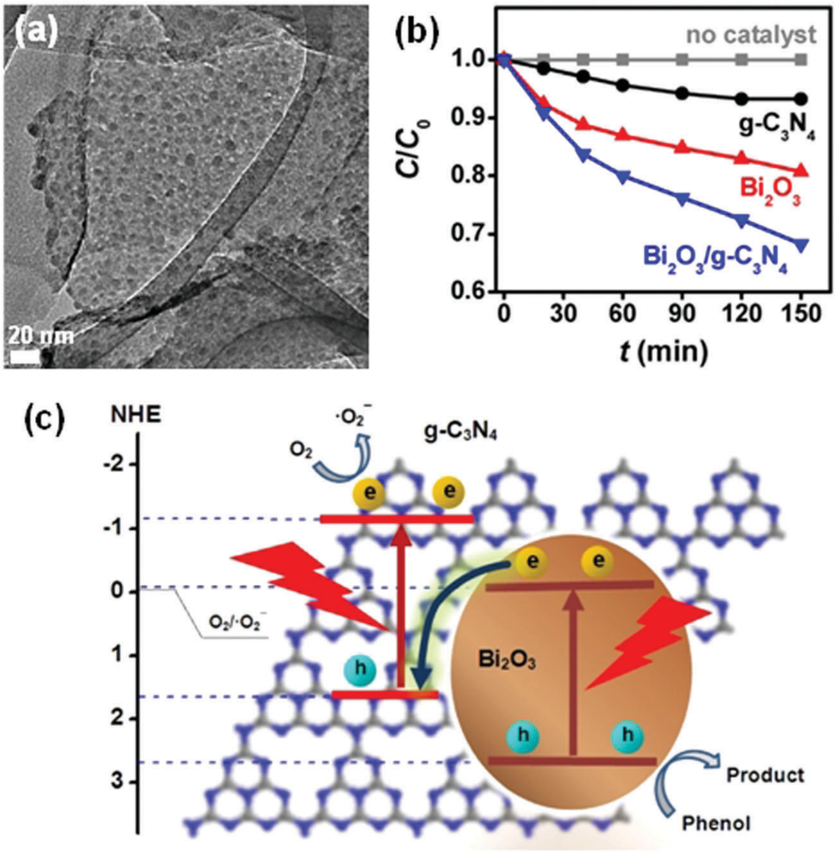

Fig. 31 (a) TEM images of a $Bi_2O_3/g-C_3N_4$ composite; (b) comparison of the photocatalytic performance of $Bi_2O_3$, $g-C_3N_4$, and $Bi_2O_3/g-C_3N_4$ in the degradation of phenol; and (c) the photocatalytic mechanism of a $Bi_2O_3/g-C_3N_4$ direct Z-scheme heterojunction. Reproduced with permission from ref. 300. Copyright 2018 Elsevier.

Table 2 Nanoscale Bi-based direct Z-scheme heterojunction photocatalysts

| Bismuthal compound | Coupled material | Method | Application | Ref. |
|---|---|---|---|---|
| $Bi_2O_3$ | $g-C_3N_4$ | Ball milling and heat treatment | MB | 301 |
| $Bi_2Sn_2O_7$ | $g-C_3N_4$ | High-temperature solid-state reaction | MB and acid red 18 | 302 |
| $Bi_2MoO_6$ | $g-C_3N_4$ | Hydrothermal method | MB | 297 |
| BiOBr | $g-C_3N_4$ | Reflux process | RhB and BPA | 303 |
| $BiOIO_3$ | $g-C_3N_4$ | Hydrothermal method | MO, RhB, and dichlorophenol | 299 |
| BiOI | CdS | Hydrothermal method | RhB | 304 |
| $Bi_2WO_6$ | $MoS_2$ | Hydrothermal method | RhB | 305 |
| $Bi_2MoO_6$ | CuO, $Co_3O_4$, NiO | Precipitation | RhB | 306 |
| $Bi_2O_3$ | $NaNbO_3$ | Ball milling method | RhB | 307 |
| $BiVO_4$ | Se film | Chemical vapor deposition | Photocurrent enhancement | 298 |
| $BiVO_4$ | SiC | Precipitation followed by calcination | $O_2$ evolution | 308 |
| BiOBr | $Bi_2MoO_6$ | Two-step coprecipitation method | RhB and CIP | 309 |
| $BiO_{1-x}Br$ | $Bi_2O_2CO_3$ | Solvothermal method | CIP | 310 |
| $BiPO_4$ | $Bi_2O_2(OH)(NO_3)$ | Hydrothermal method | Dichlorophenol | 311 |
| $MoS_2/BiOI/AgI$ |  | Precipitation | RhB | 312 |
| $BiVO_4/ZnIn_2S_4/g-C_3N_4$ |  | Impregnation and calcination | Congo red and metronidazole | 313 |

Rhodamine B, RhB; methylene blue, MB; methyl orange, MO; bisphenol A, BPA; ciprofloxacin, CIP.

loaded a $Bi_2O_3/BiOCl$ heterojunction on a prepared graphene sand composite using a wet impregnation method. The obtained composite showed an improved performance over that of $Bi_2O_3/BiOCl$ for the mineralization of ampicillin and oxytetracycline. The improvement was attributed to the electron trapping role of the graphitic carbon on the graphene sand composite. When $Bi_2WO_6$ microspheres were wrapped with GO using a freeze-drying dehydration method, they exhibited a higher activity than that of pure $Bi_2WO_6$ on the photocatalytic degradation of RhB due to the improved separation of the electrons and holes by GO.[323] GQDs possess a small particle size and high specific surface area. Therefore, GQDs are more favorable for the surface modification of

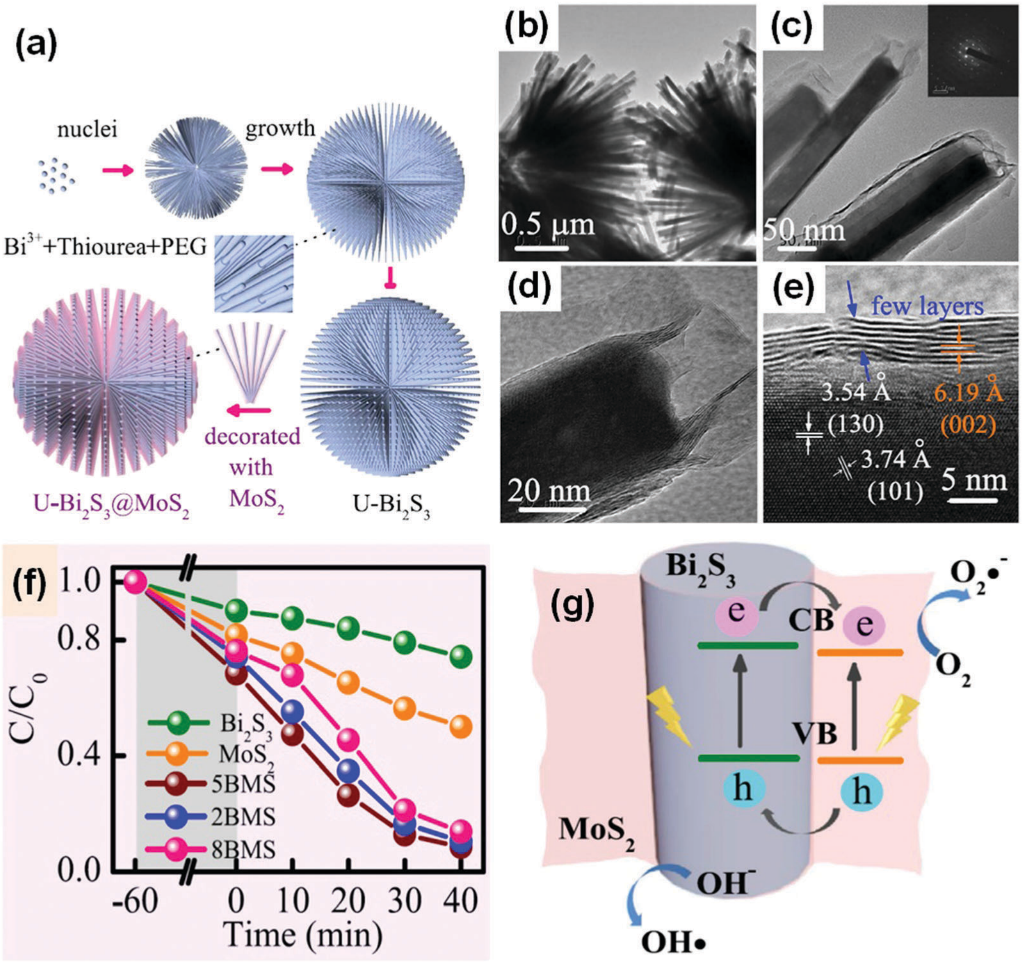

Fig. 32 (a) Schematic illustration of the formation of $MoS_2$-decorated $Bi_2S_3$ (BMS); (b–d) TEM and (e) HRTRM images of $MoS_2$-decorated $Bi_2S_3$; (f) comparison of the photocatalytic performance of RhB on $MoS_2$, $Bi_2S_3$ and BMS (2MBS, 5MBS, and 8MBS present in molar ratios of $Mo^{4+}$-to-$Bi^{3+}$ of 20%, 50%, and 80%) under visible-light irradiation; and (g) a schematic diagram of the charge transfer at a $MoS_2$/$Bi_2S_3$ heterojunction. Reproduced with permission from ref. 315. Open Access 2017 Springer Nature.

photocatalysts. For example, $Bi_2MoO_6$ decorated with GQDs *via* a self-assembly approach, showed a remarkable increase in photocatalytic degradation efficiency of different target pollutants, including BPA, MB, TC, CIP, and phenol.[324] Nevertheless, GO or RGO materials may suffer from instability in long-term reactions. Subramanian and colleagues[325] found that RGO coupled with $Bi_2Ti_2O_7$ might suffer from decomposition and result in a reduced performance of the composite after long-term illumination in an oxidation environment (Fig. 33a and b). The degradation of RGO was attributed to the oxidation by the formed $^{\bullet}$OH (Fig. 33c). Several conductive polymers, such as polyaniline, polypyrrole, and polythiophene, can play the role of electron scavenger and promote the electron migration in bismuthal photocatalysts.[326–328] However, the conductivities of these polymers are much weaker than those of noble metal and carbon materials. Thus, the related research is less reported. Usually, amorphous carbon is not suitable for electron trapping because of its poor conductivity. Nevertheless, it also plays a positive role in the enhancement of photocatalytic activity due to it enhancing the visible light absorption and carrier separation of the photocatalyst.[329]

Introducing vacancies or elements with different chemical valence states may also improve the performance of photocatalysts. Wang *et al.*[330] introduced vacancies into the surface of $Bi_6S_2O_{15}$ nanowires by increasing the molar ratio of $Na_2SO_4$ and $Bi(NO_3)_3$ from 1 : 3 to 3 : 1 during hydrothermal synthesis. The light absorption of vacancy $Bi_6S_2O_{15}$ nanowires at 370–500 nm was stronger than that of pure $Bi_6S_2O_{15}$ nanowires. Vacancy $Bi_6S_2O_{15}$ nanowires also showed improved photocatalytic activity for the degradation of phenol and MB. The enhancement was attributed to the improved visible-light response induced by the surface vacancies (Fig. 34). Zhang and colleagues[331] treated $BiVO_4$ at different temperatures under different atmospheres. The sample treated at 973 K in $N_2$ exhibited the best activity for the formation of EG from aldehyde. The enhancement was attributed to the formation of $V^{4+}$. $Bi_2WO_6$ with a large fraction of {100} high-energy facets showed relatively high efficiency in the photocatalytic degradation of diclofenac, because ''Bi–O'' dimer vacancy pairs formed on the {100} facets could bring about a narrower band gap and less photoexcited charge recombination.[332] Moderate oxygen-deficient defects in BiOBr

Table 3 Surface modification strategies for nanoscale Bi-based photocatalysts

| Modifier | Bi-Based material | Method | Target material of enhanced performance | Ref. |
|---|---|---|---|---|
| Semiconductor | | | | |
| $MoS_2$ | $Bi_2S_3$ | Hydrothermal method | RhB | 315 |
| g-$C_3N_4$ | $Bi_2O_4$ | Hydrothermal method | MO | 335 |
| CdS | $BiVO_4$ | Solvothermal method | $H_2$ generation | 336 |
| $Cu_2O$ | $Bi_2WO_6$ | Interfacial self-assembly | MB | 337 |
| AgBr QDs | $Bi_2WO_6$ | Precipitation–deposition | MB and phenol | 338 |
| g-BN | BiOI | Solvothermal method | RhB | 339 |
| g-BN | BiOCl | Microwave-assisted method | Cr(VI) reduction | 340 |
| g-BN | $BiPO_4$ | Solvothermal method | Enrofloxacin | 341 |
| $Bi_2O_3$ QDs | $BiVO_4$ | Calcination | RhB | 248 |
| $Bi_2O_4$ | BiOBr | Alkali posttreatment under light irradiation | MO | 276 |
| BiOI | $Bi_2MoO_6$ | Deposition–precipitation | MO | 342 |
| BiOBr | $BiPO_4$ | Hydrothermal method | MB | 343 |
| Carbon material | | | | |
| Carbon | $Bi_4Ti_3O_{12}$ | Coprecipitation | MO | 344 |
| Carbon | $Bi_2MoO_6$ | Two-step hydrothermal method | RhB | 345 |
| Carbon microspheres | $BiFeO_3$ | Hydrothermal method | RhB | 346 |
| Carbon microspheres | $Bi_{0.5}Dy_{0.5}VO_4$ | Self-assembly | $H_2$ generation | 347 |
| Carbon nanotubes | $Bi_4O_5Br_2$ | Solvothermal method | Tetracycline hydrochloride and RhB | 163 |
| Carbon dots | BiOI | Immersion | MO | 348 |
| CQDs | $Bi_{20}TiO_{32}$ | Oil bath | Isoproturon | 349 |
| CQDs | $Bi_4O_5I_2$ | Solvothermal method | RhB | 350 |
| CQDs | BiOI | Hydrothermal method | RhB | 351 |
| GO | $BiVO_4$ | Hydrothermal method | RhB | 352 |
| GO | BiOCl | Two-step synthesis | RhB | 353 |
| GO | $BiO_xI_y$ | Hydrothermal method | Crystal violet | 354 |
| GO | $BiFeO_3$ | Ultrasonic treatment | BPA | 355 |
| GO | $Bi_2O_2CO_3$ | Precipitation | Gaseous NO | 356 |
| GO | $Bi_2WO_6$ | Liquid nitrogen freezing and freeze-drying dehydration | RhB | 323 |
| GO | BiOI | Self-assembly | Phenol | 357 |
| RGO | BiOI | Hydrothermal method | MO | 358 |
| RGO | BiOBr | Two-step hydrothermal method | Higher activity for MO than for RhB | 359 |
| RGO | $Bi_{25}FeO_{40}$ | Hydrothermal method | MO | 360 |
| RGO | $Bi_2WO_6$ | Wrapped | RhB | 361 |
| RGO | $Bi_2S_3$ | Hydrothermal method | 2,4-Dichlorophenol | 362 |
| RGO | $BiPO_4$ | Solvothermal method | Chlorpyrifos detection | 363 |
| Graphene | Ag/$BiOBr_{0.2}I_{0.8}$ | Combined solvothermal method and photodeposition | RhB | 364 |
| Graphene | $BiOCl_{0.7}Br_{0.3}$ | Solvothermal method | RhB | 365 |
| Graphene | $Bi_2O_2CO_3$ | Hydrothermal method | RhB | 366 |
| Ag and graphene | $Bi_2WO_6$ | Hydrothermal method followed by photodeposition | RhB | 367 |
| GQDs | $Bi_2MoO_6$ | Self-assembly | BPA, MB, TC, CIP, and phenol | 324 |
| Au and RGO | $Bi_2MoO_6$ | Solvothermal synthesis and photochemical reduction | RhB | 368 |
| Ag and graphene | $Bi_2Fe_4O_9$ | Multistep synthesis | MB | 369 |
| Metal and ion | | | | |
| Pd | $Bi_2MO_6$ | Photoreduction | Phenol | 370 |
| Pd | $Bi_2WO_6$ | Chemical deposition | RhB | 371 |
| Pd | BiOBr | Solvothermal method | RhB and CIP | 372 |
| Pd | m-$BiVO_4$/BiOBr | Reduction in the dark | Polychlorinated biphenyls | 373 |
| Pt | BiOBr | Photodeposition | *p*-Nitrophenol | 374 |
| Pt | $BiFeO_3$ | Impregnation and thermal reduction | MO | 375 |
| Pt | $Bi_2WO_6$ | Chemical reduction | Rhodamine 6G | 376 |
| Pt | $Bi_2WO_6/TiO_2$ | Photodeposition | $CO_2$ reduction | 377 |
| Au | BiOCl | Photodeposition | Formaldehyde | 378 |
| Au | $BiVO_4$ | Pulsed laser deposition | Congo red and water splitting | 379 |
| Au | $BiPO_4$ | Solvothermal method | CO oxidation | 380 |
| Au | $Bi_2O_2CO_3$ | Hydrothermal method | NO | 381 |
| Ag | $BiFeO_3$ film | Sol spin coating and annealing | $O_2$ evolution | 382 |
| Ag | BiOBr | Solvothermal method | Tetracycline hydrochloride | 383 |
| Ag | $BiVO_4$ | Hydrothermal method | Reduced electron-transfer resistance | 384 |
| Ag | $Bi_4Ti_3O_{12}$ | Sonochemical method | RhB | 385 |
| Ag | $Bi_2WO_6$ | Irradiation | RhB | 386 |
| Bi | $Bi_2WO_6$ | *In situ* reduction | Phenol | 319 |
| Bi | $Bi_2WO_6$ nanorod | Hydrothermal reaction | Rh6G | 387 |
| Bi | $Bi_2MoO_6$ | Solvothermal reduction | Rh6G | 388 |
| Bi | $BiPO_4$ | Solvothermal treatment | MB | 389 |
| Bi | BiOBr | Reduction reaction at room temperature | MO | 390 |
| Bi | BiOI/CNFs | Solvothermal method | MO | 391 |
| Cr | $Bi_4Ti_3O_{12}$ | Sol–gel hydrothermal process | $H_2$ generation | 69 |

Table 3 (*continued*)

| Modifier | Bi-Based material | Method | Target material of enhanced performance | Ref. |
|---|---|---|---|---|
| Ni | BiOI | Photo-assisted deposition | Reducing Cr(VI) to Cr(III) | 392 |
| Fe(III) | $Bi_2O_2CO_3$ | Impregnation | MO | 393 |
| Fe | $Bi_2Ti_2O_7$ | Precipitation | MO | 394 |
| $Fe_2O_3$ | Macroporous $BiVO_4$ | Impregnation | 4-Nitrophenol | 395 |
| $CoO_x$ | $BiFeO_3$ | Photodeposition | $O_2$ evolution | 396 |
| Rh(III) | BiOCl | Impregnation | Gaseous acetaldehyde (Vis) | 397 |
| Organic material | | | | |
| Polythiophene | $Bi_2MoO_6$ | *In situ* chemical oxidative polymerization | RhB | 326 |
| Polyaniline | $Bi_2O_2CO_3$ | Low-temperature chemical method | RhB | 327 |
| PVP | BiOBr | Solvothermal method | RhB | 328 |
| MIL-101 (MOF) | $BiVO_4$ | Hydrothermal method | RhB | 398 |
| Ionic liquid | $BiPO_4$ | Hydrothermal method | RhB | 399 |
| Surface defect | | | | |
| Bi defects | $Bi_6S_2O_{15}$ | Hydrothermal method | Phenol | 330 |
| Dimer vacancy | $Bi_2WO_6$ | Solvothermal method | Diclofenac | 332 |
| Defect | $BiPO_4$ | Ball milling | MB | 400 |

GO: graphene oxide; RGO: reduced graphene oxide; MOF: metal–organic framework; CQDs: carbon quantum dots; GQDs: graphene quantum dots; Rh6G: Rhodamine 6G; MB: methylene blue; PEDOT:PSS: poly(3,4-ethylenedioxythiophene):poly(styrenesulfonate).

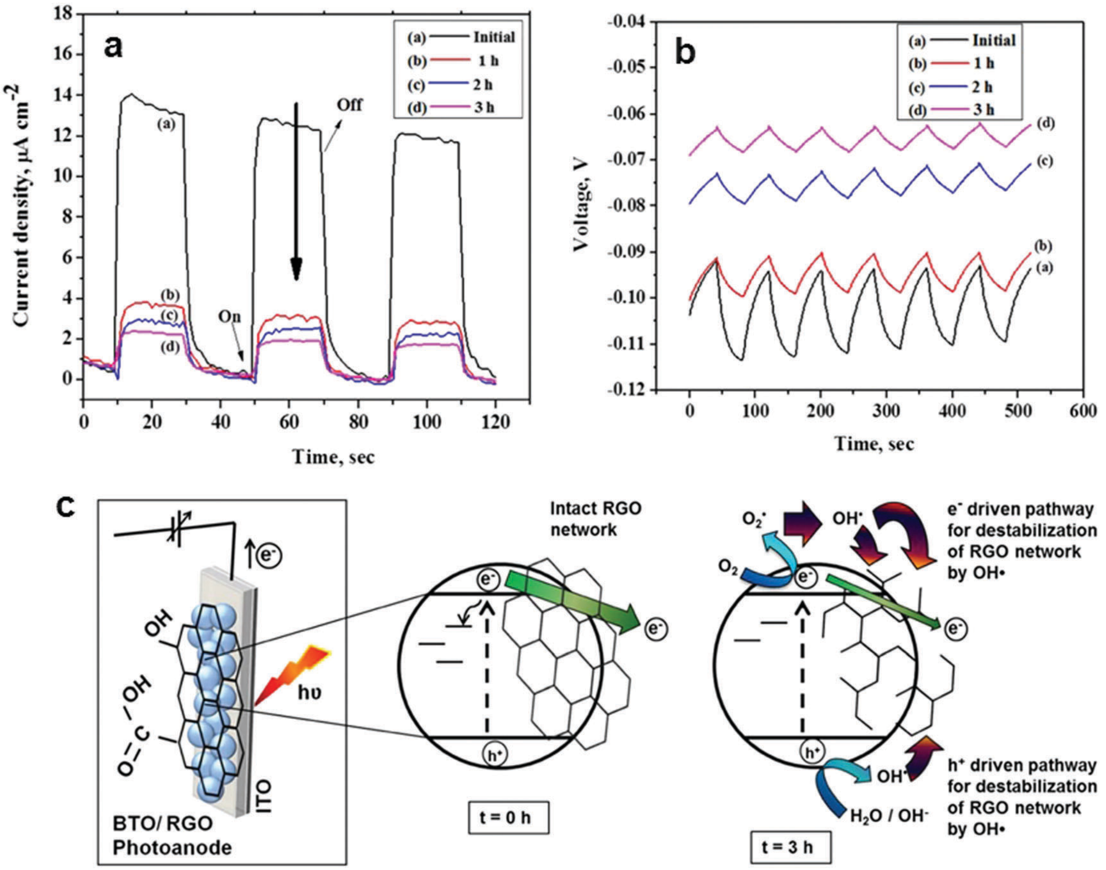

Fig. 33 (a) $I/t$ and (b) $V/t$ curves of the $Bi_2Ti_2O_7$/RGO composite (BTO/RGO) during long-term light irradiation and (c) the degradation mechanism of the RGO on a BTO/RGO film under light illumination for 3 h in an air-equilibrated solution. Reproduced with permission from ref. 325. Copyright 2016 Electrochemical Society.

also play an indispensable role for superior photocatalytic $CO_2$ reduction, by acting as the active sites for $CO_2$ adsorption and activation, trapping photogenerated electrons and thus impact upon the recombination of the electron–hole pairs.[333] Oxygen vacancies were also found to have a positive influence on the performance of BiOCl on photocatalytic $CO_2$ reduction because oxygen vacancies can induce exciton dissociation and provide more photo-induced electrons for $CO_2$ reduction.[334]

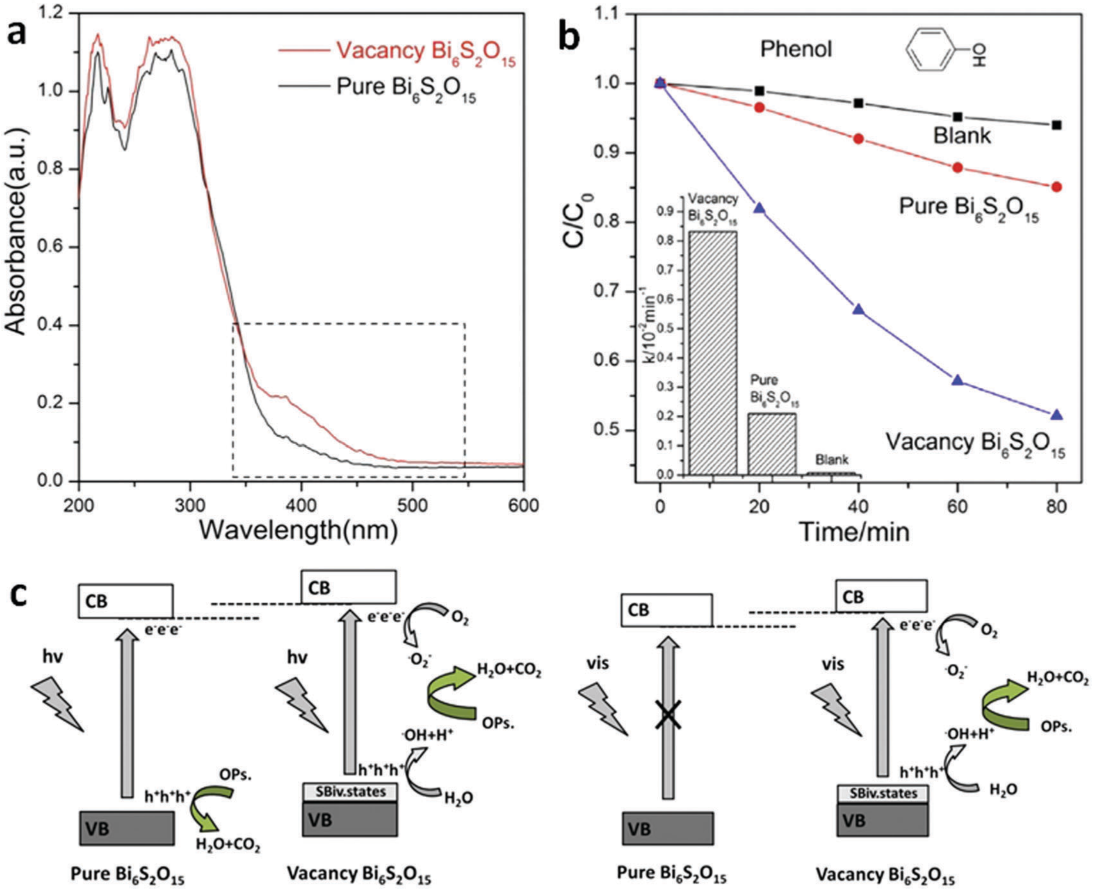

Fig. 34 (a) UV-visible diffuse reflectance spectra of pure $Bi_6S_2O_{15}$ and vacancy $Bi_6S_2O_{15}$ nanowires; (b) degradation rate constant $k$ of pure $Bi_6S_2O_{15}$ and vacancy $Bi_6S_2O_{15}$ nanowire photocatalysts; (c) schematic diagram of the carrier separation and photocatalytic reaction of pure $Bi_6S_2O_{15}$ and vacancy $Bi_6S_2O_{15}$ nanowires under UV-visible irradiation. Reproduced with permission from ref. 330. Copyright 2015 Elsevier.

# Conclusions and prospects

A layered structure and excellent visible-light response endow Bi-based photocatalysts with excellent photocatalytic activity and promising prospects for application in the fields of environmental science and energy. Studies centered on Bi-based photocatalysts will be beneficial for the future development of photocatalysts. Considerable work has been performed to control the composition, morphology, and structure of these catalysts to improve the photocatalytic performance of Bi-based photocatalysts. These photocatalysts are used for the visible-light photocatalytic degradation of organic pollutants, $H_2$ generation, water splitting, and $CO_2$ reduction. Although significant progress has been achieved, great efforts are still required to further explore the advantages of Bi-based photocatalysts as visible-light photocatalysts. The following five aspects deserve special attention:

(1) Previous studies on Bi-based photocatalysts have mainly focused on the photocatalytic degradation of organic pollutants. Few studies have reported on the application of these photocatalysts in photocatalytic $H_2$ generation, water splitting, and $CO_2$ reduction. Several investigations have focused on $BiVO_4$. The main obstacle in the study of Bi-based photocatalysts is the less negative CB and the poor reducing abilities of bismuthal compounds. More bismuthal materials should be extensively explored to overcome these obstacles. The construction of nanosized direct Z-scheme heterojunctions by coupling bismuthal semiconductors with semiconductors that have a more negative CB is a promising method for exploring Bi-based photocatalysts for reduction applications.

(2) Bi-based photocatalyst photodegradation has been primarily evaluated in aqueous solutions instead of under gaseous conditions. The latter condition is favorable for the use of Bi-based photocatalysts because visible light can be more fully utilized in the gas phase. The removal of formaldehyde and benzene from air is important for environmental remediation and indoor air purification. Therefore, extending the application of Bi-based photocatalysts to the degradation of gaseous contaminants is meaningful.

(3) The aim of photocatalysis is to solve serious environmental and energy problems in the world. We hope that this review can further stimulate the research into and application of Bi-based photocatalytic materials in the near future. We believe that the understanding and knowledge on Bi-based photocatalysts can be greatly enhanced and the experimental and characterization methods improved.

(4) Theoretical simulations can provide new insight into understanding the photocatalytic mechanism and relationship

between the microstructure and performance. The theoretical investigations on Bi-based photocatalytic materials should be further strengthened, which will contribute to a deep understanding on the surfaces, interfaces, nanostructures and activity at the atomic and molecular level of the material properties.

(5) Although Bi-based photocatalysts have been continuously investigated over the past ten years, their photocatalytic performance is still far from the requirements for practical application. More research work is still needed to reach their real application.

## Conflicts of interest

There are no conflicts to declare.

## Acknowledgements

This work was supported by the NSFC (21573170, 51320105001, U1705251 and 21433007), the Self-determined and Innovative Research Funds of SKLWUT (2017-ZD-4), and the Natural Science Foundation of Hubei Province of China (No. 2015CFA001). The project was also supported by the Internal Research Grant (RG 11/2016-2017R), and the EdUHK and General Research Fund (GRF 18301117) by RGC of the HK government. The work was also supported by the Natural Science Foundation of Hunan Province of China (2018JJ2457).

## References

1 K. Maeda, K. Teramura, D. L. Lu, T. Takata, N. Saito, Y. Inoue and K. Domen, *Nature*, 2006, **440**, 295.

2 Z. Huang, L. Pan, J. Zou, X. Zhang and L. Wang, *Nanoscale*, 2014, **6**, 14044.

3 P. Reddy, P. Reddy, E. Kwon, K. H. Kim, T. Akter and S. Kalagara, *Environ. Int.*, 2016, **91**, 94.

4 P. Zhou, J. Yu and M. Jaroniec, *Adv. Mater.*, 2014, **26**, 4920.

5 O. Ola and M. M. Maroto-Valer, *J. Photochem. Photobiol., C*, 2015, **24**, 16.

6 J. Low, B. Cheng and J. Yu, *Appl. Surf. Sci.*, 2017, **392**, 658.

7 S. Cao and J. Yu, *J. Photochem. Photobiol., C*, 2016, **27**, 72.

8 J. Low, J. Yu and W. Ho, *J. Phys. Chem. Lett.*, 2015, **6**, 4244.

9 Q. Xiang, B. Cheng and J. Yu, *Angew. Chem., Int. Ed.*, 2015, **54**, 11350.

10 C. Trellu, E. Mousset, Y. Pechaud, D. Huguenot, E. D. van Hullebusch, G. Esposito and M. A. Oturan, *J. Hazard. Mater.*, 2016, **306**, 149.

11 S. Cao, F. F. Tao, Y. Tang, Y. Li and J. Yu, *Chem. Soc. Rev.*, 2016, **45**, 4747.

12 W. Ong, Z. Lin and K. Domen, *Part. Part. Syst. Charact.*, 2018, **35**, 1700371.

13 K. H. Leong, A. Abd Aziz, L. C. Sim, P. Saravanan, M. Jang and D. Bahnemann, *Beilstein J. Nanotechnol.*, 2018, **9**, 628.

14 X. Chen, N. Li, Z. Kong, W. Ong and X. Zhao, *Mater. Horiz.*, 2018, **5**, 9.

15 W. Ong, *Front. Mater.*, 2017, **4**, 11.

16 Y. W. Phuan, W. Ong, M. N. Chong and J. D. Ocon, *J. Photochem. Photobiol., C*, 2017, **33**, 54.

17 Z. Li, X. Meng and Z. Zhang, *J. Photochem. Photobiol., C*, 2018, **35**, 39.

18 W. Ong, L. Tan, S. Chai, S. Yong and A. R. Mohamed, *ChemSusChem*, 2014, **7**, 690.

19 W. Ong, L. Tan, Y. H. Ng, S. Yong and S. Chai, *Chem. Rev.*, 2016, **116**, 7159.

20 E. Rahmanian, R. Malekfar and M. Pumera, *Chem. – Eur. J.*, 2018, **24**, 18.

21 W. Han, Z. Li, Y. Li, X. Fan, F. Zhang, G. Zhang and W. Peng, *Front. Chem.*, 2017, **5**, 84.

22 D. Zeng, W. Xu, W. J. Ong, J. Xu, H. Ren, Y. Chen, H. Zheng and D. L. Peng, *Appl. Catal., B*, 2018, **221**, 47.

23 D. Zeng, L. Xiao, W. J. Ong, P. Wu, H. Zheng, Y. Chen and D. L. Peng, *ChemSusChem*, 2017, **10**, 4624.

24 S. Zeng, P. Kar, U. K. Thakur and K. Shankar, *Nanotechnology*, 2018, **29**, 052001.

25 Y. Wu, Y. Chaing, C. Huang, S. Wang and H. Yang, *Dyes Pigm.*, 2013, **98**, 25.

26 H. Fan, T. Jiang, H. Li, D. Wang, L. Wang, J. Zhai, D. He, P. Wang and T. Xie, *J. Phys. Chem. C*, 2012, **116**, 2425.

27 H. He, J. Yin, Y. P. Li, Y. Zhang, H. Qiu, J. Xu, T. Xu and C. Wang, *Appl. Catal., B*, 2014, **156**, 35.

28 A. E. Nogueira, E. Longo, E. R. Leite and E. R. Camargo, *Ceram. Int.*, 2015, **41**, 12073.

29 Z. Ni, Y. Sun, Y. Zhang and F. Dong, *Appl. Surf. Sci.*, 2016, **365**, 314.

30 L. Zhang and Y. Zhu, *Catal. Sci. Technol.*, 2012, **2**, 694.

31 Y. Zhu, Y. Liu, Y. Lv, Q. Ling, D. Liu and Y. Zhu, *J. Mater. Chem. A*, 2014, **2**, 13041.

32 T. Gao, Z. Chen, Q. Huang, F. Niu, X. Huang, L. Qin and Y. Huang, *Rev. Adv. Mater. Sci.*, 2015, **40**, 97.

33 H. F. Cheng, B. B. Huang and Y. Dai, *Nanoscale*, 2014, **6**, 2009.

34 L. Xu, Y. Wan, H. Xie, Y. Huang, X. Qiao, L. Qin and H. J. Seo, *J. Am. Ceram. Soc.*, 2016, **99**, 3964.

35 H. B. Luong, H. T. Le Thi, V. C. Nguyen, T. K. Nguyen, V. T. Duong, V. T. Trinh and D. D. Dang, *Mater. Lett.*, 2016, **164**, 631.

36 X. Zhang, Y. Yang, H. Li, X. Zou and Y. Wang, *Prog. Chem.*, 2016, **28**, 1550.

37 R. He, S. Cao and J. Yu, *Acta Phys.-Chim. Sin.*, 2016, **32**, 2841.

38 R. He, S. Cao, P. Zhou and J. Yu, *Chin. J. Catal.*, 2014, **35**, 989.

39 X. Jin, L. Ye, H. Xie and G. Chen, *Coord. Chem. Rev.*, 2017, **349**, 84.

40 B. Lamm, B. J. Trzesniewski, H. Doscher, W. A. Smith and M. Stefik, *ACS Energy Lett.*, 2018, **3**, 112.

41 J. Di, J. Xia, H. Li, S. Guo and S. Dai, *Nano Energy*, 2017, **41**, 172.

42 L. Chen, J. He, Y. Liu, P. Chen, C. Au and S. Yin, *Chin. J. Catal.*, 2016, **37**, 780.

43 N. Serpone and A. V. Emeline, *J. Phys. Chem. Lett.*, 2012, **3**, 673.

44 W. Yu, J. Zhang and T. Peng, *Appl. Catal., B*, 2016, **181**, 220.

45 M. S. Akple, J. Low, Z. Qin, S. Wageh, A. A. Alghamdi, J. Yu and S. Liu, *Chin. J. Catal.*, 2015, **36**, 2127.

46 K. Qi, B. Cheng, J. Yu and W. Ho, *J. Alloys Compd.*, 2017, **727**, 792.

47 R. Abe, *J. Photochem. Photobiol., C*, 2010, **11**, 179.

48 J. Zai, F. Cao, N. Liang, K. Yu, Y. Tian, H. Sun and X. Qian, *J. Hazard. Mater.*, 2017, **321**, 464.

49 J. Di, J. Chen, M. Ji, Q. Zhang, L. Xu, J. Xia and H. Li, *Chem. Eng. J.*, 2017, **313**, 1477.

50 M. Gao, D. Zhang, X. Pu, H. Li, W. Li, X. Shao, D. Lv, B. Zhang and J. Dou, *Sep. Purif. Technol.*, 2016, **162**, 114.

51 H. Zheng, W. Guo, S. Li, R. Yin, Q. Wu, X. Feng, N. Ren and J. Chang, *Catal. Commun.*, 2017, **88**, 68.

52 P. Dumrongrojthanath, T. Thongtem, A. Phuruangrat and S. Thongtem, *Res. Chem. Intermed.*, 2016, **42**, 5087.

53 L. Zhang, Z. Tang, W. Lau, W. Yin, S. Hu and L. Liu, *Phys. Chem. Chem. Phys.*, 2017, **19**, 20968.

54 W. Meng, R. Hu, J. Yang, Y. Du, J. Li and H. Wang, *Chin. J. Catal.*, 2016, **37**, 1283.

55 J. Han, G. Zhu, M. Hojamberdiev, J. Peng and P. Liu, *J. Mater. Sci.*, 2016, **51**, 2057.

56 Z. Liang, Y. Cao, Y. Li, J. Xie, N. Guo and D. Jia, *Appl. Surf. Sci.*, 2016, **390**, 78.

57 D. Wu, S. Yue, W. Wang, T. An, G. Li, H. Y. Yip, H. Zhao and P. K. Wong, *Appl. Catal., B*, 2016, **192**, 35.

58 Y. Wei, X. Wei, S. Guo, Y. Huang, G. Zhu and J. Zhang, *Mater. Sci. Eng., B*, 2016, **206**, 79.

59 V. Senthil, T. Badapanda, A. Chithambararaj, A. C. Bose and S. Panigrahi, *Int. J. Hydrogen Energy*, 2016, **41**, 22856.

60 J. Li, L. Cai, J. Shang, Y. Yu and L. Zhang, *Adv. Mater.*, 2016, **28**, 4059.

61 Z. S. Liu, Z. L. Liu, J. L. Liu, J. W. Zhang, T. F. Zhou and X. Ji, *Mater. Res. Bull.*, 2016, **76**, 256.

62 D. Liu, J. Huang, L. Cao, X. Tao and B. Zhang, *J. Mater. Sci.: Mater. Electron.*, 2016, **27**, 2473.

63 H. Jung, S. Y. Chae, H. Kim, B. K. Min and Y. J. Hwang, *Catal. Commun.*, 2016, **75**, 18.

64 L. Shan and Y. Liu, *J. Mol. Catal. A: Chem.*, 2016, **416**, 1.

65 Y. Huang, H. Li, W. Fan, F. Zhao, W. Qiu, H. Ji and Y. Tong, *ACS Appl. Mater. Interfaces*, 2016, **8**, 27859.

66 H. Li, Z. Yang, J. Zhang, Y. Huang, H. Ji and Y. Tong, *Appl. Surf. Sci.*, 2017, **423**, 1188.

67 Y. Jiang, J. Hu and J. Li, *RSC Adv.*, 2016, **6**, 39810.

68 H. Li, W. Li, S. Gu, F. Wang and H. Zhou, *Catal. Sci. Technol.*, 2016, **6**, 3510.

69 Z. Chen, X. Jiang, C. Zhu and C. Shi, *Appl. Catal., B*, 2016, **199**, 241.

70 M. Hasan, M. A. Basith, M. A. Zubair, M. S. Hossain, R. Mahbub, M. A. Hakim and M. F. Islam, *J. Alloys Compd.*, 2016, **687**, 701.

71 X. Han, S. Dong, C. Yu, Y. Wang, K. Yang and J. Sun, *J. Alloys Compd.*, 2016, **685**, 997.

72 B. Anke, M. Rohloff, M. G. Willinger, W. Hetaba, A. Fischer and M. Lerch, *Solid State Sci.*, 2017, **63**, 1.

73 X. Nie, W. Wulayin, T. Song, M. Wu and X. Qiao, *Appl. Surf. Sci.*, 2016, **387**, 351.

74 V. Kumar and S. Singh, *Appl. Surf. Sci.*, 2016, **386**, 78.

75 S. Gu, W. Li, F. Wang, H. Li and H. Zhou, *Catal. Sci. Technol.*, 2016, **6**, 1870.

76 R. P. Antony, T. Baikie, S. Y. Chiam, Y. Ren, R. R. Prabhakar, S. K. Batabyal, S. C. J. Loo, J. Barber and L. H. Wong, *Appl. Catal., A*, 2016, **526**, 21.

77 B. Liu, J. Li, W. Yang, X. Zhang, X. Jiang and Y. Bando, *Small*, 2017, **13**, 1701998.

78 I. Tsuji, H. Kato, H. Kobayashi and A. Kudo, *J. Am. Chem. Soc.*, 2004, **126**, 13406.

79 T. Jing and Y. Dai, *Acta Phys.-Chim. Sin.*, 2017, **33**, 295.

80 H. Huang, X. Li, X. Han, N. Tian, Y. Zhang and T. Zhang, *Phys. Chem. Chem. Phys.*, 2015, **17**, 3673.

81 K. Ren, J. Liu, J. Liang, K. Zhang, X. Zheng, H. Luo, Y. Huang, P. Liu and X. Yu, *Dalton Trans.*, 2013, **42**, 9706.

82 Y. Bai, L. Ye, T. Chen, P. Wang, L. Wang, X. Shi and P. K. Wong, *Appl. Catal., B*, 2017, **203**, 633.

83 J. Zhang, Q. Han, J. Zhu and X. Wang, *J. Colloid Interface Sci.*, 2016, **477**, 25.

84 T. Wu, X. Li, D. Zhang, F. Dong and S. Chen, *J. Alloys Compd.*, 2016, **671**, 318.

85 Y. Zhang, X. Sun, G. Yang, Y. Zhu, H. Si, J. Zhang and Y. Li, *Mater. Sci. Semicond. Process.*, 2016, **41**, 193.

86 Q. Qin, Y. Guo, D. Zhou, Y. Yang and Y. Guo, *Appl. Surf. Sci.*, 2016, **390**, 765.

87 X. Sun, Y. Zhang, C. Li, Z. Zhang, Z. Peng, H. Si, J. Zhang and Y. Li, *J. Alloys Compd.*, 2015, **638**, 254.

88 Z. Zhao, Q. Liu and W. Dai, *Sci. Rep.*, 2016, **6**, 31449.

89 K. V. Terebilenko, K. L. Bychkov, V. N. Baumer, N. S. Slobodyanik, M. V. Pavliuk, A. Thapper, I. I. Tokmenko, I. M. Nasieka and V. V. Strelchuk, *Dalton Trans.*, 2016, **45**, 3895.

90 L. Lu, M. Lv, G. Liu and X. Xu, *Appl. Surf. Sci.*, 2017, **391**, 535.

91 X. Xiao, C. Liu, R. Hu, X. Zuo, J. Nan, L. Li and L. Wang, *J. Mater. Chem.*, 2012, **22**, 22840.

92 J. Xia, M. Ji, J. Di, B. Wang, S. Yin, M. He, Q. Zhang and H. Li, *J. Alloys Compd.*, 2017, **695**, 922.

93 X. Jin, L. Ye, H. Wang, Y. Su, H. Xie, Z. Zhong and H. Zhang, *Appl. Catal., B*, 2015, **165**, 668.

94 F. Chang, J. Luo, X. Wang, Y. Xie, B. Deng and X. Hu, *J. Colloid Interface Sci.*, 2015, **459**, 136.

95 C. Wang, X. Zhang, X. Song, W. Wang and H. Yu, *ACS Appl. Mater. Interfaces*, 2016, **8**, 5320.

96 J. Xia, Y. Ge, J. Di, L. Xu, S. Yin, Z. Chen, P. Liu and H. Li, *J. Colloid Interface Sci.*, 2016, **473**, 112.

97 R. Li, F. Xie, J. Liu, Y. Wang, Y. Wang, X. Zhang and C. Fan, *Dalton Trans.*, 2016, **45**, 9182.

98 J. Di, J. Xia, M. Ji, S. Yin, H. Li, H. Xu, Q. Zhang and H. Li, *J. Mater. Chem. A*, 2015, **3**, 15108.

99 L. Ye, X. Jin, C. Liu, C. Ding, H. Xie, K. H. Chu and P. K. Wong, *Appl. Catal., B*, 2016, **187**, 281.

100 S. S. Batool, S. Hassan, Z. Imran, K. Rasool, M. Ahmad and M. A. Rafiq, *Int. J. Environ. Sci. Technol.*, 2016, **13**, 1497.

101 Z. Jiang, Y. Liu, M. Li, T. Jing, B. Huang, X. Zhang, X. Qin and Y. Dai, *Sci. Rep.*, 2016, **6**, 22727.
102 K. C. Chitrada, R. Gakhar, D. Chidambaram, E. Aston and K. S. Raja, *J. Electrochem. Soc.*, 2016, **163**, H546.
103 M. Maisano, M. V. Dozzi and E. Selli, *J. Photochem. Photobiol., C*, 2016, **28**, 29.
104 S. Y. Jeong, K. S. Choi, H. Shin, T. L. Kim, J. Song, S. Yoon, H. W. Jang, M. Yoon, C. Jeon, J. Lee and S. Lee, *ACS Appl. Mater. Interfaces*, 2017, **9**, 505.
105 H. L. Tan, R. Amal and Y. H. Ng, *ACS Appl. Mater. Interfaces*, 2016, **8**, 28607.
106 F. Duan, X. Wang, T. Tan and M. Chen, *Phys. Chem. Chem. Phys.*, 2016, **18**, 6113.
107 H. Li, T. Hu, J. Liu, S. Song, N. Du, R. Zhang and W. Hou, *Appl. Catal., B*, 2016, **182**, 431.
108 L. Yang, G. Zhang, H. Wang, X. Bai, X. Shen, J. Liu and D. Gao, *CrystEngComm*, 2016, **18**, 3683.
109 T. Hu, H. Li, R. Zhang, N. Du and W. Hou, *RSC Adv.*, 2016, **6**, 31744.
110 T. Wu, L. Liu, M. Pi, D. Zhang and S. Chen, *Appl. Surf. Sci.*, 2016, **377**, 253.
111 H. L. Tan, X. Wen, R. Amal and Y. H. Ng, *J. Phys. Chem. Lett.*, 2016, **7**, 1400.
112 Y. Hu, G. Chen, C. Li, Y. Zhou, J. Sun, S. Hao and Z. Han, *J. Mater. Chem. A*, 2016, **4**, 5274.
113 X. Li, C. Zhu, Y. Song, D. Du and Y. Lin, *RSC Adv.*, 2017, **7**, 10235.
114 J. Di, J. Xia, M. Ji, L. Xu, S. Yin, Z. Chen and H. Li, *J. Mater. Chem. A*, 2016, **4**, 5051.
115 B. Zhang, Y. Li, J. Luo, H. Zhao, J. Zhao, G. Dong, Y. Zhu and C. Wang, *Appl. Surf. Sci.*, 2017, **391**, 499.
116 S. Bharathkumar, M. Sakar and S. Balakumar, *J. Phys. Chem. C*, 2016, **120**, 18811.
117 Y. Li, Y. Zhao, G. Wu and J. Zhao, *Inorg. Chem.*, 2016, **55**, 4897.
118 L. Yang, Q. Han, X. Wang and J. Zhu, *Chem. Eng. J.*, 2015, **262**, 169.
119 Z. Liu, Q. Lu, C. Wang, J. Liu and G. Liu, *J. Alloys Compd.*, 2015, **651**, 29.
120 J. Jin and T. He, *Appl. Surf. Sci.*, 2017, **394**, 364.
121 S. Sun, Q. An, W. Wang, L. Zhang, J. Liu and W. A. I. Goddard, *J. Mater. Chem. A*, 2017, **5**, 201.
122 S. Wang, X. Hai, X. Ding, K. Chang, Y. Xiang, X. Meng, Z. Yang, H. Chen and J. Ye, *Adv. Mater.*, 2017, **29**, 1701774.
123 P. Yang, T. Deng, D. Zhao, P. Feng, D. Pine, B. F. Chmelka, G. M. Whitesides and G. D. Stucky, *Science*, 1998, **282**, 2244.
124 X. Li, J. Yu and M. Jaroniec, *Chem. Soc. Rev.*, 2016, **45**, 2603.
125 J. Fu, B. Zhu, C. Jiang, B. Cheng, W. You and J. Yu, *Small*, 2017, **13**, 1603938.
126 L. Qi, B. Cheng, W. Ho, G. Liu and J. Yu, *ChemNanoMat*, 2015, **1**, 58.
127 Z. Liu, J. Liu, Z. Liu, J. Niu and P. Feng, *Mater. Res. Bull.*, 2016, **81**, 119.
128 Z. Qin, H. Tian, T. Su, H. Ji and Z. Guo, *RSC Adv.*, 2016, **6**, 52665.
129 T. Jia, X. Wang, F. Long, J. Li, Z. Kang, F. Fu, G. Sun and J. Chen, *Crystals*, 2016, **6**, 140.
130 J. Zhang, Q. Han, X. Wang, J. Zhu and G. Duan, *Mater. Lett.*, 2016, **162**, 218.
131 M. Zhou, W. Li, Y. Du, D. Kong, Z. Wang, Y. Meng, X. Sun, T. Yan, D. Kong and J. You, *J. Nanopart. Res.*, 2016, **18**, 346.
132 H. Li, J. Liu, T. Hu, N. Du, S. Song and W. Hou, *Mater. Res. Bull.*, 2016, **77**, 171.
133 R. He, S. Cao, J. Yu and Y. Yang, *Catal. Today*, 2016, **264**, 221.
134 Y. Wang, Z. Li, H. Yu and C. Feng, *Funct. Mater. Lett.*, 2016, **9**, 1650059.
135 A. Sarka, A. B. Ghosh, N. Saha, D. N. Srivastava, P. Paul and B. Adhikary, *J. Colloid Interface Sci.*, 2016, **483**, 49.
136 G. Zhao, W. Liu, J. Li, Q. Lv, W. Li and L. Liang, *Appl. Surf. Sci.*, 2016, **390**, 531.
137 L. Chen, J. Wang, D. Meng, X. Wu, Y. Wang and E. Zhong, *Mater. Lett.*, 2016, **162**, 150.
138 Z. Liang, Y. Cao, H. Qin and D. Jia, *Mater. Res. Bull.*, 2016, **84**, 397.
139 Q. Zhang, J. Chen, Y. Xie, M. Wang and X. Ge, *Appl. Surf. Sci.*, 2016, **368**, 332.
140 K. Qian, Z. Jiang, H. Shi, W. Wei, C. Zhu and J. Xie, *Mater. Lett.*, 2016, **183**, 303.
141 M. Wang, X. Xi, C. Gong, X. L. Zhang and G. Fan, *Mater. Res. Bull.*, 2016, **74**, 258.
142 R. Kashfi-Sadabad, S. Yazdani, A. Alemi, D. H. Tran, R. Ramprasad and M. T. Pettes, *Langmuir*, 2016, **32**, 10967.
143 Y. Zhou, X. Meng, L. Tong, X. Zeng and X. Chen, *Energies*, 2016, **9**, 764.
144 J. Li, X. Liu, Z. Sun and L. Pan, *Ceram. Int.*, 2015, **41**, 8592.
145 L. Hou, H. Hua, L. Gan and C. Yuan, *Mater. Lett.*, 2015, **159**, 35.
146 L. Zong, P. Cui, F. Qin, K. Zhao, Z. Wang and R. Yu, *Mater. Res. Bull.*, 2017, **86**, 44.
147 Y. Tang, C. Yang, K. Li, F. Jing, R. Liu, D. Wu and J. Jia, *J. Colloid Interface Sci.*, 2017, **491**, 273.
148 Y. Ying, F. Tao, T. Hong and L. Wang, *Mater. Sci. Semicond. Process.*, 2015, **32**, 82.
149 L. Li, X. Huang, J. Zhang, W. Zhang, F. Ma, Z. Xiao, S. Gai, D. Wang and N. Li, *J. Colloid Interface Sci.*, 2015, **443**, 13.
150 R. Y. Lee, H. Hwang, T. H. Kim and W. Choi, *ACS Appl. Mater. Interfaces*, 2016, **8**, 3366.
151 X. Zhang, R. Li, Y. Wang, X. Zhang, Y. Wang and C. Fan, *Mater. Lett.*, 2016, **174**, 126.
152 S. P. Patil, B. Bethi, G. H. Sonawane, V. S. Shrivastava and S. Sonawane, *J. Ind. Eng. Chem.*, 2016, **34**, 356.
153 Q. Wang, D. Jiao, Y. Bai, J. Zhong, L. Zhao, X. Yong, J. Tong and J. Li, *Mater. Lett.*, 2015, **161**, 267.
154 B. Li, H. Huang, Y. Guo and Y. Zhang, *Appl. Surf. Sci.*, 2015, **353**, 1179.
155 Q. Tong, Y. Dong, X. Wang, P. Yan and D. He, *NANO*, 2015, **10**, 1550077.
156 Y. Shi, Y. Hu, L. Zhang, Z. Yang, Q. Zhang, H. Cui, X. Zhu, J. Wang, J. Chen and K. Wang, *Appl. Clay Sci.*, 2017, **137**, 249.

157 L. Li, Z. Ma, F. Bi, H. Li, W. Zhang and H. He, *J. Adv. Oxid. Technol.*, 2016, **19**, 310.

158 Z. Guo, P. Li, H. Che, G. Wang, C. Wu, X. Zhang and J. Mu, *Ceram. Int.*, 2016, **42**, 4517.

159 Y. Shen, X. Yu, W. Lin, Y. Zhu and Y. Zhang, *Appl. Surf. Sci.*, 2017, **399**, 67.

160 S. Kumar, S. Sharma, S. Sood, A. Umar and S. K. Kansal, *Ceram. Int.*, 2016, **42**, 17551.

161 M. Zhang, C. Shao, X. Zhang and Y. Liu, *CrystEngComm*, 2015, **17**, 7276.

162 B. Weng, F. Xu and F. Yu, *Mater. Lett.*, 2015, **145**, 70.

163 J. Di, M. Ji, J. Xia, X. Li, W. Fan, Q. Zhang and H. Li, *J. Mol. Catal. A: Chem.*, 2016, **424**, 331.

164 G. Jiang, X. Li, M. Lan, T. Shen, X. Lv, F. Dong and S. Zhang, *Appl. Catal., B*, 2017, **205**, 532.

165 Z. Zhao, W. Zhang, X. Lv, Y. Sun, F. Dong and Y. Zhang, *Environ. Sci.: Nano*, 2016, **3**, 1306.

166 D. Xia, L. Hu, C. He, W. Pan, T. Yang, Y. Yang and D. Shu, *Chem. Eng. J.*, 2015, **279**, 929.

167 S. Wang, J. Yun, B. Luo, T. Butburee, P. Peerakiatkhajohn, S. Thaweesak, M. Xiao and L. Wang, *J. Mater. Sci. Technol.*, 2017, **33**, 1.

168 X. Zhang, Y. Liu, Q. Zhang and Y. Zhou, *Prog. Chem.*, 2016, **28**, 1560.

169 S. Cao, J. Low, J. Yu and M. Jaroniec, *Adv. Mater.*, 2015, **27**, 2150.

170 R. Marschall, *Adv. Funct. Mater.*, 2014, **24**, 2421.

171 H. Wang, L. Zhang, Z. Chen, J. Hu, S. Li, Z. Wang, J. Liu and X. Wang, *Chem. Soc. Rev.*, 2014, **43**, 5234.

172 X. Meng and Z. Zhang, *J. Mol. Catal. A: Chem.*, 2016, **423**, 533.

173 B. N. Nunes, L. F. Paula, Í. A. Costa, A. E. H. Machado, L. G. Paterno and A. O. T. Patrocinio, *J. Photochem. Photobiol., C*, 2017, **32**, 1.

174 D. Li and W. Shi, *Chin. J. Catal.*, 2016, **37**, 792.

175 J. Low, J. Yu, M. Jaroniec, S. Wageh and A. A. Alghamdi, *Adv. Mater.*, 2017, **29**, 1601694.

176 Y. Liu, G. Zhu, J. Gao, M. Hojamberdiev, H. Lu, R. Zhu, X. Wei and P. Liu, *J. Alloys Compd.*, 2016, **688**, 487.

177 L. Fan, B. Wei, L. Xu, Y. Liu, W. Cao, N. Ma and H. Gao, *NANO*, 2016, **11**, 1650095.

178 M. Yan, Y. Hua, F. Zhu, W. Gu, J. Jiang, H. Shen and W. Shi, *Appl. Catal., B*, 2017, **202**, 518.

179 M. Zhang, J. Qin, P. Yu, B. Zhang, M. Ma, X. Zhang and R. Liu, *Beilstein J. Nanotechnol.*, 2018, **9**, 789.

180 Y. Huang, W. Fan, B. Long, H. Li, F. Zhao, Z. Liu, Y. Tong and H. Ji, *Appl. Catal., B*, 2016, **185**, 68.

181 Y. Guo, P. Wang, J. Qian, J. Hou, Y. Ao and C. Wang, *Catal. Sci. Technol.*, 2018, **8**, 486.

182 C. Lv, G. Chen, X. Zhou, C. Zhang, Z. Wang, B. Zhao and D. Li, *ACS Appl. Mater. Interfaces*, 2017, **9**, 23748.

183 J. Li, G. Zhan, Y. Yu and L. Zhang, *Nat. Commun.*, 2016, **7**, 11480.

184 L. Chen, J. He, Q. Yuan, Y. Liu, C. Au and S. Yin, *J. Mater. Chem. A*, 2015, **3**, 1096.

185 R. He, J. Zhang, J. Yu and S. Cao, *J. Colloid Interface Sci.*, 2016, **478**, 201.

186 X. Liu and Y. Kang, *Mater. Lett.*, 2016, **164**, 229.

187 Y. Huang, Y. Wei, J. Wang, D. Luo, L. Fan and J. Wu, *Appl. Surf. Sci.*, 2017, **423**, 119.

188 X. Dang, X. Zhang, Y. Chen, X. Dong, G. Wang, C. Ma, X. Zhang, H. Ma and M. Xue, *J. Nanopart. Res.*, 2015, **17**, 93.

189 Y. Li, S. Wu, L. Huang, H. Xu, R. Zhang, M. Qu, Q. Gao and H. Li, *J. Phys. Chem. Solids*, 2015, **76**, 112.

190 D. Xiong, G. Huang, B. Zhou, Q. Yan, A. Pan and W. Huang, *J. Colloid Interface Sci.*, 2016, **464**, 103.

191 M. Nawaz, *J. Photochem. Photobiol., A*, 2017, **332**, 326.

192 L. Long, A. Zhang, Y. Huang, X. Zhang and H. Yu, *J. Mater. Chem. A*, 2015, **3**, 4301.

193 Y. Ao, L. Xu, P. Wang, C. Wang, J. Hou and J. Qian, *Dalton Trans.*, 2015, **44**, 11321.

194 D. Zhou, H. Yang, Y. Tu, Y. Tian, Y. Cai, Z. Hu and X. Zhu, *Nanoscale Res. Lett.*, 2016, **11**, 193.

195 H. Sun, J. Li, G. Zhang and N. Li, *J. Mol. Catal. A: Chem.*, 2016, **424**, 311.

196 Y. Guo, J. Li, Z. Gao, X. Zhu, Y. Liu, Z. Wei, W. Zhao and C. Sun, *Appl. Catal., B*, 2016, **192**, 57.

197 W. Shan, Y. Hu, Z. Bai, M. Zheng and C. Wei, *Appl. Catal., B*, 2016, **188**, 1.

198 Y. Hu, C. Dong, K. Wu, S. Xia, X. Li and X. Wei, *Mater. Lett.*, 2015, **147**, 69.

199 J. An, G. Zhang, R. Zheng and P. Wang, *J. Environ. Sci.*, 2016, **48**, 218.

200 F. Niu, D. Chen, L. Qin, N. Zhang, J. Wang, Z. Chen and Y. Huang, *ChemCatChem*, 2015, **7**, 3279.

201 Y. Xing, W. Que, X. Yin, Z. He, X. Liu, Y. Yang, J. Shao and L. B. Kong, *Appl. Surf. Sci.*, 2016, **387**, 36.

202 S. Li, K. Xu, S. Hu, W. Jiang, J. Zhang, J. Liu and L. Zhang, *Appl. Surf. Sci.*, 2017, **397**, 95.

203 N. Bao, Z. Yin, Q. Zhang, S. He, X. Hu and X. Miao, *Ceram. Int.*, 2016, **42**, 1791.

204 M. Zalfani, B. van der Schueren, Z. Hu, J. C. Rooke, R. Bourguiga, M. Wu, Y. Li, G. Van Tendeloo and B. Su, *J. Mater. Chem. A*, 2015, **3**, 21244.

205 Y. Huang, M. Fu and T. He, *Acta Phys.-Chim. Sin.*, 2015, **31**, 1145.

206 J. Xu, W. Wang, J. Wang and Y. Liang, *Appl. Surf. Sci.*, 2015, **349**, 529.

207 J. Li, M. Cui, Z. Guo, Z. Liu and Z. Zhu, *Mater. Lett.*, 2015, **151**, 75.

208 G. Joshi, J. K. Pandey, S. Singh and R. Sharma, *Korean J. Chem. Eng.*, 2017, **34**, 500.

209 J. Yin, S. Huang, Z. Jian, Z. Wang and Y. Zhang, *Mater. Sci. Semicond. Process.*, 2015, **34**, 198.

210 X. Chang, T. Wang, P. Zhang, J. Zhang, A. Li and J. Gong, *J. Am. Chem. Soc.*, 2015, **137**, 8356.

211 K. Trzcinski, M. Szkoda, K. Siuzdak, M. Sawczak and A. Lisowska-Oleksiak, *Appl. Surf. Sci.*, 2016, **388**, 753.

212 C. Yang, Y. Huang, F. Li and T. Li, *J. Mater. Sci.*, 2016, **51**, 1032.

213 X. Sun, H. Zhang, J. Wei, Q. Yu, P. Yang and F. Zhang, *Mater. Sci. Semicond. Process.*, 2016, **45**, 51.

214 J. Zhang, L. Huang, L. Yang, Z. Lu, X. Wang, G. Xu, E. Zhang, H. Wang, Z. Kong, J. Xi and Z. Ji, *J. Alloys Compd.*, 2016, **676**, 37.

215 Z. Zhu, Y. Yan and J. Li, *J. Mater. Sci.*, 2016, **51**, 2112.

216 X. Liu, Q. Lu and C. Wang, *Mater. Lett.*, 2015, **154**, 81.

217 S. Issarapanacheewin, K. Wetchakun, S. Phanichphant, W. Kangwansupamonkon and N. Wetchakun, *Mater. Lett.*, 2015, **156**, 28.

218 J. Li, C. Yu, W. Fang, L. Zhu, W. Zhou and Q. Fan, *Chin. J. Catal.*, 2015, **36**, 987.

219 L. Chen, H. Hua, Q. Yang and C. Hu, *Appl. Surf. Sci.*, 2015, **327**, 62.

220 R. Tang, H. Su, S. Duan, Y. Sun, L. Li, X. Zhang, S. Zeng and D. Sun, *RSC Adv.*, 2015, **5**, 41949.

221 J. Li, X. Liu, Z. Sun and L. Pan, *J. Colloid Interface Sci.*, 2016, **463**, 145.

222 W. Chen, G. Duan, T. Liu, S. Chen and X. Liu, *Mater. Sci. Semicond. Process.*, 2015, **35**, 45.

223 S. Jonjana, A. Phuruangrat, S. Thongtem, O. Wiranwetchayan and T. Thongtem, *Mater. Lett.*, 2016, **180**, 93.

224 S. Jonjana, A. Phuruangrat, T. Thongtem and S. Thongtem, *Mater. Lett.*, 2016, **172**, 11.

225 M. Xu and W. Zhang, *Eur. J. Inorg. Chem.*, 2016, 826.

226 A. Dittmer, J. Menze, B. Mei, J. Strunk, H. S. Luftman, R. Gutkowski, I. E. Wachs, W. Schuhmann and M. Muhler, *J. Phys. Chem. C*, 2016, **120**, 18191.

227 S. N. Lou, J. Scott, A. Iwase, R. Amal and Y. H. Ng, *J. Mater. Chem. A*, 2016, **4**, 6964.

228 Z. Wan and G. Zhang, *J. Mater. Chem. A*, 2015, **3**, 16737.

229 S. Yin, J. Di, M. Li, Y. Sun, J. Xia, H. Xu, W. Fan and H. Li, *J. Mater. Sci.*, 2016, **51**, 4769.

230 X. Wang, H. Hu, S. Chen, K. Zhang, J. Zhang, W. Zou and R. Wang, *Mater. Chem. Phys.*, 2015, **158**, 67.

231 X. Wang, Q. Ni, D. Zeng, G. Liao, Y. Wen, B. Shan and C. Xie, *Appl. Surf. Sci.*, 2016, **396**, 590.

232 D. Jiang, X. Du, D. Chen, Y. Li, N. Hao, J. Qian, H. Zhong, T. You and K. Wang, *Carbon*, 2016, **102**, 10.

233 R. Jiang, H. Y. Zhu, J. B. Li, F. Q. Fu, J. Yao, S. T. Jiang and G. M. Zeng, *Appl. Surf. Sci.*, 2016, **364**, 604.

234 X. Li, L. Wang, L. Zhang and S. Zhuo, *Appl. Surf. Sci.*, 2017, **419**, 586.

235 Y. Ao, K. Wang, P. Wang, C. Wang and J. Hou, *Appl. Catal., B*, 2016, **194**, 157.

236 X. Wen, C. Zhang, C. Niu, L. Zhang, G. Zeng and X. Zhang, *Catal. Commun.*, 2017, **90**, 51.

237 O. Mehraj, N. A. Mir, B. M. Pirzada and S. Sabir, *Appl. Surf. Sci.*, 2015, **332**, 419.

238 G. Dai, J. Yu and G. Liu, *J. Phys. Chem. C*, 2011, **115**, 7339.

239 K. Wang, C. Shao, X. Li, F. Miao, N. Lu and Y. Liu, *Materials*, 2016, **9**, 90.

240 O. Mehraj, B. M. Pirzada, N. A. Mir, M. Z. Khan and S. Sabir, *Appl. Surf. Sci.*, 2016, **387**, 642.

241 Y. Sun, X. Xiao, X. Dong, F. Dong and W. Zhang, *Chin. J. Catal.*, 2017, **38**, 217.

242 S. Lee, Y. Park, D. Pradhan and Y. Sohn, *J. Ind. Eng. Chem.*, 2016, **35**, 231.

243 J. Xia, M. Ji, J. Di, B. Wang, S. Yin, Q. Zhang, M. He and H. Li, *Appl. Catal., B*, 2016, **191**, 235.

244 T. A. Gadhi, A. Hernandez-Gordillo, M. Bizarro, P. Jagdale, A. Tagliaferro and S. E. Rodil, *Ceram. Int.*, 2016, **42**, 13065.

245 L. Shan, G. Wang, D. Li, X. San, L. Liu, L. Dong and Z. Wu, *Dalton Trans.*, 2015, **44**, 7835.

246 M. Mao, F. Chen, C. Zheng, J. Ning, Y. Zhong and Y. Hu, *J. Alloys Compd.*, 2016, **688**, 1080.

247 Y. Cheng, H. Wang, Y. Zhu, F. Liao, Z. Li and J. Li, *J. Mater. Sci.: Mater. Electron.*, 2015, **26**, 1268.

248 C. Lv, G. Chen, J. Sun, C. Yan, H. Dong and C. Li, *RSC Adv.*, 2015, **5**, 3767.

249 D. Peng, Z. Zou, F. Long, J. He and T. Zhang, *Ionics*, 2016, **22**, 2347.

250 Q. Zhao, X. Liu, Y. Xing, Z. Liu and C. Du, *J. Mater. Sci.*, 2017, **52**, 2117.

251 S. Han, J. Li, K. Yang and J. Lin, *Chin. J. Catal.*, 2015, **36**, 2119.

252 L. Cheng and Y. Kang, *Catal. Commun.*, 2015, **72**, 16.

253 Y. Mi, H. Li, Y. Zhang, R. Zhang and W. Hou, *Appl. Surf. Sci.*, 2017, **423**, 1062.

254 X. Li, Y. Li, J. Shen and M. Ye, *Ceram. Int.*, 2016, **42**, 3154.

255 A. Rauf, M. S. A. S. Shah, G. H. Choi, U. B. Humayoun, D. H. Yoon, J. W. Bae, J. Park, W. Kim and P. J. Yoo, *ACS Sustainable Chem. Eng.*, 2015, **3**, 2847.

256 Y. Liu, M. Zhang, L. Li and X. Zhang, *Catal. Commun.*, 2015, **60**, 23.

257 F. Dong, X. Feng, Y. Zhang, C. Gao and Z. Wu, *RSC Adv.*, 2015, **5**, 11714.

258 Y. Wu, Q. Han, L. Wang, X. Wang and J. Zhu, *Mater. Chem. Phys.*, 2017, **187**, 72.

259 Y. Liu, G. Zhu, J. Peng, J. Gao, C. Wang and P. Liu, *J. Mater. Sci.: Mater. Electron.*, 2017, **28**, 2172.

260 X. Zhang, L. Zhang, J. Hu, C. Pan and C. Hou, *Appl. Surf. Sci.*, 2015, **346**, 33.

261 P. Madhusudan, J. Ran, J. Zhang, J. Yu and G. Liu, *Appl. Catal., B*, 2011, **110**, 286.

262 X. Zou, Y. Dong, X. Zhang, Y. Cui, X. Ou and X. Qi, *Appl. Surf. Sci.*, 2017, **391**, 525.

263 Y. Ma, Y. Jia, L. Wang, M. Yang, Y. Bi and Y. Qi, *Phys. Chem. Chem. Phys.*, 2016, **18**, 5091.

264 X. Lin, D. Liu, X. Guo, N. Sun, S. Zhao, L. Chang, H. Zhai and Q. Wang, *J. Phys. Chem. Solids*, 2015, **76**, 170.

265 Q. W. Cao, Y. F. Zheng and X. C. Song, *Ceram. Int.*, 2016, **42**, 14533.

266 Z. Dai, F. Qin, H. Zhao, F. Tian, Y. Liu and R. Chen, *Nanoscale*, 2015, **7**, 11991.

267 Z. Xiang, Y. Wang, D. Zhang and P. Ju, *J. Ind. Eng. Chem.*, 2016, **40**, 83.

268 T. He, D. Wu and Y. Tan, *Mater. Lett.*, 2016, **165**, 227.

269 C. Feng, D. Wang, B. Jin and Z. Jiao, *RSC Adv.*, 2015, **5**, 75947.

270 L. Hao, H. Huang, Y. Guo, X. Du and Y. Zhang, *Appl. Surf. Sci.*, 2017, **420**, 303.

271 T. Yan, M. Sun, H. Liu, T. Wu, X. Liu, Q. Yan, W. Xu and B. Du, *J. Alloys Compd.*, 2015, **634**, 223.

272 X. Liu, Y. Su, Q. Zhao, C. Du and Z. Liu, *Sci. Rep.*, 2016, **6**, 28689.

273 H. Huang, K. Xiao, T. Zhang, F. Dong and Y. Zhang, *Appl. Catal., B*, 2017, **203**, 879.

274 S. Tu, M. Lu, X. Xiao, C. Zheng, H. Zhong, X. Zuo and J. Nan, *RSC Adv.*, 2016, **6**, 44552.

275 Y. Si, J. Li, J. Zhong, J. Zeng, S. Huang, W. Yuan, M. Li and J. Ding, *Curr. Appl. Phys.*, 2016, **16**, 240.

276 D. Wu, L. Ye, S. Yue, B. Wang, W. Wang, H. Y. Yip and P. K. Wong, *J. Phys. Chem. C*, 2016, **120**, 7715.

277 H. Qian, M. Lai, X. Huang, W. Wang, C. Xu, H. Yong, Y. Wen and Y. Zhou, *Surf. Rev. Lett.*, 2016, **23**, 1650032.

278 W. S. Dos Santos, M. Rodriguez, A. S. Afonso, J. P. Mesquita, L. L. Nascimento, A. O. T. Patrocinio, A. C. Silva, L. C. A. Oliveira, J. D. Fabris and M. C. Pereira, *Sci. Rep.*, 2016, **6**, 31406.

279 J. Ke, J. Liu, H. Sun, H. Zhang, X. Duan, P. Liang, X. Li, M. O. Tade, S. Liu and S. Wang, *Appl. Catal., B*, 2017, **200**, 47.

280 Q. Wang, X. Shi, E. Liu, J. C. Crittenden, X. Ma, Y. Zhang and Y. Cong, *J. Hazard. Mater.*, 2016, **317**, 8.

281 Y. Zhang, M. Park, H. Y. Kim, B. Ding and S. Park, *Appl. Surf. Sci.*, 2016, **384**, 192.

282 C. Zeng, Y. Hu, Y. Guo, T. Zhang, F. Dong, X. Du, Y. Zhang and H. Huang, *Appl. Catal., B*, 2016, **194**, 62.

283 S. Chou, C. Chen, Y. Dai, J. Lin and W. W. Lee, *RSC Adv.*, 2016, **6**, 33478.

284 W. Li, P. Li, Y. Liu, B. Zhang, H. Zhang, W. Geng and Q. Zhang, *ChemCatChem*, 2015, **7**, 4163.

285 J. Yu, S. Wang, J. Low and W. Xiao, *Phys. Chem. Chem. Phys.*, 2013, **15**, 16883.

286 J. Low, C. Jiang, B. Cheng, S. Wageh, A. A. Al-Ghamdi and J. Yu, *Small Methods*, 2017, **1**, 1700080.

287 W. Yu, J. Chen, T. Shang, L. Chen, L. Gu and T. Peng, *Appl. Catal., B*, 2017, **219**, 693.

288 K. Qi, B. Cheng, J. Yu and W. Ho, *Chin. J. Catal.*, 2017, **38**, 1936.

289 T. Di, B. Zhu, B. Cheng, J. Yu and J. Xu, *J. Catal.*, 2017, **352**, 532.

290 J. Liu, B. Cheng and J. Yu, *Phys. Chem. Chem. Phys.*, 2016, **18**, 31175.

291 A. J. Bard, *J. Photochem.*, 1979, **10**, 59.

292 Q. Wang, T. Hisatomi, Q. Jia, H. Tokudome, M. Zhong, C. Wang, Z. Pan, T. Takata, M. Nakabayashi, N. Shibata, Y. Li, I. D. Sharp, A. Kudo, T. Yamada and K. Domen, *Nat. Mater.*, 2016, **15**, 611.

293 H. Tada, T. Mitsui, T. Kiyonaga, T. Akita and K. Tanaka, *Nat. Mater.*, 2006, **5**, 782.

294 Y. Sasaki, H. Kato and A. Kudo, *J. Am. Chem. Soc.*, 2013, **135**, 5441.

295 M. Wang, Q. Han, L. Li, L. Tang, H. Li, Y. Zhou and Z. Zou, *Nanotechnology*, 2017, **28**, 274002.

296 Q. Liu, J. Huan, N. Hao, J. Qian, H. Mao and K. Wang, *ACS Appl. Mater. Interfaces*, 2017, **9**, 18369.

297 J. Lv, K. Dai, J. Zhang, L. Geng, C. Liang, Q. Liu, G. Zhu and C. Chen, *Appl. Surf. Sci.*, 2015, **358**, 377.

298 S. N. F. M. Nasir, H. Ullah, M. Ebadi, A. A. Tahir, J. S. Sagu and M. A. M. Teridi, *J. Phys. Chem. C*, 2017, **121**, 6218.

299 W. Wang, H. Cheng, B. Huang, X. Liu, X. Qin, X. Zhang and Y. Dai, *J. Colloid Interface Sci.*, 2015, **442**, 97.

300 R. He, J. Zhou, H. Fu, S. Zhang and C. Jiang, *Appl. Surf. Sci.*, 2018, **430**, 273.

301 J. Zhang, Y. Hu, X. Jiang, S. Chen, S. Meng and X. Fu, *J. Hazard. Mater.*, 2014, **280**, 713.

302 X. Zhao, J. Yu, H. Cui and T. Wang, *J. Photochem. Photobiol., A*, 2017, **335**, 130.

303 C. Liu, Q. Wu, M. Ji, H. Zhu, H. Hou, Q. Yang, C. Jiang, J. Wang, L. Tian, J. Chen and W. Hou, *J. Alloys Compd.*, 2017, **723**, 1121.

304 C. Song, Y. Feng, W. Shi and C. Liu, *CrystEngComm*, 2016, **18**, 7796.

305 F. Wang, W. Li, S. Gu, H. Li, X. Wu, C. Ren and X. Liu, *J. Photochem. Photobiol., A*, 2017, **335**, 140.

306 H. Li, T. Hu, R. Zhang, J. Liu and W. Hou, *Appl. Catal., B*, 2016, **188**, 313.

307 S. Chen, Y. Hu, L. Ji, X. Jiang and X. Fu, *Appl. Surf. Sci.*, 2014, **292**, 357.

308 D. Wang, Z. Guo, Y. Peng and W. Yuan, *Chem. Eng. J.*, 2015, **281**, 102.

309 S. Wang, X. Yang, X. Zhang, X. Ding, Z. Yang, K. Dai and H. Chen, *Appl. Surf. Sci.*, 2017, **391**, 194.

310 J. Ding, Z. Dai, F. Qin, H. Zhao, S. Zhao and R. Chen, *Appl. Catal., B*, 2017, **205**, 281.

311 G. Liu, S. You, H. Huang, M. Ma and N. Ren, *Chemosphere*, 2017, **171**, 702.

312 M. J. Islam, D. A. Reddy, N. S. Han, J. Choi, J. K. Song and T. K. Kim, *Phys. Chem. Chem. Phys.*, 2016, **18**, 24984.

313 W. Jo and T. S. Natarajan, *J. Colloid Interface Sci.*, 2016, **482**, 58.

314 W. Fang, M. Xing and J. Zhang, *J. Photochem. Photobiol., C*, 2017, **32**, 21.

315 M. Li, J. Wang, P. Zhang, Q. Deng, J. Zhang, K. Jiang, Z. Hu and J. Chu, *Sci. Rep.*, 2017, **7**, 42484.

316 K. Hu, Z. Li, S. Chen, J. Bian, Y. Qu, J. Tang and L. Jing, *Part. Part. Syst. Charact.*, 2018, **35**, 1700320.

317 H. Hirakawa, S. Shiota, Y. Shiraishi, H. Sakamoto, S. Ichikawa and T. Hirai, *ACS Catal.*, 2016, **6**, 4976.

318 K. R. Yoon, J. W. Ko, D. Youn, C. B. Park and I. Kim, *Green Chem.*, 2016, **18**, 944.

319 S. Yu, Y. Zhang, M. Li, X. Du and H. Huang, *Appl. Surf. Sci.*, 2017, **391**, 491.

320 X. Dong, W. Zhang, Y. Sun, J. Li, W. Cen, Z. Cui, H. Huang and F. Dong, *J. Catal.*, 2018, **357**, 41.

321 X. Li, J. Yu, S. Wageh, A. A. Al-Ghamdi and J. Xie, *Small*, 2016, **12**, 6640.

322 B. Priya, P. Raizada, N. Singh, P. Thakur and P. Singh, *J. Colloid Interface Sci.*, 2016, **479**, 271.

323 J. Zhai, H. Yu, H. Li, L. Sun, K. Zhang and H. Yang, *Appl. Surf. Sci.*, 2015, **344**, 101.

324 Y. Hao, X. Dong, X. Wang, S. Zhai, H. Ma and X. Zhang, *J. Mater. Chem. A*, 2016, **4**, 8298.

325 J. Selvaraj, S. Gupta, R. Anand, S. Fiechter and V. R. Subramanian, *J. Electrochem. Soc.*, 2016, **163**, H147.

326 Z. Zhang, T. Zheng, J. Xu and H. Zeng, *J. Mater. Sci.*, 2016, **51**, 3846.

327 Z. Zhao, Y. Zhou, F. Wang, K. Zhang, S. Yu and K. Cao, *ACS Appl. Mater. Interfaces*, 2015, **7**, 730.

328 Y. Li, Z. Wang, B. Huang, Y. Dai, X. Zhang and X. Qin, *Appl. Surf. Sci.*, 2015, **347**, 258.

329 Q. Hao, R. Wang, H. Lu, C. Xie, W. Ao, D. Chen, C. Ma, W. Yao and Y. Zhu, *Appl. Catal., B*, 2017, **219**, 63.

330 J. Wang, W. Jiang, D. Liu, Z. Wei and Y. Zhu, *Appl. Catal., B*, 2015, **176**, 306.

331 Z. Shen, S. Xie, W. Fan, Q. Zhang, Z. Xie, W. Yang, Y. Wang, J. Lin, X. Wu, H. Wan and Y. Wang, *Catal. Sci. Technol.*, 2016, **6**, 6485.

332 G. Zhang, Z. Hu, M. Sun, Y. Liu, L. Liu, H. Liu, C. Huang, J. Qu and J. Li, *Adv. Funct. Mater.*, 2015, **25**, 3726.

333 X. Y. Kong, W. P. C. Lee, W. Ong, S. Chai and A. R. Mohamed, *ChemCatChem*, 2016, **8**, 3074.

334 Z. Ma, P. Li, L. Ye, Y. Zhou, F. Su, C. Ding, H. Xie, Y. Bai and P. K. Wong, *J. Mater. Chem. A*, 2017, **5**, 24995.

335 H. Y. Wang, Z. S. Liu, Y. L. Zhao, J. N. Niu and P. Z. Feng, *Mater. Res. Bull.*, 2017, **89**, 253.

336 F. Q. Zhou, J. C. Fan, Q. J. Xu and Y. L. Min, *Appl. Catal., B*, 2017, **201**, 77.

337 L. Liu, L. Ding, Y. Liu, W. An, S. Lin, Y. Liang and W. Cui, *Appl. Surf. Sci.*, 2016, **364**, 505.

338 D. Wang, L. Guo, Y. Zhen, L. Yue, G. Xue and F. Fu, *J. Mater. Chem. A*, 2014, **2**, 11716.

339 D. Liu, Z. Jiang, C. Zhu, K. Qian, Z. Wu and J. Xie, *Dalton Trans.*, 2016, **45**, 2505.

340 H. Xu, Z. Wu, M. Ding and X. Gao, *Mater. Des.*, 2017, **114**, 129.

341 Z. Chen, X. Chen, J. Di, Y. Liu, S. Yin, J. Xia and H. Li, *J. Colloid Interface Sci.*, 2017, **492**, 51.

342 F. Chen, C. Niu, Q. Yang, X. Li and G. Zeng, *Ceram. Int.*, 2016, **42**, 2515.

343 W. An, W. Cui, Y. Liang, J. Hu and L. Liu, *Appl. Surf. Sci.*, 2015, **351**, 1131.

344 J. Chen, W. Mei, C. Liu, C. Hu, Q. Huang, N. Chen, J. Chen, R. Zhang and W. Hou, *Mater. Lett.*, 2016, **172**, 184.

345 Y. Sun, J. Wu, T. Ma, P. Wang, C. Cui and D. Ma, *Appl. Surf. Sci.*, 2017, **403**, 141.

346 C. Wu, F. Zhang and X. Zhou, *J. Mater. Sci.: Mater. Electron.*, 2015, **26**, 7496.

347 Q. Wang, D. Jiao, Y. Wu, H. Guo, H. She, J. Li, J. Zhong, F. Wang and J. Tong, *Int. J. Hydrogen Energy*, 2016, **41**, 16032.

348 B. Long, Y. Huang, H. Li, F. Zhao, Z. Rui, Z. Liu, Y. Tong and H. Ji, *Ind. Eng. Chem. Res.*, 2015, **54**, 12788.

349 R. Xie, L. Zhang, H. Xu, Y. Zhong, X. Sui and Z. Mao, *Chem. Eng. J.*, 2017, **310**, 79.

350 M. Ji, J. Xia, J. Di, B. Wang, S. Yin, L. Xu, J. Zhao and H. Li, *J. Colloid Interface Sci.*, 2016, **478**, 324.

351 J. Di, J. Xia, M. Ji, L. Xu, S. Yin, Q. Zhang, Z. Chen and H. Li, *Carbon*, 2016, **98**, 613.

352 C. Yu, S. Dong, J. Zhao, X. Han, J. Wang and J. Sun, *J. Alloys Compd.*, 2016, **677**, 219.

353 Y. Zhang, M. Park, H. Kim and S. Park, *J. Alloys Compd.*, 2016, **686**, 106.

354 S. Chou, W. Chung, L. Chen, Y. Dai, W. Lin, J. Lin and C. Chen, *RSC Adv.*, 2016, **6**, 82743.

355 T. Soltani and B. Lee, *Chem. Eng. J.*, 2016, **306**, 204.

356 W. Zhang, F. Dong and W. Zhang, *Appl. Surf. Sci.*, 2015, **358**, 75.

357 R. He, S. Cao, D. Guo, B. Cheng, S. Wageh, A. A. Al-Ghamdi and J. Yu, *Ceram. Int.*, 2015, **41**, 3511.

358 R. Vinoth, S. G. Babu, R. Ramachandran and B. Neppolian, *Appl. Surf. Sci.*, 2017, **418**, 163.

359 X. Yu, J. Shi, L. Feng, C. Li and L. Wang, *Appl. Surf. Sci.*, 2017, **396**, 1775.

360 X. Wang, W. Mao, Q. Wang, Y. Zhu, Y. Min, J. Zhang, T. Yang, J. Yang, X. Li and W. Huang, *RSC Adv.*, 2017, **7**, 10064.

361 H. Wang, Y. Liang, L. Liu, J. Hu and W. Cui, *Appl. Surf. Sci.*, 2017, **392**, 51.

362 Y. Chen, G. Tian, G. Mao, R. Li, Y. Xiao and T. Han, *Appl. Surf. Sci.*, 2016, **378**, 231.

363 J. Qian, Z. Yang, C. Wang, K. Wang, Q. Liu, D. Jiang, Y. Yan and K. Wang, *J. Mater. Chem. A*, 2015, **3**, 13671.

364 H. Liu, Z. Chen and Y. Wang, *J. Photochem. Photobiol., A*, 2016, **326**, 30.

365 G. Tang, J. Dong, K. Wu, W. Liang, D. Zhou, S. Ma, H. Tang and C. Li, *Ceram. Int.*, 2016, **42**, 5607.

366 P. Madhusudan, J. Yu, W. Wang, B. Cheng and G. Liu, *Dalton Trans.*, 2012, **41**, 14345.

367 J. Low, J. Yu, Q. Li and B. Cheng, *Phys. Chem. Chem. Phys.*, 2014, **16**, 1111.

368 J. Bi, W. Fang, L. Li, X. Li, M. Liu, S. Liang, Z. Zhang, Y. He, H. Lin, L. Wu, S. Liu and P. K. Wong, *J. Alloys Compd.*, 2015, **649**, 28.

369 Z. Hu, S. K. Lua and T. Lim, *ACS Sustainable Chem. Eng.*, 2015, **3**, 2726.

370 X. Meng and Z. Zhang, *Appl. Surf. Sci.*, 2017, **392**, 169.

371 J. Zhang, T. Chen, H. Lu, Z. Yang, F. Yin, J. Gao, Q. Liu and Y. Tu, *Appl. Surf. Sci.*, 2017, **404**, 282.

372 J. Di, J. X. Xia, S. Yin, H. Xu, L. Xu, Y. G. Xu, M. Q. He, H. M. Li and J. G. Wang, *Mater. Technol.*, 2015, **30**, 113.

373 M. Palmai, E. M. Zahran, S. Angaramo, S. Balint, Z. Paszti, M. R. Knecht and L. G. Bachas, *J. Mater. Chem. A*, 2017, **5**, 529.

374 W. Guo, Q. Qin, L. Geng, D. Wang, Y. Guo and Y. Yang, *J. Hazard. Mater.*, 2016, **308**, 374.

375 F. Niu, D. Chen, L. Qin, T. Gao, N. Zhang, S. Wang, Z. Chen, J. Wang, X. Sun and Y. Huang, *Sol. Energy Mater. Sol. Cells*, 2015, **143**, 386.

376 Y. Yu, S. Lu and S. Bao, *J. Nanopart. Res.*, 2015, **17**, 323.

377 S. Murcia-Lopez, V. Vaiano, M. C. Hidalgo, J. A. Navio and D. Sannino, *Photochem. Photobiol. Sci.*, 2015, **14**, 678.

378 X. Yan, X. Zhu, R. Li and W. Chen, *J. Hazard. Mater.*, 2016, **303**, 1.

379 N. V. Chien, W. S. Chang, J. Chen, K. Tsai, W. Tzeng, Y. Lin, H. Kuo, H. Liu, K. Chang, W. Chou, C. Wu, Y. Chen, C. Luo, Y. Hsu and Y. Chu, *Nano Energy*, 2015, **15**, 625.

380 P. Zhang, H. Yu, J. Li, H. Zhao, B. Zhu, W. Huang and S. Zhang, *RSC Adv.*, 2016, **6**, 15304.

381 R. Wang, X. Li, W. Cui, Y. Zhang and F. Dong, *New J. Chem.*, 2015, **39**, 8446.

382 P. Yilmaz, D. Yeo, H. Chang, L. Loh and S. Dunn, *Nanotechnology*, 2016, **27**, 345402.

383 J. Di, J. Xia, M. Ji, B. Wang, S. Yin, Y. Huang, Z. Chen and H. Li, *Appl. Catal., B*, 2016, **188**, 376.

384 J. Li, J. Zhou, H. Hao and Z. Zhu, *Mater. Lett.*, 2016, **170**, 163.

385 D. P. Dutta and A. K. Tyagi, *Mater. Res. Bull.*, 2016, **74**, 397.

386 Q. Wu, Y. Cui, L. Yang, G. Zhang and D. Gao, *Sep. Purif. Technol.*, 2015, **142**, 168.

387 S. Lu, Y. Yu, S. Bao and S. Liao, *RSC Adv.*, 2015, **5**, 85500.

388 M. Jin, S. Lu, L. Ma and M. Gan, *Appl. Surf. Sci.*, 2017, **396**, 438.

389 F. Tian, H. Zhao, G. Li, Z. Dai, Y. Liu and R. Chen, *ChemSusChem*, 2016, **9**, 1579.

390 Y. Guo, Y. Zhang, N. Tian and H. Huang, *ACS Sustainable Chem. Eng.*, 2016, **4**, 4003.

391 Y. Chen, B. Liu, J. Chen, D. Chen, X. Yan, W. Xiao, L. Ge, M. Tu, Q. Wang and Z. Wang, *Mater. Lett.*, 2015, **161**, 289.

392 E. S. Baeissa, *Desalin. Water Treat.*, 2016, **57**, 28939.

393 S. Liu, P. Deng, G. Dai, Y. Liang and S. Zhang, *Ceram. Int.*, 2016, **42**, 10094.

394 W. Ragsdale, S. Gupta, K. Conard, S. Delacruz and V. R. Subramanian, *Appl. Catal., B*, 2016, **180**, 442.

395 K. Zhang, Y. Liu, J. Deng, S. Xie, H. Lin, X. Zhao, J. Yang, Z. Han and H. Dai, *Appl. Catal., B*, 2017, **202**, 569.

396 S. J. A. Moniz, D. Pugh, C. S. Blackman, J. Tang and C. J. Carmalt, *Cryst. Growth Des.*, 2016, **16**, 3818.

397 J. Hu, X. Wu, C. Huang, W. Fan and X. Qiu, *Appl. Surf. Sci.*, 2016, **387**, 45.

398 Y. Xu, M. Lv, H. Yang, Q. Chen, X. Liu and F. Wei, *RSC Adv.*, 2015, **5**, 43473.

399 H. Lv, J. Guang, Y. Liu, H. Tang, P. Zhang, Y. Lu and J. Wang, *RSC Adv.*, 2015, **5**, 100625.

400 Y. Zhu, Q. Ling, Y. Liu, H. Wang and Y. Zhu, *Appl. Catal., B*, 2016, **187**, 204.